PHYSICAL REVIEW D

PARTICLES AND FIELDS

THIRD SERIES, VOLUME 26, NUMBER 7 1 OCTOBER 1982

Experimental study of single-particle inclusive hadron scattering and associated multiplicities

A. E. Brenner, D. C. Carey, J. E. Elias, P. H. Garbincius, G. Mikenberg,* and V. A. Polychronakos†
Fermi National Accelerator Laboratory, Batavia, Illinois 60510

W. Aitkenhead,‡ D. S. Barton,† G. W. Brandenburg,§ W. Busza, T. Dobrowolski, J. I. Friedman, H. W. Kendall, T. Lyons, B. Nelson, L. Rosenson, W. Toy,** R. Verdier, and L. Votta††
Massachusetts Institute of Technology, Cambridge, Massachusetts 02139

M. T. Chiaradia, C. DeMarzo, C. Favuzzi, G. Germinario, L. Guerriero, P. LaVopa, G. Maggi, F. Posa, G. Selvaggi, P. Spinelli, and F. Waldner
Istituto di Fisica and Istituto Nazionale di Fisica Nucleare, Bari, Italy

R. Meunier
CERN, Geneva, Switzerland

D. Cutts, R. S. Dulude,‡‡ R. E. Lanou, Jr., and J. T. Massimo
Brown University, Providence, Rhode Island 02912

(Received 13 January 1982)

An experiment using the Fermilab Single Arm Spectrometer (SAS) facility and an associated nonmagnetic vertex detector studied the reactions $a+p\to c+X$, where a and c were $\pi^{\pm}$, $K^{\pm}$, p, or $\bar{p}$. Extensive measurements were made at 100 and 175 GeV/c beam momenta with the outgoing hadrons detected in the SAS covering a kinematic range $0.12<x<1.0$ and $p_T<1.25$ GeV/c. Additional data covering a more restricted range in x were also gathered at 70 GeV/c incident momentum. In this high-statistics experiment, the identification of both the incoming and outgoing charged hadrons were made with a total of eight Čerenkov counters. New and extensive single-particle inclusive data for charged-particle production in low-p_T hadronic fragmentation are presented. The average associated charged-particle multiplicity and pseudorapidity distributions are also given.

I. INTRODUCTION

Inclusive scattering results from hadronic interactions have yielded a great deal of information on the basic physical processes involved. In a manner which is complementary to the study of complete hadron jets by calorimetry, models which describe inclusive scattering within the quark-parton framework have provided information about the substructure of hadrons. In such models of inclusive scattering the identification of the produced particles provides indirect information on the flavor of the participating quarks.

This paper is a data-summary report of a high-statistics inclusive scattering experiment with complete particle identification of the incoming and outgoing charged hadrons. This experiment, designated E118, was performed using the Single Arm Spectrometer facility[1] at Fermilab. The associated charged-particle multiplicities and angular distributions were measured simultaneously using a nonmagnetic vertex detector. The reactions studied were $a+p\to c+X$ where a and c were charged pions, kaons, protons, or antiprotons. Most of the data were taken at two beam momenta, 100 and 175 GeV/c. The kinematic range covered by the

 ©1982 The American Physical Society

TABLE I. M6 beam species ratios for 400-GeV incident protons.

Beam momentum (GeV/c)	Polarity	π	K	p
100	(+)	0.60	0.04	0.36
100	(−)	0.93	0.04	0.03
175	(+)	0.10	0.01	0.89
175	(−)	0.96	0.03	0.01

outgoing hadrons in Feynman x was $0.12 < x < 1.0$ and in transverse momentum was $p_T < 1.25$ GeV/c. A small amount of additional data was taken with a positive 70-GeV/c beam spanning an x range $0.75 < x < 0.97$, with the same p_T limit. Within these ranges, data were taken at more than three hundred separate kinematic settings. Previous publications report on the importance of resonance production[2] via one-pion exchange in reactions yielding π^- for large values of Feynman x, on the power-law behavior in $(1-x)$ for the cross sections,[3] and on the determination of the pion and kaon structure functions.[4] New analyses of triple-Regge parametrizations,[5] and of the associated charged-hadron multiplicity[6,7] in hadron reactions are discussed here.

The apparatus used for this experiment is described in Sec. II and the analysis procedures are described in Secs. III and IV of this paper. The spectrometer data are presented in Sec. V together with fitted parametrizations of the x and p_T dependence and triple-Regge representations. In Sec. VI, the vertex-detector data are presented giving the associated charge multiplicities and their angular distributions. Finally, a summary of results and conclusions presented here and earlier appear in Sec. VII.

II. THE APPARATUS

The apparatus for this experiment, much of it previously described in detail,[1] consisted of the

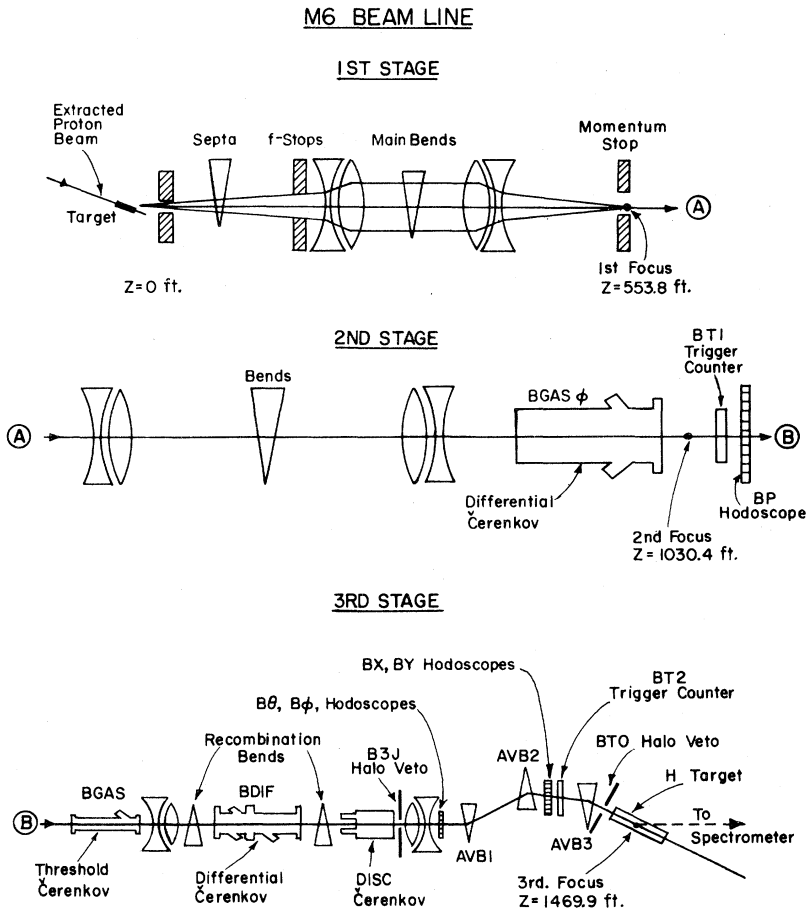

FIG. 1. The three stages of the Fermilab Meson Laboratory M6 beam line.

TABLE II. Hodoscope properties.

Name	z position (ft)	Element size (mm)	Decode sense	No. of elements
BP	1032	2.5	Horizontal	30
$B\theta$	1397	3	Horizontal	8
$B\phi$	1398	3	Vertical	8
Bx	1450	3	Horizontal	11
By	1450	3	Vertical	8
$S\phi$	1555	3	Vertical	16

M6E beam line in the Meson Laboratory together with the Fermilab Single Arm Spectrometer (SAS) augmented by a nonmagnetic vertex detector. In this section, the major features will be outlined with special emphasis on modifications made for this experiment.

A. The beam

The M6E beam line had a production angle of 2.7 mrad relative to the primary proton beam and could transport up to 6×10^6 hadrons/pulse into the experimental area. The momentum could be centered in the range from 20 to 175 GeV/c with a 1% momentum bite. With 400-GeV primary protons incident upon the 8-in.-long beryllium production target, the observed pion, kaon, and proton ratios at the hydrogen target are listed in Table I.

A schematic drawing of the beam is shown in Fig. 1. See Ref. 1 for detailed phase-space and optics contours. Scintillation-counter hodoscopes were placed at the appropriate positions in the beam to determine the momenta, angles, and positions of the transmitted particles. The properties and element sizes of the hodoscopes are given in Table II. In all cases, the elements were overlapped by $\frac{1}{3}$ counter widths to give finer position resolution.

The beam trigger counters BT1, BT2, B3J, and BT0 were plastic scintillation counters located in the last stage of the beam line. BT1 and BT2 spanned the usable beam phase space, and a coincidence between them formed the primary beam trigger. B3J and BT0 were adjustable hole counters that were used to veto halo around the incident beam. The beam trigger for data taking was

$$\mathrm{BT}=\mathrm{BT1}\cdot\mathrm{BT2}\cdot\overline{\mathrm{B3J}}\cdot\overline{\mathrm{BT0}}\ .$$

TABLE III. Beam dimensions at the hydrogen target.

$\Delta p/p$	$\pm0.5\%$
$\Delta\theta$	±0.2 mrad
$\Delta\phi$	±0.2 mrad
Δx	±5 mm
Δy	±2 mm

The beam dimensions at the hydrogen target are given in Table III.

Elements BGAS0, BGAS, BDIF, and BDISC were pressurized gas Čerenkov counters in the beam.[8–11] Their properties are summarized in Table IV. BGAS0 and BGAS were the beam pion threshold detectors, while BDIF and BDISC were differential counters pressurized to detect protons and kaons, respectively. With this system of counters, the beam particle type could be determined on an event-by-event basis for $\gtrsim95\%$ of the incident particles at normal operating intensity. This allowed data to be taken simultaneously for incident π's, K's, and protons. Unidentified or ambiguous beam particles were discarded from the incident flux samples. The lepton content of the beam was always less than 0.5%.

The scattering angle between the beam and spectrometer axes was varied by changing the vertical pitch of the beam as it passed through the target.[1] This was accomplished by a set of three angle-varying bend (AVB) magnets. This is shown in Fig. 2, which also defines the coordinate systems used. Several targets were located on a rotating turntable, shown in Fig. 3, which could also be tilted to match the beam angle. The target was rotated and tilted by remote control between data runs. The data reported on here were taken with the 20-in.-long liquid-hydrogen-filled target cell and a complementary 20-in. empty cell. A typical data point had contributions from target-full and -empty runs each with the beam pitched alternatively up and down to minimize systematic offsets.

TABLE IV. Beam and spectrometer Čerenkov counters.

Name	Ref.	Effective length (ft)	Čerenkov mode	Čerenkov angle (mrad)
BGAS0	8	82	threshold	
BGAS	11	59	threshold	≤ 10
BDIF	9	34	differential	10
BDISC	10	16.4	differential	24.5 ± 0.25
SDIF	9	34	differential	10 or 8.5
SGAS1	11	103	threshold	≤ 8
SGAS2	11	46.5	threshold	≤ 10
SGAS3	11	22.5	threshold	≤ 14

B. The spectrometer

The Single Arm Spectrometer as shown in Fig. 4 was a separate magnetic-transport system which was used to analyze fast forward particles scattered from the target. Measurements were made of the momentum, angle, position, and identity of one particle resulting from each interaction in the target. ST1 and ST2 were the spectrometer trigger counters located, respectively, at the momentum focus and at the end of the spectrometer. A coincidence was required between these counters to indicate the presence of a charged particle within the spectrometer aperture. A spectrometer event (SEV) trigger (ST) was then defined as

$$\mathrm{ST} = \mathrm{ST1} \cdot \mathrm{ST2} \cdot \mathrm{BT} \, .$$

On each trigger, the coordinates of the scattered particle were measured using multiwire proportional counters which were positioned at four locations along the spectrometer. The properties of these chambers are given in Table V. Momentum and spatial coordinates at the target were decoded from the x,y position information measured by these detectors. The resolution of these measurements and the aperture of the spectrometer are given in Table VI. Here the fractional momentum $(\Delta p/p)$ is the fractional deviation of a particle's momentum from the spectrometer setting.

The spectrometer optics were slightly modified with respect to those described in Ref. 1 to increase further the angular acceptance. To reduce point-to-point systematic errors, a single spectrometer tune was employed over the entire range of momentum from 20 to 175 GeV/c.

The determination of the fractional-momentum deviation from the central spectrometer setting, $(\Delta p/p)$, was independent of the position and angle of the scattered particle at the target. The first wire planes H11 and H12 were used to measure the particle position in front of the spectrometer bends, and wire planes H21, H22, H3, and H4 to measure the angle and position of the particle after it left the bend magnets (see Fig. 4). The momentum of the particle could then be determined from the change in trajectory angle caused by the bending magnets.

As in the beam line, the spectrometer had several gas Čerenkov counters[9,11] for identifying particle type. These were SDIF, SGAS1, SGAS2, and SGAS3 (see Table IV). SDIF was a dual-channel differential counter and the three SGAS counters were threshold counters. At momenta above 100 GeV/c, the SGAS counters were used to identify pions. Light falling on the coincidence ring mirror of the SDIF differential Čerenkov

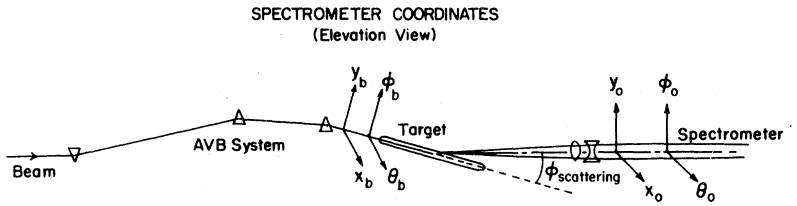

FIG. 2. The angle the spectrometer subtended relative to the incident beam direction was adjusted using an angle-varying bend (AVB) magnetic system bending in the vertical plane of the incident beam. The three magnets of the AVB are shown here in relation to the target and the spectrometer.

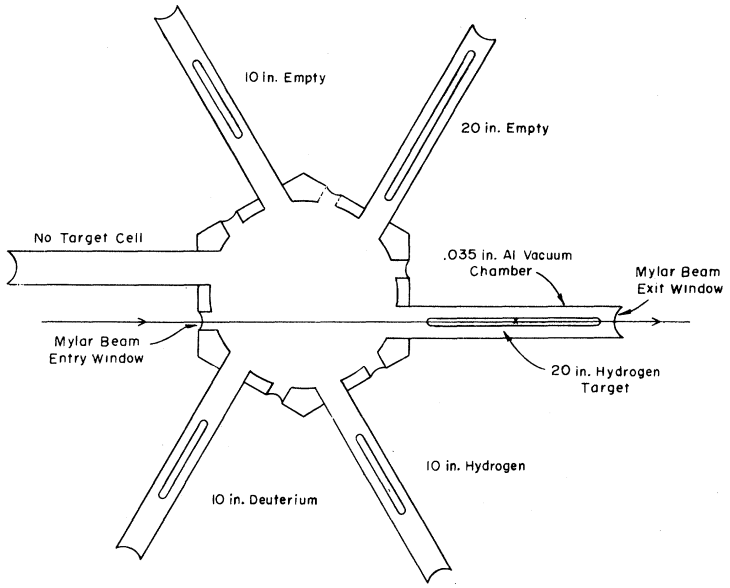

FIG. 3. Plan view of the target turntable assembly. The turntable contained 10- and 20-in.-long targets each of hydrogen, deuterium, and empty-target cells.

counter signaled the presence of a proton. In the absence of a pion signature, a signal in the veto mirror of SDIF defined a kaon. For increased efficiency at spectrometer momenta below 100 GeV/c, SGAS2 was pressurized to count kaons as well as pions. Appendix A contains a discussion of the spectrometer Čerenkov-counter particle-identification strategy.

Electromagnetic and hadronic shower counters and a 15-foot-long steel-loaded counter telescope at the end of the spectrometer were used to tag events with leptonlike triggers. This information was helpful in determining corrections for pion and kaon decays in flight in which daughter particles were emitted within the spectrometer-trigger aperture.

Periodically, the spectrometer was set at zero degrees and tuned to the beam momentum. The incident beam then passed through the spectrometer providing verifications of spectrometer tune, alignment, and transformation coefficients as well as a calibration of the detectors.

C. Vertex detector

The 20-in. liquid hydrogen (0.06 absorption length) target was surrounded by a nonmagnetic vertex detector. The primary purpose of this detector system was to measure the associated charged-particle multiplicities and pseudorapidity distributions for single-particle inclusive events triggered by the SAS. The vertex detector and liquid-hydrogen target were mounted on a tilt

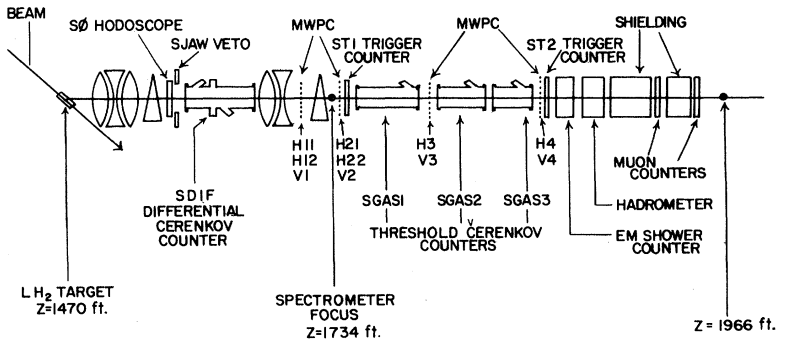

FIG. 4. The Single Arm Spectrometer instrumentation. The quadrupole polarities are indicated for the nonbend, vertical plane.

TABLE V. Spectrometer wire chambers (2 mm wire spacing).

Name	z position (ft)	No. of wires
$H11$	1639.7	64
$H12$	1641.1	64
$V1$	1640.4	32
$H21$	1733.6	64
$H22$	1734.3	64
$V2$	1732.4	32
$H3$	1845.0	160
$V3$	1745.7	64
$H4$	1925.5	160
$V4$	1926.4	64

frame to maintain alignment along the incident beam while the beam was pitched vertically to vary the p_T of the trigger reaction. A schematic layout showing the relative positions of the vertex-detector components is shown in Fig. 5.

Three separate detector systems, all with hexagonal geometry were used to cover the full angular range: the forward multiplicity Čerenkov counters (MC's), the mid-range multiwire proportional chambers (PC's), and the wide-angle target-recoil hodoscopes (MT and MB). Two adjacent detector regions allowed substantial overlap for tracks originating from any vertex within the hydrogen target. Table VII lists the detector properties.

The multiplicity Čerenkov counters,[12] MC, composed of six $\frac{1}{2}$-in.-thick (0.02 absorption length) Pilot 425 lucite wedge-shaped members, detected charged particles within 1.8° of the incident beam. The incident beam and spectrometer trigger particle also passed through the MC's. This required short resolving times and high-rate capability. The Čerenkov-light output was independent of the velocity for particles with $\beta > 0.9$ allowing detection of multiple particles in a single MC by pulse-height analysis.

Multiwire proportional chambers[13] (PC's) covered the angular range 1.5° to 24°. In addition to track counting, the PC array was used to reconstruct the interaction-vertex position for each event, since knowledge of the vertex position is necessary for studying angular distributions for an extended target. The nine sense planes were arranged in three packages providing three wire hits for each track in each of three projections rotated 120° between views. There were 2600 sense wires of 0.080-in. spacing in the entire vertex detector. Hexagonal kapton plugs of 0.002-in. thickness were used to deaden the beam region of the PC's, which corresponded to the active region of the MC's.

The hexagonal target hodoscope (MT and MB) counters covered the region beyond 22°. The double layer of scintillators discriminated against δ rays while maintaining sensitivity to stopping protons. A coincidence between the inner (MT) and outer (MB) counters signaled a penetrating particle. Stopping recoil protons were detected by requiring a 6-times-minimum energy deposition in the inner MT layer without requiring a MT·MB coincidence. The MT counters formed three hexagonal barrels along the beam. Each set of three MT counters was backed up by a single MB counter for a total of eighteen MT and six MB counters.

The overall resolving time of the vertex detector was determined by the 40-nsec charge-collection time of the multiwire proportional chambers. Accidental rates and PC wire currents limited the luminosity to 1.5×10^5 interactions/second or 3×10^6 incident hadrons/second.

The performance of the vertex-detector components was monitored by the off-line analysis of frequent runs with an interaction trigger which was decoupled from the SAS. The trigger for these runs was BT·IT, where IT was a ring-shaped scintillation counter with a hole for the beam which was located immediately downstream of the MC array.

D. Electronics

To trigger an event it was required that a charged particle be observed in both the beam and

TABLE VI. Spectrometer aperture and resolution.

	Resolution	Aperture
θ horizontal angle	±0.09 mrad	±1.3 mrad
ϕ vertical angle	±0.10 mrad	±0.8 mrad
x position	±0.9 mm	±10 mm
y position	±0.9 mm	±10 mm
$(\Delta p/p)$ fractional momentum	±0.12%	±3.25%

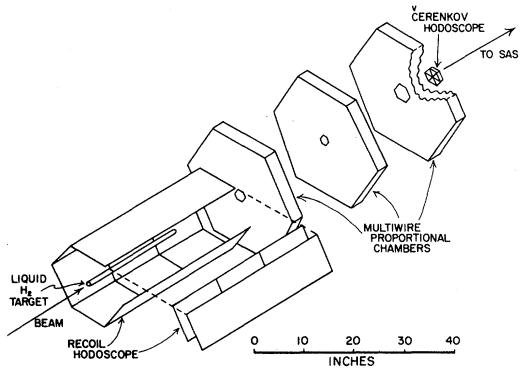

FIG. 5. The arrangement of the apparatus in the target region showing the target hodoscope and the downstream vertex detector.

spectrometer. When a spectrometer-event (SEV) trigger occurred, the status of all the detectors was latched in a CAMAC system and read into a PDP-11 computer. The complete event buffer was written onto magnetic tape; part of the information was saved for on-line analysis and monitoring.

In addition to forming the trigger, the fast electronics provided extensive scaler information on the flux of each beam and spectrometer particle type, along with the various trigger rates. These scalers were gated on only when the computer was ready to take data, thus doing away with dead-time corrections.

A prescaled sample of beam particles without spectrometer trigger was also selected during each beam pulse. These beam events (BEV's) gave the phase space, detection efficiencies, and resolutions for beam particles, whether or not they scattered into the spectrometer. The mixture of π's K's, and p's could also be independently checked using this beam-event sample.

III. SPECTROMETER DATA ANALYSIS

The first step in the analysis of the spectrometer data was a selection of those spectrometer events that could be decoded without error and also occurred in the region of uniform spectrometer acceptance. Next, the yield of good spectrometer events and the corresponding incident beam flux were used to calculate and store run-by-run cross sections. Finally, the various runs were combined, full-minus-empty-target subtractions were made and AVB up and down averages were taken over

TABLE VII. Vertex-detector characteristics (all measurements in inches).

Counter	z position[a]	Type of light detected	Element size
Multiplicity detectors			
MC1–6	67.9	Čerenkov	2.0 (on a side, equilateral triangle)
MT1–6	−5.0	scintillation	8.5×10.0
MT7–12	+5.0	scintillation	8.5×10.0
MT13–18	+15.0	scintillation	8.5×10.0
MB1–6	+5.0	scintillation	8.5×30.0
IT	68.4	scintillation	hole trigger counter
Multiwire proportional chambers			
Sense plane	z position[a]	Plug size	Coordinate measured
PC11	25.1	1.5×1.8	U_1
PC12	24.5	1.5×1.8	U_2
PC13	23.9	1.5×1.8	U_3
PC21	45.8	1.0×1.2	U_1
PC22	45.2	1.0×1.2	U_2
PC23	44.6	1.0×1.2	U_3
PC31	63.6	3.3×3.8	U_1
PC32	63.0	3.3×3.8	U_2
PC33	62.4	3.3×3.8	U_3

[a]All z positions are given relative to the center of the 20-in. hydrogen target.

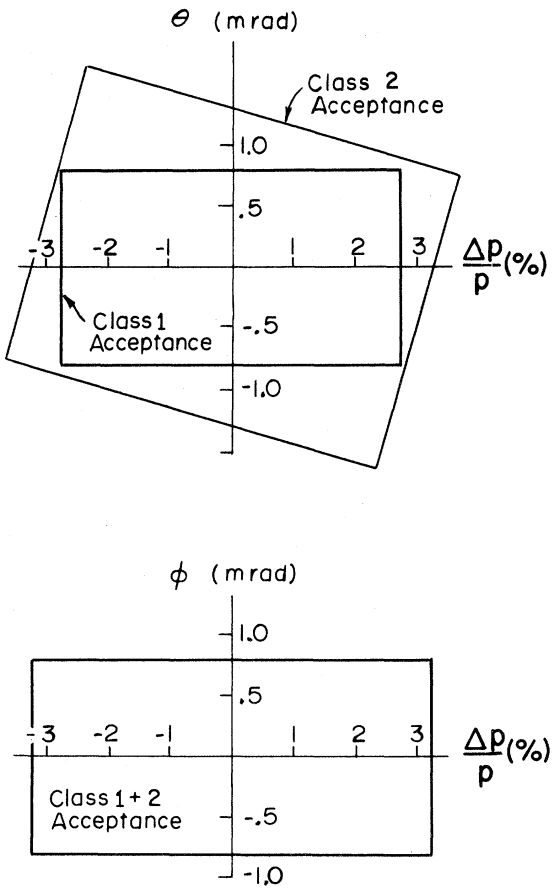

FIG. 6. The acceptance of the spectrometer for the two analyses performed on the data.

similar runs. The procedures used in carrying out the analysis are described here.

A. Event selection

For spectrometer events, the coordinates of the beam and spectrometer particles were calculated and the particle types in the beam and spectrometer were determined from the recorded Čerenkov patterns. The event was discarded if the requirements for a good particle track in the spectrometer wire chambers, an unambiguous beam Čerenkov pattern, and a good beam hodoscope pattern were not all met. All spectrometer Čerenkov patterns were given particle assignments; corrections were later made to resolve ambiguities. If the spectrometer particle coordinates were within the good acceptance region, the event was binned in spectrometer production coordinates $\theta,\phi,(\Delta p/p)$ as shown in Fig. 2, and stored for the cross-section calculation.

The yields of two different classes of events were saved. The acceptance regions for these classes are illustrated in Fig. 6. The first class of events came from the central uniform spectrometer acceptance region with aperture $\Delta\Omega(\Delta p/p)=14.1$ μsr %. The second acceptance class took advantage of the full spectrometer size. For this class, events were accepted from a parallelpiped in the $\theta,\phi,(\Delta p/p)$ space whose size was 25 μsr %. Comparisons between these classes for high-statistics processes validated the second acceptance class. These results agreed with a second independent analysis using a Monte Carlo calculation[14] of the larger spectrometer acceptance.

Final cross sections were determined using the data from each spectrometer kinematic setting as a single bin. Finer-grained information was used for acceptance cuts and for resolution corrections, which compensated for nonlinear variation of the cross section over the spectrometer acceptance. In this case, the event yields were integrated over θ and ϕ in Fig. 6, but were separated into seven $\Delta p/p$ bins. This allowed systematic study of overlapping data between adjacent x bins in the region $x>0.8$. The fine binning procedure was also used in triple-Regge fits to leading-particle channels $a+p\rightarrow a+X$ where there would be rapid variation of the cross section across a single coarse data bin.

For beam events (BEV's), coordinate and particle type information was decoded using the same Čerenkov and hodoscope criteria employed for the SEV sample. This determined the respective fraction of good beam triggers for pions, kaons, and protons. The beam phase-space distributions were checked to verify that all acceptable beam particles of one type had nearly equal probability to scatter into the spectrometer.

Finally, the beam fluxes of pions, kaons, protons, and total beam triggers were accumulated. These fluxes were saved along with the event yields for the calculation of cross sections.

B. Cross-section calculation

Using the stored yields and fluxes the cross sections were calculated for the 3 (beam particles)$\times$3 (spectrometer particles)=9 (different reaction channels) simultaneously for each run. The invariant cross section for the reaction $ap\rightarrow cX$ is given by

$$E\frac{d^3\sigma(a,c)}{dp^3}=\frac{E}{p^2}\frac{d^3\sigma(a,c)}{dp\,d\Omega}=\frac{Y(a\rightarrow c)}{F(a)}\frac{E}{p^3}\frac{A}{\Delta\Omega(\Delta p/p)N_0\rho l}\,, \tag{1}$$

where $\Delta\Omega(\Delta p/p)$ is the acceptance of the spectrometer, N_0 is Avogadro's number, ρ is the density of hydrogen in the target, l is the length of the target, $Y(a \rightarrow c)$ is the yield, $F(a)$ is the flux, A is the atomic number of hydrogen, and E,p are the energy and momentum of the scattered particle c in the laboratory frame.

Normalized empty-target subtractions were made. Next, data with opposite scattering angles (AVB polarity) were averaged, producing cross sections indexed by reaction type, beam momentum, Feynman x, and transverse momentum p_T, representing the uncorrected cross sections.

To calibrate the aperture, it was first established through a set of studies that the physical aperture stops (magnet pole faces, etc.) were not shadowing the good acceptance region. Then it was necessary to find the transformation between the true scattering coordinates θ, ϕ, and $(\Delta p/p)$ (two angles and fractional momentum) and the spectrometer exit coordinates measured by the spectrometer wire planes. For this purpose, the program TRANSPORT (Ref. 14) was used. This program provided a second-order description of the transformation between $x,y,\theta,\phi,(\Delta p/p)$ (production coordinates at the target) and $x_0,y_0,\theta_0,\phi_0,(\Delta p/p)_0$ (coordinates measured in the spectrometer) with $(\Delta p/p)_0 = (\Delta p/p)$. Using this transformation, the systematic uncertainties in alignment, magnetic excitations, and resolutions were combined to yield an estimated 7% total systematic uncertainty in the spectrometer acceptance. This is the largest source of systematic error for the cross sections.

As an independent check of the acceptance, both elastic and inelastic cross sections were measured where experimental data from other groups existed. The elastic-differential-cross-section data for incident beam momenta 70 GeV/c positive polarity, 100 GeV/c both polarities, and 175 GeV/c negative polarity agreed in both slope and intercept to within 10% of the Ayres *et al.*[1] data. This is consistent within the combined error of these two experiments. Inelastic data at 100 GeV/c in the channel $pp \rightarrow pX$ were compared with data from Johnson *et al.*[15] and Sannes *et al.*[16] The data agreed within the estimated 7% systematic normalization uncertainty.

C. Systematic corrections

There were several important corrections applied during the analysis. They are listed here in decreasing order of importance. The residual uncertainties in these systematic corrections are listed in Table VIII.

TABLE VIII. Systematic uncertainties.

Transport and acceptance	7% overall
	3% point to point
Transmission and decay loss	$P_{\text{spect}} > 50$ GeV/c
protons	1%
pions	1%
kaons	2%
Multiple scattering in spectrometer at low momentum	
≥ 50 GeV	$<0.5\%$
30 GeV	3%
20 GeV	4.5%
Particle misidentification	
Beam	0.1%
Spectrometer $ap \rightarrow aX$	0.5%
Spectrometer $ap \rightarrow bX$	1–30 %
Spectrometer-wire-chamber loss	$<0.5\%$
Double-scattering correction	1.8%
Radiative corrections	1.3%
Double rf bunches	0.5–1 %
Electrons in beam	$<0.5\%$
Muons in beam	$<0.5\%$

1. Transmission and decay loss in the spectrometer

Over the 500-foot length of the spectrometer, there was a significant probability for particle decay, absorption or scattering out of the acceptance. The fractions of particles transmitted at various energies were determined experimentally to $\pm 2\%$ accuracy from special runs in which an incident beam was run directly into the spectrometer at various energies. The results are shown in Fig. 7. The transmitted fraction was lowest for kaons, ranging from 36% at 30 GeV/c to 90% at 170 GeV/c. Pion and proton transmissions were comparable and were near 70% and 95%, respectively, for these momenta. Decays into either muons or electrons within the spectrometer aperture could be tagged and vetoed on an event-by-event basis using the calorimeter and transmission counters downstream of ST2.

2. Particle misidentification in the spectrometer

The four gas Čerenkov counters in the spectrometer gave five independent signals; thus, there were $2^5=32$ Čerenkov patterns. However, some of the Čerenkov patterns were ambiguous and could be produced by more than one particle type. Nevertheless, each spectrometer event was initially classified as π, K, or proton on the basis of its Čerenkov pattern. The particle misidentification correction (Appendix A) rectified cross-section errors due to

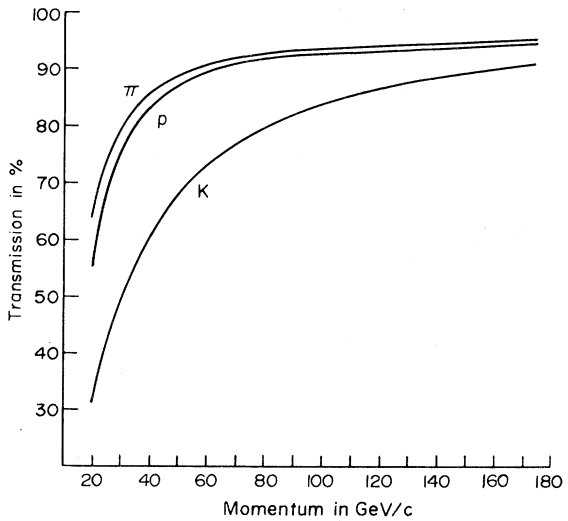

FIG. 7. The spectrometer transmission for π, K, and protons as a function of spectrometer momentum. These curves include the effects of nuclear and multiple scattering as well as decays.

these ambiguities. The probabilities of misidentifying pions or protons in the spectrometer were typically less than 1%, whereas the misidentification probabilities for kaons were typically 7% above 100 GeV and 11% below 100 GeV.

3. Spectrometer-wire-chamber tracking loss

A few percent of the spectrometer events could not be properly tracked because of inefficiencies in the wire chambers and because of ambiguities arising from interactions in the spectrometer. These interactions led to the detection of more than one particle in some of the wire chambers. This tracking loss was measured using runs in which the unscattered beam passed directly through the spectrometer, and was found to be 2% at 20-GeV/c spectrometer momentum, gradually increasing to 3% at 175 GeV/c.

4. Double scattering

The hydrogen target was 20 in. long, corresponding to about 6% of an absorption length. The probability that a particle that scattered more than once in the hydrogen target and would be detected was calculated[17] and the resulting small correction was parametrized as a function of x and p_T. The average magnitude of this double scattering correction was less than 2% over most of the kinematic range studied. At low spectrometer momenta, the correction increased to as much as 6% while the uncertainty in this correction was estimated to be less than 2%.

5. Radiative corrections

During the scattering, either the incident or scattered particle may radiate photons in the bremsstrahlung process. The photon emission will affect the kinematics of the emitting particle and, therefore, the cross section as a function of the kinematics. The radiative correction[17] to leading-particle reactions due to the elastic radiative tail averaged 2%. The inelastic radiative corrections also averaged 2%.

6. Other effects

Several other effects that might affect the cross-section results have been considered. In each case,

these effects were shown to be small. They are as follows.

(a) Simultaneous presence of two beam particles. These events were effectively rejected by their ambiguous signature in a beam hodoscope or the beam Čerenkov counters or large pulse heights in the beam trigger counters. The residual error was less than 0.5%.

(b) Electron contamination in the beam. Direct lepton production from the meson target was small, so that most electrons that entered the beam line came from π^0 gamma conversions. The electron flux in the primary beam was measured with a shower counter at the end of the spectrometer and was found to be less than 0.5% of the hadron flux at 100 GeV/c.

(c) Muon contamination in the beam. Few muons were produced directly at the production target. Muons were produced quite copiously from decays of pions in the primary beam line. However, due to the 1% momentum acceptance of the beam line, most decay muons were swept from the beam by the bend magnets. The measured muon contamination at the hydrogen target was less than 0.5%.

IV. VERTEX-DETECTOR DATA ANALYSIS

A. Event selection

For those spectrometer-event triggers which were completely reconstructed, were within all aperture and software cuts, and had unambiguous Čerenkov particle identification, the vertex-detector data-analysis processing was invoked. It was further required that there be no other beam particle incident within ± 3 rf bunches (± 55 nsec) of the spectrometer trigger to minimize background due to out-of-time tracks from events in nearby rf bunches. Events were discarded if there were more than one beam particle in an rf bunch as detected by ambiguous beam Čerenkov patterns or large pulse heights in beam trigger counters. The standard scattering up/scattering down, target-full, and target-empty data cycles were followed to minimize scattering angle offsets and to perform empty-target subtractions.

In addition to normal spectrometer triggers, the vertex-detector data were also analyzed for noninteracting beam triggers (BEV, for beam events) and special total-cross-section, or minimum-bias, triggers described below. These subsidiary triggers were primarily used for monitoring and calibrating the vertex detector.

B. Analysis

The tracking algorithm for the multiwire proportional chambers first found a vertex by extrapolating hits in each projection back to the target. A fit combining all three projections determined the x,y,z coordinates of the interaction vertex. Tracks were discarded until an acceptable χ^2 was attained, and the discarded tracks were examined for a second vertex. Using thin nuclear targets, the PC vertex resolution was measured to be $\sigma_z = 1.8$ cm. For low-multiplicity events, if no vertex was found, the center of the target was used to compute the track coordinates. The three PC packages were analyzed beginning with the downstream one. The most probable set of points was then found, each point having a hit in all three projections. Lines were drawn from these points to the vertex including three-dimensional hits in other packages within a 4-mm width. The found tracks were scanned, deleting those ambiguous tracks which shared too many common projections. Two PC tracks within 6 mm were treated as a single track.

Multiple particles could be identified in a single MC by pulse-height analysis. For a set of events, the average number of prongs in each counter was determined by fitting the summed pulse-height distribution with spectra expected for 0,1,2,3, . . . particle events. To get the multiplicity in each MC on an event-by-event basis, the pulse-height cut between n and $n+1$ particles was chosen such that the number of events with n particles misidentified as $n+1$ particle events equaled the number of events with $n+1$ particles misidentified as events with n particles, thereby preserving the average multiplicity for that set of events. In those cases where a single MC appeared to have more than three particles detected, it was assumed that a secondary interaction occurred in the lucite counter and the true multiplicity for that counter was set to one. The percentage of good events with more than three particles in a single MC was estimated to be appreciably less than 1%.

Wide-angle particles were detected by a coincidence between the inner MT counter and the corresponding MB counter. A coincidence was not required for particles stopping in the inner counter provided there was at least a six-times-minimum energy deposition in the MT counter.

The overall multiplicity and angular distribution for each event were then determined by combining the results from the three vertex-detector systems. Coincidences between the overlapping regions of the individual detectors were checked to prevent

double counting. The charged-particle distribution was integrated over azimuthal angle and stored in six polar-angle bins for each reaction channel and kinematic setting. Empty-target subtractions were performed on all distributions at this point.

C. Corrections

For each reaction type, the raw charged-prong count N_{0i} was measured. To extract the true charged-prong count N_{Tj}, there is a linear transformation

$$N_{0i}=\sum_j M_{ij}N_{Tj} \ , \tag{2}$$

where M_{ij} is the probability of an event with j charged prongs being measured as having i charged particles. The elements M_{ij} were determined using a Monte Carlo method which simulated events with both charged and neutral particles, including the vertex-detector response.[7,18]

In the Monte Carlo calculation, two related methods were used to generate the outgoing hadron distribution. Reconstructed Fermilab 30-in. bubble-chamber events for 100 GeV pp interactions[19] were used for the charged tracks. Extra neutral tracks were generated using a p_T-limited phase-space Monte Carlo method to balance momentum.[20] The number of extra neutrals was generated as a Poisson distribution using the average number of K^0, π^0, and Λ^0 measured in bubble-chamber data.[21]

The second method involved generating both charged and neutral particles using the p_T-limited phase-space Monte Carlo program. This method also generated simulated events which were triggered by the detected spectrometer particle. The recoiling hadrons were generated for the appropriate missing mass $M_X{}^2$ and recoil momenta. The overall single-particle distributions generated were constrained to reproduce the inclusive data measured by the spectrometer. The two methods were found to be in good agreement with each other and with data taken using a total-cross-section trigger (see subsection D).

The generated events of a given multiplicity j were then propagated through the vertex detector taking the following effects into account: two or more particles in the same MT·MB counter, δ rays, multiple scattering, ionization energy loss, elastic and inelastic scattering, γ-ray conversion,

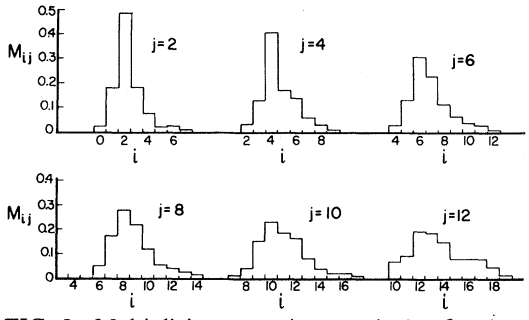

FIG. 8. Multiplicity correction matrix M_{ij} for the 100 GeV, $x=0.6$, $p_T=0.3$ GeV/c kinematic setting. M_{ij} represents the probability of an event with j charged prongs being detected as an event with i charged prongs as calculated by Monte Carlo methods. The efficiency for detecting the spectrometer trigger particle by the vertex detector is also included, giving j=even prong topologies.

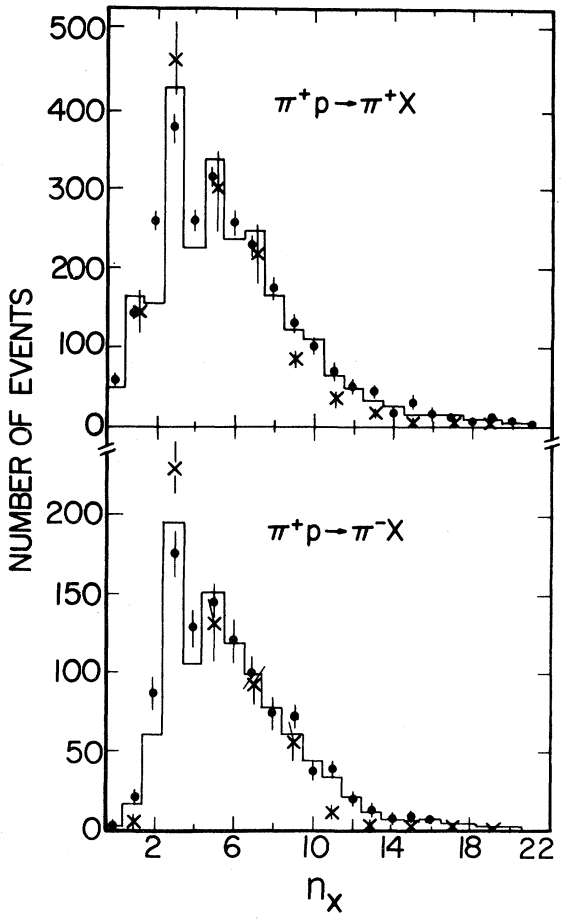

FIG. 9. Associated-charged-prong distributions n_X for $\pi^+p\to\pi^\pm X$ at 100 GeV, $x=0.6$, $p_T=0.3$ GeV/c. ●=raw observed prong distribution N_{0i}; ×=corrected prong distribution N_{Tj} divided by a factor of 2 to account for odd-even prong normalizations; the histogram is the fitted prong distribution $\sum_j M_{ij}N_{Tj}$.

TABLE IX. Corrections for average inelastic charged multiplicity. Uncorrected $\pi^- p \to X$ average $=7.43 \pm 0.10$. Final corrected $\pi^- p \to X$ average $=6.79 \pm 0.11$.

Correction type	Correction	Uncertainty
(A) Physics effects		
δ-ray production	−0.70	0.10
γ conversions in target region	−0.29	0.03
K_S^0 decays	−0.10	0.05
Λ^0 decays	−0.07	0.02
Secondary interactions	−0.70	0.05
(B) Equipment-response correction		
MC efficiency[a] and pulse-height errors	0.10	0.02
Wire-chamber efficiency and tracking-algorithm failure	0.52	0.10
MT and MB efficiency[a] and backward loss of solid angle	0.15	0.03
(C) Other sources		
Elastic-cross-section subtraction	0.48	0.06
Inelastic two-prong loss	−0.03	0.03
Total correction	−0.64	±0.17[b]

[a]Note that these corrections include γ-ray conversions in the counters.
[b]Total correction uncertainty is the uncertainty in each correction added in quadrature. Note that the final quoted error does not include the 0.17.

and the decays of neutral particles. The measured detector inefficiencies, misalignments, and responses were also included in the analysis. The distribution in the number of the particles detected by the vertex detector produced the transform matrix

$$M_{ij} = \frac{\text{number of } j\text{-prong events detected as } i \text{ prongs}}{\text{number of simulated events with } j \text{ prongs}} . \quad (3)$$

As an example, the matrix elements for 100 GeV, $x=0.6$, $p_T=0.3$ GeV/c are shown in Fig. 8. The charged-prong distribution N_{Tj} was calculated by least-squares minimization of

TABLE X. Total cross sections in mb.

Channel	Momentum (GeV)	This experiment	Reference 23
$\pi^+ p$	100	23.4±0.9	23.3±0.1
$\pi^+ p$	175	22.9±1.2	23.6±0.1
$K^+ p$	100	18.4±1.7	18.9±0.1
$K^+ p$	175	18.2±1.8	19.6±0.1
pp	100	38.7±1.3	38.4±0.1
pp	175	39.6±1.1	38.8±0.1
$\pi^- p$	100	23.9±0.7	24.0±0.1
$\pi^- p$	175	23.4±0.8	24.2±0.1
$K^- p$	100	20.8±1.2	20.4±0.1
$K^- p$	175	21.4±1.1	20.7±0.1
$\bar{p}p$	100	40.4±1.2	42.0±0.2
$\bar{p}p$	175	41.2±1.7	41.6±0.5

TABLE XI. Mean inelastic charged multiplicity.

Reaction	Incident beam momentum (GeV/c)	This experiment Mean	This experiment Dispersion	Other experiments Mean	Other experiments Dispersion	Ref.
π^+p	100	6.75±0.16	3.33±0.12	6.62±0.07	3.19±0.05	24
π^-p	100	6.79±0.11	3.15±0.08	6.79±0.08	3.39±0.04	25
π^+p	175	7.55±0.21	3.67±0.14			
π^-p	175	7.83±0.14	3.81±0.10			
K^+p	100	6.95±0.25	3.33±0.18	6.65±0.31	3.34±0.19	26
K^-p	100	6.76±0.18	3.17±0.10			
K^+p	175	7.61±0.37	3.85±0.21			
K^-p	175	7.56±0.18	3.63±0.11	7.33±0.21	3.51±0.15	27[a]
pp	100	6.44±0.17	3.24±0.13	6.37±0.06	3.26±0.05	24
$\bar{p}p$	100	6.52±0.11	3.13±0.09	6.74±0.05	3.26±0.05	28
pp	175	7.54±0.15	3.71±0.10			
$\bar{p}p$	175	7.36±0.24	3.81±0.17			

[a]Results at 147 GeV/c.

$$\chi^2=\sum_i\left[\frac{(N_{0i}-\sum_j M_{ij}N_{Tj})^2}{\sigma_i{}^2}\right], \tag{4}$$

where σ_i is the statistical error on the number of events N_{0i} of apparent multiplicity i. A problem regarding the oscillation of the fitted charged-prong coefficients in the high-multiplicity tail was solved by smoothing the low-statistics bins with the formula

$$N_{Tj}=ae^{-bj} \tag{5}$$

for j greater than twice the average multiplicity. For rare channels, such as $\bar{p}p\to K^+X$, with less than 100 detected events, a correction ratio of (fitted $\langle n\rangle$/raw$\langle n\rangle$) was determined for a much-higher-statistics process measured simultaneously, such as $\pi^-p\to\pi^+X$. A similar least-squares matrix approach was used to correct the pseudorapidity distributions. Examples of the raw, corrected, and fitted charged-prong distributions are shown in Fig. 9.

Three data sets were used to calibrate the Monte Carlo and detector models. Noninteracting beam particles produced δ rays in the hydrogen target. By studying the vertex-detector response to these beam triggers, the difficult to model major backgrounds due to production, absorption, multiple scattering and transport of very low energy electrons through the hydrogen target and detector were determined. Elastic-scattering data were used to calibrate the response of the MT and MB counters to slow recoil protons. Finally, as discussed in the next subsection, good agreement of

TABLE XII. Inelastic charged-topology cross sections in mb at 100 GeV/c.

Charged prongs	π^+p This expt.	π^+p Ref. 24	pp This expt.	pp Ref. 24	π^-p This expt.	π^-p Ref. 25	$\bar{p}p$ This expt.	$\bar{p}p$ Ref. 28
2	2.5±0.9	2.4 ±0.2	3.7±0.9	4.9±0.3	1.9 ±0.6	2.0 ±0.3	4.6 ±0.6	3.6 ±0.3
4	4.2±0.5	4.7 ±0.2	8.9±0.9	7.3±0.3	4.8 ±0.4	4.8 ±0.1	8.0 ±0.7	8.1 ±0.2
6	4.4±0.6	4.8 ±0.2	7.0±0.9	7.0±0.3	5.0 ±0.5	5.2 ±0.1	8.3 ±0.9	8.3 ±0.2
8	4.0±0.8	3.6 ±0.2	4.3±1.0	5.6±0.2	3.9 ±0.6	4.3 ±0.1	4.9 ±1.1	6.9 ±0.2
10	2.5±0.8	2.6 ±0.2	4.4±0.8	3.7±0.2	2.8 ±0.6	2.5 ±0.1	4.4 ±1.1	4.1 ±0.1
12	1.6±0.5	1.3 ±0.1	1.7±0.2	1.7±0.1	1.7 ±0.4	1.4 ±0.1	3.0 ±0.7	2.2 ±0.1
14	0.5±0.1	0.5 ±0.1	0.7±0.2	0.8±0.1	0.5 ±0.1	0.6 ±0.04	0.8 ±0.4	0.9 ±0.1
16	0.2±0.1	0.13±0.03	0.3±0.1	0.2±0.04	0.12±0.10	0.13±0.03	0.2 ±0.1	0.4 ±0.04
18	0.1±0.1	0.04±0.02	0.1±0.05	0.1±0.02	0.03±0.01	0.05±0.01	0.06±0.06	0.12±0.02
20		0.02±0.01		0.1±0.1		0.01±0.018		0.04±0.01
All	20.0±0.9	20.2 ±0.2	31.3±1.2	31.4±0.2	20.7 ±0.7	21.0 ±0.2	34.2 ±1.1	35.6 ±0.4

TABLE XIII. Inelastic charged-topology cross sections in mb.

Charged prongs \ Beam momentum (GeV/c)	100 K^+p	100 K^-p	175 π^+p	175 K^+p	175 pp	175 π^-p	175 K^-p	175 $\bar{p}p$
2	1.7±0.9	2.1±0.5	1.9±0.8	2.1±1.6	3.7±0.8	2.2±0.5	1.5±1.0	4.0±2.0
4	3.5±0.5	3.8±0.5	3.7±0.7	2.6±0.9	5.4±0.8	3.7±0.4	3.7±0.5	6.8±1.2
6	3.8±0.6	4.9±0.7	4.2±0.9	3.4±1.1	6.5±1.0	3.6±0.5	3.4±0.7	6.9±1.7
8	3.2±0.6	2.9±0.7	3.6±1.0	3.6±1.3	5.9±1.0	3.7±0.6	3.7±0.8	7.0±2.3
10	2.3±0.5	2.8±0.7	2.5±1.0	2.3±1.2	4.2±1.0	2.9±0.4	2.7±0.5	3.5±1.5
12	1.1±0.5	1.3±0.4	2.7±0.7	1.5±0.7	3.7±0.8	1.7±0.3	1.5±0.3	3.3±1.5
14	0.5±0.1	0.4±0.2	1.0±0.5	0.5±0.5	1.5±0.2	1.0±0.3	0.8±0.3	1.7±0.5
16	0.2±0.1	0.1±0.1	0.4±0.3		0.6±0.2	0.6±0.2	0.5±0.2	0.9±0.3
18	0.1±0.1	0.05±0.05	0.1±0.1		0.3±0.1	0.4±0.1	0.2±0.1	0.5±0.3
20					0.1±0.06	0.2±0.1	0.1±0.1	0.3±0.2
22						0.13±0.07		
Total inelastic cross section	16.4±1.6	18.4±1.1	20.2±1.1	17.1±1.7	31.7±1.0	19.9±0.7	18.1±1.1	34.9±1.6

the corrected multiplicities and charged-prong distributions with those observed in previous bubble-chamber experiments verified the validity of these calibrations.

D. Correction-procedure verification

A simple transmission trigger was developed which was sensitive to the total hadronic cross section. This allowed the properties of the particles measured with the vertex detector using a minimal-bias trigger to be compared with similar bubble-chamber results. A small scintillation counter was placed at the momentum-dispersed focus of the spectrometer. The scattering angle was set to zero degrees and the spectrometer was tuned to the beam momentum. Particles that met the criteria for beam particles, but failed to fire this scintillation counter, were candidates for inelastic interactions and produced a trigger for the vertex detector. The largest loss for such a total-cross-section measurement was from low-t, high-x scatters that struck the transmission veto counter. False triggers due to scattering or absorption in the spectrometer were removed by subtraction of empty-target runs.

There are two sources of systematic error for the total inelastic multiplicities and topological cross sections. Uncertainty in the elastic-event subtraction can contaminate the two-prong topology and shift the average multiplicity by about 0.06 of a charged particle. The other source of systematic error is in the modeling of the detector system and in the parametrization of neutral-particle production and background used in the Monte Carlo program. The set of physical effects considered and the detector-system modeling are summarized in Table IX, together with the actual corrections applied to the 100-GeV π^-p data. For all reactions, the systematic uncertainty from these effects in the average charged multiplicity is $\lesssim 3\%$ of the multiplicity. The understanding and treatment of this source of error are directly applicable to the associated multiplicity data.

The total cross sections measured in this experiment are listed in Table X. These were corrected for elastic events vetoed by the spectrometer[1] ($\sim 20\%$ and 50% at 100 and 175 GeV/c, respectively) as well as for the loss of low-t ($|t| \leq 0.04$

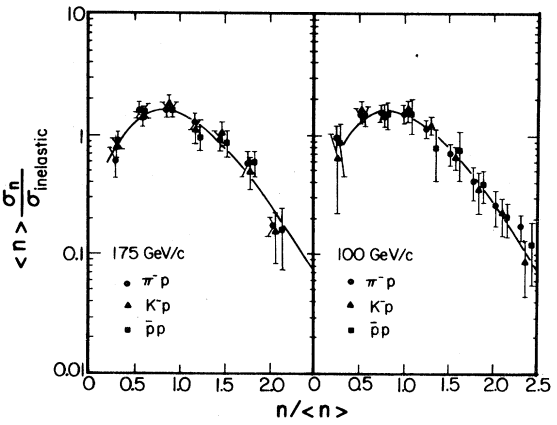

FIG. 10. KNO scaling data for negative beam, total-cross-section trigger. The curve is the KNO fit (Ref. 30) for $pp \to X$ reactions.

TABLE XIV. Complete data set of inclusive cross sections $E\,d^3\sigma/dp^3$ in mb/(GeV^2/c^3) at 100 and 175 GeV/c at constant Feynman-x values. The errors shown below each entry include both statistical and estimated systematic errors in quadrature. In addition, there is an overall 7% absolute normalization uncertainty. The notation for reactions is $a,c \equiv a+p \to c+X$.

	p_T			(a) 100 GeV/c $x=0.200$					
	(GeV/c)	0.100	0.200	0.300	0.500		0.100	0.200	0.300	0.500
π^+,π^+		11.37	10.90	9.17	4.92	π^-,π^-	11.25	8.96	7.50	3.23
		0.68	0.41	0.29	0.43		1.23	0.50	0.29	0.29
π^+,K^+		1.22	0.98	0.66	0.49	π^-,K^-	1.16	0.94	0.55	
		0.38	0.23	0.17	0.36		0.59	0.22	0.14	
π^+,p		1.13	0.71	0.68	0.24	$\pi^-,\bar{p}$	0.33	0.39	0.57	0.36
		0.24	0.13	0.10	0.18		0.28	0.14	0.08	0.10
K^+,π^+		11.43	7.04	5.74	4.08	K^-,π^-	11.20	8.65	5.04	4.78
		2.63	1.29	1.06	2.32		5.60	2.12	1.06	1.48
K^+,K^+		5.24		2.61		K^-,K^-		5.98	4.47	
		3.02		1.55				2.65	1.94	
p,π^+		17.88	12.33	9.37	3.22	$\bar{p},\pi^-$	27.80	9.54	9.01	
		1.10	0.58	0.39	0.47		11.88	3.58	1.74	
p,K^+		1.11	0.73	0.76		$\bar{p},\bar{p}$	13.99			
		0.44	0.26	0.24			10.34			
p,p		3.40	4.06	3.74	2.17					
		0.61	0.35	0.30	0.46					

	p_T			(b) 100 GeV/c	$x=0.300$				
	(GeV/c)	0.100	0.150	0.200	0.250	0.300	0.400	0.500	0.625	0.750
π^+,π^+		8.42	8.93	7.71	7.10	6.37	5.17	3.58	2.30	1.18
		0.44	0.27	0.24	0.23	0.22	0.18	0.15	0.13	0.11
π^+,K^+		0.82	0.95	0.94	0.74	0.66	0.45	0.35	0.19	0.12
		0.20	0.14	0.14	0.12	0.12	0.10	0.08	0.07	0.07
π^+,p		0.70	0.80	0.69	0.55	0.65	0.51	0.43	0.26	0.11
		0.14	0.09	0.08	0.08	0.08	0.06	0.05	0.05	0.05
K^+,π^+		4.20	4.80	6.53	5.43	3.71	2.72	2.88	0.84	
		2.37	1.17	1.55	0.71	0.61	0.61	0.57	0.46	
K^+,K^+		5.28	5.34	3.56	3.03	2.59	2.59	1.16	1.29	
		1.71	1.29	0.80	0.95	0.85	1.27	0.73	0.81	
p,π^+		12.91	11.69	8.74	6.73	5.50	3.49	2.44	1.69	0.80
		0.75	0.41	0.35	0.31	0.27	0.22	0.16	0.15	0.13
p,K^+		0.77	0.79	0.61	0.71	0.96	0.44	0.44	0.16	
		0.26	0.17	0.14	0.14	0.16	0.13	0.12	0.10	
p,p		7.12	7.37	6.63	6.35	5.62	3.95	2.90	1.77	0.82
		0.60	0.36	0.34	0.32	0.29	0.24	0.18	0.16	0.14
π^-,π^-		8.38	7.47	7.67	6.85	6.02	4.52	2.98	1.92	0.95
		0.27	0.26	0.21	0.15	0.13	0.11	0.13	0.08	0.07
π^-,K^-		0.80	0.53	0.60	0.61	0.43	0.38	0.28	0.17	0.13
		0.12	0.11	0.09	0.07	0.05	0.05	0.05	0.03	0.03
$\pi^-,\bar{p}$		0.61	0.47	0.45	0.48	0.42	0.35	0.22	0.14	0.07
		0.07	0.07	0.05	0.04	0.04	0.03	0.04	0.03	0.03
K^-,π^-		4.35	4.95	7.59	3.93	3.99	3.11	2.14	0.89	0.41
		1.92	1.20	1.43	0.59	0.51	0.41	0.51	0.36	0.31
K^-,K^-		4.28	4.56	2.96	4.09	2.92	1.33	0.84	1.35	0.74
		1.26	1.21	0.90	0.68	0.61	0.53	0.65	0.47	0.53
$\bar{p},\pi^-$		8.29	9.59	9.59	7.00	5.61	3.47	2.35	1.77	0.88
		1.96	1.52	1.38	0.86	0.70	0.61	0.69	0.49	0.53
$\bar{p},\bar{p}$		7.04	4.41	6.84	5.51	4.50	3.44	2.78	2.51	1.05
		1.55	1.43	1.26	0.87	0.67	0.55	0.73	0.59	0.58
π^+,π^-		5.04	4.61	4.29	3.96	3.52	2.80	1.76	0.90	
		0.22	0.16	0.15	0.15	0.14	0.13	0.11	0.07	

TABLE XIV. (*Continued.*)

(b) 100 GeV/c $x=0.300$ (*continued*)

p_T (GeV/c)	0.100	0.150	0.200	0.250	0.300	0.400	0.500	0.625	0.750
π^+,K^-	0.45	0.58	0.41	0.63	0.40	0.24	0.15	0.15	
	0.13	0.10	0.08	0.09	0.07	0.07	0.06	0.05	
$\pi^+,\bar{p}$	0.40	0.34	0.30	0.27	0.26	0.21	0.16	0.06	
	0.06	0.05	0.04	0.05	0.04	0.04	0.04	0.03	
K^+,π^-	2.69	3.55	3.08	2.17	2.83	1.99	0.96	0.61	
	1.20	0.57	0.52	0.51	0.48	0.53	0.50	0.40	
p,π^-	4.45	3.90	3.28	3.07	2.71	1.99	1.33	0.80	
	0.28	0.20	0.17	0.17	0.16	0.14	0.12	0.08	
p,K^-	0.25	0.17	0.24	0.18	0.19	0.20			
	0.08	0.06	0.07	0.06	0.07	0.10			
$p,\bar{p}$	0.13	0.10	0.10	0.06	0.09				
	0.04	0.03	0.03	0.03	0.04				
π^-,π^+	4.37	4.64	3.93	4.10	3.48	2.83	1.77	0.77	0.38
	0.31	0.28	0.27	0.23	0.19	0.16	0.12	0.06	0.04
π^-,K^+	0.59	0.58	0.72	0.52	0.44	0.27	0.18	0.10	0.06
	0.16	0.15	0.13	0.11	0.11	0.08	0.06	0.04	0.03
π^-,p	0.46	0.32	0.52	0.64	0.53	0.32	0.26	0.18	0.06
	0.13	0.13	0.10	0.08	0.08	0.07	0.05	0.03	0.02
K^-,π^+		3.99	8.64	3.52	2.01	2.31	1.03	0.75	
		1.26	2.24	1.14	0.81	0.74	0.57	0.42	
$\bar{p},\pi^+$	6.25	3.52	5.13	3.01	3.25	2.39	2.06	1.05	0.97
	1.63	1.63	1.68	1.45	1.34	1.10	1.02	0.65	0.45

(c) 100 GeV/c $x=0.600$

p_T (GeV/c)	0.200	0.300	0.400	0.500	0.625	0.750	1.000	1.250
π^+,π^+	6.06	4.34	0.55	1.58	0.95	0.55	0.18	0.06
	0.20	0.09	0.08	0.04	0.03	0.2	0.01	0.01
π^+,K^+	0.35	0.24	0.16	0.16	0.11	0.08	0.02	
	0.06	0.03	0.03	0.02	0.01	0.01	0.01	
π^+,p	0.22	0.17	0.17	0.14	0.12	0.07	0.03	0.01
	0.04	0.02	0.02	0.01	0.01	0.01	0.01	0.00
K^+,π^+		1.34	0.48	0.51	0.23	0.12		
		0.19	0.18	0.11	0.08	0.06		
K^+,K^+	1.67	1.45	1.12	0.98	0.74	0.43		0.04
	0.65	0.28	0.29	0.16	0.13	0.09		0.04
p,π^+	0.90	0.81	0.53	0.35	0.21	0.13	0.04	0.01
	0.12	0.05	0.05	0.03	0.02	0.01	0.01	0.00
p,K^+	0.13	0.13	0.13	0.09	0.04	0.04		
	0.05	0.02	0.03	0.02	0.01	0.01		
p,p	14.15	10.00	6.67	4.37	2.60	1.50	0.37	0.14
	0.46	0.20	0.18	0.10	0.07	0.05	0.02	0.01
π^-,π^-	5.79	4.12	2.59	1.52	0.91	0.53	0.18	0.05
	0.14	0.06	0.07	0.05	0.03	0.02	0.01	0.00
π^-,K^-	0.23	0.19	0.17	0.12	0.08	0.06	0.02	0.01
	0.04	0.02	0.03	0.02	0.01	0.01	0.00	0.00
$\pi^-,\bar{p}$	0.11	0.10	0.09	0.08	0.05	0.04	0.02	0.00
	0.02	0.01	0.01	0.01	0.01	0.01	0.00	0.00
K^-,π^-		1.16	0.75	0.26	0.26	0.14	0.05	
		0.24	0.20	0.14	0.10	0.08	0.05	
K^-,K^-	2.72	1.93	1.03	0.80	0.56	0.52	0.20	
	0.55	0.25	0.28	0.21	0.14	0.12	0.08	
$\bar{p},\pi^-$	0.68	1.38	0.81	0.58		0.12		
	0.46	0.20	0.23	0.19		0.10		
$\bar{p},\bar{p}$	10.91	8.05	6.66	3.76	2.69	1.33	0.42	
	1.16	0.52	0.60	0.42	0.31	0.19	0.11	

TABLE XIV. *(Continued.)*

p_T (GeV/c)	(d) 100 GeV/c $x=0.920$ 0.300	0.400	0.500	0.625	0.750	1.000	1.250
π^+,π^+	6.11	4.33	2.80	1.54	0.83	0.23	0.06
	0.12	0.11	0.05	0.04	0.02	0.01	0.01
π^+,K^+	0.23	0.13	0.07	0.04	0.02		
	0.02	0.02	0.01	0.01	0.00		
K^+,K^+	3.83	3.35	1.89	1.38	0.78	0.26	
	0.42	0.40	0.21	0.18	0.11	0.09	
p,p	15.01	9.19	5.17	2.48	1.15	0.25	0.03
	0.27	0.23	0.10	0.07	0.04	0.02	0.01
π^-,π^-	5.77	4.34	2.70	1.44	0.76	0.20	0.05
	0.09	0.10	0.06	0.04	0.03	0.01	0.00
π^-,K^-	0.15	0.09	0.06	0.02	0.01	0.00	
	0.02	0.02	0.01	0.01	0.00	0.00	
K^-,K^-	3.73	3.19	2.00	1.18	0.38	0.20	
	0.35	0.39	0.27	0.17	0.10	0.05	
$\bar{p},\bar{p}$	13.16	9.88	5.29	2.17	0.75	0.22	
	0.67	0.50	0.42	0.27	0.15	0.07	

p_T (GeV/c)	(e) 175 GeV/c $x=0.300$ 0.150	0.225	0.300	0.400	0.500	0.625	0.750	0.850
π^+,π^+	8.60	7.42	6.22	4.85	3.70	2.10	1.21	0.69
	0.37	0.30	0.29	0.23	0.18	0.12	0.07	0.06
π^+,K^+	0.70	0.90	0.63	0.40	0.39	0.26	0.17	0.07
	0.15	0.13	0.11	0.08	0.08	0.05	0.04	0.03
π^+,p	0.82	0.82	0.61	0.38	0.32	0.15	0.18	0.07
	0.14	0.10	0.10	0.08	0.06	0.04	0.03	0.03
K^+,π^+	4.58	4.10	3.41	4.14	2.08	1.11	0.68	0.50
	1.17	1.15	0.85	0.78	0.60	0.34	0.23	0.24
K^+,K^+	3.70	3.11	4.01	1.87	1.33	1.86	0.45	
	0.80	0.85	0.84	0.77	0.69	0.48	0.27	
p,π^+	10.39	7.25	5.11	3.91	2.45	1.50	0.83	0.50
	0.21	0.18	0.16	0.17	0.09	0.06	0.03	0.03
p,K^+	0.77	0.66	0.54	0.41	0.32	0.19	0.12	0.05
	0.08	0.08	0.07	0.07	0.04	0.03	0.02	0.02
p,p	6.81	5.78	5.24	3.97	2.86	1.68	0.99	0.60
	0.17	0.16	0.16	0.17	0.10	0.06	0.04	0.03
π^-,π^-	7.45	6.75	6.20	4.87	3.45	2.16	1.14	
	0.22	0.21	0.12	0.09	0.07	0.05	0.04	
π^-,K^-	0.55	0.51	0.61	0.41	0.33	0.22	0.12	
	0.09	0.09	0.06	0.04	0.04	0.02	0.02	
$\pi^-,\bar{p}$	0.41	0.43	0.42	0.34	0.29	0.17	0.12	
	0.06	0.06	0.03	0.03	0.02	0.01	0.01	
K^-,π^-	8.84	5.74	3.85	2.86	2.21	1.34	0.63	
	1.50	1.37	0.57	0.46	0.40	0.24	0.22	
K^-,K^-	6.28	3.33	3.00	2.65	1.68	0.90	0.55	
	1.36	0.99	0.62	0.49	0.45	0.25	0.29	
$\bar{p},\pi^-$	12.25	7.37	5.12	4.02	3.16	1.72	0.68	
	2.37	2.19	0.95	0.73	0.65	0.44	0.51	
$\bar{p},\bar{p}$	5.14	5.89	5.17	3.03	1.46	2.05	0.74	
	1.95	1.49	1.01	0.68	0.70	0.45	0.47	
π^+,π^-	4.76	3.61	3.86	2.78	1.85	0.78	0.43	0.24
	0.25	0.22	0.22	0.18	0.15	0.08	0.05	0.06
π^+,K^-	0.48	0.53	0.29	0.36	0.29	0.16	0.05	
	0.10	0.10	0.09	0.10	0.08	0.05	0.03	

TABLE XIV. (*Continued.*)

p_T (GeV/c)	(e) 175 GeV/c $x=0.300$ (*continued*) 0.150	0.225	0.300	0.400	0.500	0.625	0.750	0.850
$\pi^+,\bar{p}$	0.46	0.52	0.25	0.31	0.18	0.08	0.08	0.08
	0.08	0.08	0.07	0.07	0.08	0.03	0.03	0.06
K^+,π^-	3.74	3.59	2.72	1.50	2.05	0.87		
	0.79	0.63	0.70	0.71	0.79	0.48		
p,π^-	3.95	3.08	2.40	1.69	1.28	0.81	0.41	0.27
	0.08	0.10	0.11	0.09	0.08	0.04	0.03	0.03
p,K^-	0.24	0.24	0.24	0.19	0.09	0.05	0.05	0.03
	0.03	0.03	0.04	0.03	0.03	0.02	0.01	0.02
$p,\bar{p}$	0.14	0.11	0.10	0.05	0.04	0.03	0.02	
	0.02	0.02	0.02	0.02	0.02	0.01	0.01	
π^-,π^+	4.01		3.21	2.73	1.77	0.88	0.42	
	0.12		0.10	0.08	0.06	0.03	0.02	
π^-,K^+	0.68		0.54	0.42	0.35	0.15	0.10	
	0.07		0.06	0.04	0.03	0.02	0.01	
π^-,p	0.44		0.37	0.26	0.25	0.15	0.10	
	0.04		0.04	0.03	0.02	0.01	0.01	
K^-,π^+	4.99		2.62	1.85	1.10	0.79	0.31	
	0.66		0.60	0.40	0.27	0.18	0.11	
$\bar{p},\pi^+$	5.24		3.17	2.24	1.33	0.98	0.71	
	1.27		0.95	0.67	0.55	0.37	0.28	

p_T (GeV/c)	(f) 175 GeV/c $x=0.600$ 0.200	0.300	0.400	0.500	0.625	0.750	0.850	1.000	1.250
π^+,π^+		3.86	2.60	1.53	0.82	0.55	0.27	0.13	0.01
		0.13	0.08	0.07	0.04	0.02	0.02	0.01	0.00
π^+,K^+		0.28	0.20	0.19	0.11	0.08	0.04	0.02	
		0.04	0.03	0.03	0.02	0.01	0.01	0.01	
π^+,p		0.28	0.20	0.18	0.11	0.09	0.03	0.02	
		0.03	0.02	0.02	0.01	0.01	0.01	0.01	
K^+,π^+		1.60	0.66	0.45	0.27	0.17	0.10	0.05	
		0.41	0.17	0.12	0.07	0.04	0.05	0.04	
K^+,K^+		1.97	1.26	1.14	0.70	0.30	0.27	0.11	
		0.31	0.23	0.18	0.11	0.06	0.06	0.05	
p,π^+		0.96	0.54	0.35	0.21	0.13	0.06	0.03	
		0.06	0.02	0.02	0.01	0.00	0.00	0.00	
p,K^+		0.10	0.09	0.08	0.05	0.03	0.01	0.01	
		0.03	0.01	0.01	0.01	0.00	0.00	0.00	
p,p		9.39	6.29	4.26	2.58	1.50	0.71	0.32	0.02
		0.18	0.06	0.07	0.03	0.01	0.01	0.01	0.00
π^-,π^-		3.89	2.49	1.41	0.85	0.43		0.15	0.06
		0.07	0.05	0.04	0.03	0.03		0.02	0.01
π^-,K^-		0.28	0.22	0.1	0.08	0.07		0.01	0.01
		0.02	0.02	0.02	0.01	0.01		0.01	0.00
$\pi^-,\bar{p}$		0.11	0.09	0.08	0.05	0.03		0.02	
		0.01	0.01	0.01	0.01	0.01		0.01	
K^-,π^-		1.45	0.77	0.45	0.37	0.25			
		0.31	0.14	0.13	0.10	0.13			
K^-,K^-		1.98	1.27	0.95	0.27	0.48		0.18	
		0.24	0.18	0.17	0.17	0.17		0.11	
$\bar{p},\pi^-$		0.68	0.71	0.39					
		0.25	0.21	0.21					
$\bar{p},\bar{p}$		9.44	6.84	4.05	1.73	1.08		0.86	
		0.80	0.64	0.54	0.44	0.51		0.29	

TABLE XIV. (*Continued.*)

p_T (GeV/c)	(f) 175 GeV/c $x=0.600$ (*continued*) 0.200	0.300	0.400	0.500	0.625	0.750	0.850	1.000	1.250
π^+,π^-	1.47	0.83	0.54	0.41	0.26	0.12	0.06		0.01
	0.08	0.05	0.05	0.04	0.03	0.01	0.01		0.00
π^+K^-	0.12	0.10	0.14	0.09	0.05	0.02	0.01		
	0.03	0.02	0.02	0.02	0.01	0.01	0.00		
$\pi^+,\bar{p}$	0.08	0.04	0.03	0.02	0.02	0.02	0.01		
	0.02	0.01	0.01	0.01	0.01	0.01	0.00		
K^+,π^-	1.19	0.46	0.34	0.12	0.08	0.13	0.03		0.02
	0.23	0.13	0.08	0.09	0.05	0.06	0.02		0.01
p,π^-	0.31	0.26	0.17	0.12	0.08	0.04	0.02		
	0.02	0.01	0.01	0.01	0.01	0.01	0.00		
p,K^-	0.02	0.01	0.01	0.01					
	0.00	0.00	0.00	0.00					

p_T (GeV/c)	(g) 175 GeV/c $x=0.920$ 0.500	0.625	0.750	1.000	1.250		(h) 175 GeV/c $x=0.940$ 0.500	0.625	0.750	1.000	1.250
π^-,π^-	2.59	1.40	0.73	0.20	0.06	π^+,π^+	3.70	2.34	1.27	0.35	0.10
	0.04	0.03	0.02	0.01	0.00		0.04	0.08	0.03	0.01	0.01
π^-,K^-	0.06	0.03	0.02			π^+,K^+	0.09	0.05	0.02		
	0.01	0.01	0.00				0.01	0.02	0.01		
K^-,K^-	1.88	1.03	0.34	0.14	0.08	K^+,K^+	2.97	2.49	1.26	0.33	0.09
	0.16	0.14	0.08	0.04	0.04		0.19	0.32	0.14	0.06	0.03
$\bar{p},\bar{p}$	5.02	2.27	1.05	0.17		p,p	7.46	3.67	1.67	0.30	0.06
	0.37	0.30	0.18	0.07			0.08	0.08	0.03	0.01	0.00

GeV^2) inelastic diffractive events.[22] The quoted errors are statistical only. The systematic error is estimated to be about 3%. The largest source of error is the uncertainty in the spectrometer acceptance for the elastic cross section ($\lesssim 1.5\%$). The excellent agreement with the data of Carroll *et al.*[23] indicates that the simple transmission trigger provided a good total-cross-section trigger.

A comparison of the mean multiplicities of charged particles measured in this experiment using the minimum bias trigger, with those measured with bubble chambers[24–28] appears in Table XI. The quoted errors are only statistical. It is evident that these measurements are in quite good agreement with the bubble-chamber measurements. Although intended as a calibration, for some channels these data represent the first multiplicity measurements at these energies.

The charged topological cross sections for $\pi^{\pm}p$, pp, and $\bar{p}p$ at 100 GeV/c are listed[24,25,28] in Table XII, also indicating good agreement with bubble-chamber measurements. Charged topological cross sections of the remaining channels are given in Table XIII. It has been shown that charged topological cross sections obey Koba-Nielsen-Olesen (KNO) scaling.[29] As an example of this, the 100 and 175 GeV/c negative-beam topological cross sections have been plotted as $\langle n\rangle\sigma_n/\sigma_{\text{inelastic}}$ vs $n/\langle n\rangle$ (Fig. 10). The data are in good agreement with the curve, which represents a KNO fit[30] to pp data over the range 50 to 300 GeV/c.

The excellent agreement with the bubble-chamber results both for the average multiplicities and for the charged-prong distributions verifies that the detector modeling and correction procedure are capable of producing accurate associated vertex data.

V. SINGLE-PARTICLE INCLUSIVE RESULTS

The inclusive data include 36 possible reactions of the type $a+p\rightarrow c+X$, where a and c are any of $\pi^{\pm}$, $K^{\pm}$, p, or $\bar{p}$ at beam momenta of both 100 and 175 GeV/c. They span a kinematic range of $0.12<x<1.0$ and $p_T<1.25$ GeV/c. Because of the rather small acceptance of the spectrometer, a grid of independent measurements was made; specifically, for each spectrometer momentum (or x) setting data were taken for several values of p_T. In this section, the x and p_T dependence of the data will be presented, and simple fitted parametrizations of the data will be given. For completeness, all the measured points are given in Tables XIV and XV, displayed as a combination of x and

TABLE XV. Complete data set of inclusive cross sections $E\,d^3\sigma/dp^3$ in mb/(GeV^2/c^3) at 100 and 175 GeV/c at constant p_T values. The errors shown below each entry include both statistical and estimated systematic errors in quadrature. In addition, there is an overall 7% absolute normalization uncertainty. The notation for reactions is $a,c \equiv a+p \to c+X$.

(a) 100 GeV/c p_T=0.200 GeV/c

	x	0.300	0.400	0.500	0.600	0.700	0.800	0.840
π^+,π^-		4.29	2.62	1.98	1.54	1.47	1.28	1.15
		0.15	0.22	0.15	0.11	0.13	0.07	0.07
π^+,K^-		0.41	0.32	0.17	0.15		0.05	0.04
		0.08	0.10	0.06	0.04		0.02	0.01
$\pi^+,\bar{p}$		0.30	0.11	0.10	0.06	0.03	0.01	
		0.04	0.06	0.03	0.02	0.02	0.00	
K^+,π^-		3.08	3.88	2.11	1.29	0.70		
		0.52	0.88	0.55	0.38	0.25		
p,π^-		3.28	2.43	1.21	0.33	0.12		
		0.17	0.23	0.13	0.06	0.04		
p,K^-		0.24	0.21	0.07				
		0.07	0.09	0.06				
$p,\bar{p}$		0.10						
		0.03						

(b) 100 GeV/c p_T=0.300 GeV/c

	x	0.200	0.300	0.400	0.500	0.600	0.700	0.800	0.840	0.880	0.920	0.940	0.960
π^+,π^+		9.17	6.37	5.15	4.50	4.34	4.29	4.35	4.78	4.94	6.11		13.14
		0.29	0.22	0.19	0.18	0.09	0.09	0.07	0.10	0.11	0.12		0.24
π^+,K^+		0.66	0.66	0.49	0.38	0.24	0.22	0.19	0.19	0.19	0.23		0.15
		0.17	0.12	0.08	0.07	0.03	0.03	0.02	0.02	0.02	0.02		0.03
π^+,p		0.68	0.65	0.45	0.33	0.17	0.11	0.04	0.05	0.03			
		0.10	0.08	0.06	0.05	0.02	0.02	0.01	0.01	0.01			
$K^+\pi^+$		5.74	3.71	2.91	2.44	1.34	0.62	0.27					
		1.06	0.61	0.62	0.52	0.19	0.19	0.13					
K^+,K^+		2.61	2.59	2.21	2.05	1.45	1.74	2.52	2.07	2.98	3.83		7.83
		1.55	0.85	0.69	0.62	0.28	0.27	0.23	0.30	0.36	0.42		0.97
p,π^+		9.37	5.50	2.34	1.78	0.81	0.37	0.06	0.06	0.02			
		0.39	0.27	0.19	0.17	0.05	0.03	0.01	0.02	0.02			
p,K^+		0.76	0.96	0.38	0.16	0.13	0.05	0.02					
		0.24	0.16	0.09	0.07	0.02	0.02	0.01					
p,p		3.74	5.62	6.41	8.51	10.00	10.72	11.75	12.54	13.61	15.01		29.34
		0.30	0.29	0.33	0.39	0.20	0.21	0.17	0.24	0.28	0.27		0.47
π^-,π^-		7.50	6.02	4.64	4.18	4.12	4.26	4.25		4.86	5.77		
		0.29	0.13	0.13	0.07	0.06	0.05	0.08		0.08	0.09		
π^-,K^-		0.55	0.43	0.35	0.26	0.19	0.20	0.15		0.12	0.15		
		0.14	0.05	0.05	0.03	0.02	0.02	0.02		0.02	0.02		
$\pi^-,\bar{p}$		0.57	0.42	0.30	0.17	0.10	0.05	0.02					
		0.08	0.04	0.03	0.02	0.01	0.01	0.01					
K^-,π^-		5.04	3.99	3.06	1.70	1.16	0.89	0.81					
		1.06	0.51	0.45	0.27	0.24	0.13	0.17					
K^-,K^-		4.47	2.92	2.08	2.34	1.93	1.87	2.20		2.99	3.73		
		1.94	0.61	0.55	0.29	0.25	0.18	0.29		0.28	0.35		
$\bar{p},\pi^-$		9.01	5.61	4.35	2.00	1.38	0.48						
		1.74	0.70	0.65	0.29	0.20	0.11						
$\bar{p},\bar{p}$			4.50	5.45	7.75	8.05	9.83	10.79		10.71	13.16		
			0.67	0.86	0.53	0.52	0.40	0.73		0.54	0.67		
π^+,π^-			3.52	2.02	1.11	0.97	0.83	0.65	0.52	0.46		0.20	
			0.14	0.07	0.04	0.04	0.03	0.03	0.03	0.02		0.02	
π^+,K^-			0.40	0.33	0.16	0.10	0.07	0.03	0.01	0.01			
			0.07	0.04	0.02	0.01	0.01	0.01	0.01	0.00			

TABLE XV. (*Continued.*)

(b) 100 GeV/c p_T=0.300 GeV/c (*continued*)

	x	0.200	0.300	0.400	0.500	0.600	0.700	0.800	0.840	0.880	0.920	0.940	0.960
$\pi^+,\bar{p}$			0.26	0.16	0.09	0.04	0.03	0.01					
			0.04	0.02	0.01	0.01	0.00	0.00					
K^+,π^-			2.83	1.11	0.66	0.57	0.26	0.16					
			0.48	0.21	0.16	0.11	0.08	0.06					
p,π^-			2.71	1.31	0.48	0.25	0.08	0.02					
			0.16	0.07	0.04	0.02	0.01	0.01					
p,K^-			0.19	0.10	0.03	0.02							
			0.07	0.03	0.01	0.01							
$p,\bar{p}$			0.09	0.03									
			0.04	0.01									
π^-,π^+		5.35	3.48	1.82	1.27	1.05	0.83	0.70		0.52			
		0.31	0.19	0.10	0.04	0.03	0.02	0.03		0.02			
π^-,K^+		0.65	0.44	0.32	0.20	0.13	0.08	0.05		0.02			
		0.16	0.11	0.05	0.02	0.01	0.01	0.01		0.01			
π^-,p		0.68	0.53	0.29	0.16	0.09	0.04	0.02					
		0.12	0.08	0.04	0.02	0.01	0.01	0.00					
K^-,π^+		2.82	2.01	1.20	1.26	0.58	0.35	0.17					
		1.27	0.81	0.42	0.20	0.09	0.06	0.06					
$\bar{p},\pi^+$		8.71	3.25	0.98	1.02	0.40	0.18						
		2.47	1.34	0.41	0.19	0.09	0.05						

(c) 100 GeV/c p_T=0.400 GeV/c

	x	0.200	0.300	0.500	0.600	0.700	0.880	0.920
π^-,π^-			4.52	2.62	2.59			4.34
			0.11	0.14	0.07			0.10
π^-,K^-			0.38	0.18	0.17			0.09
			0.05	0.04	0.03			0.02
$\pi^-,\bar{p}$			0.35	0.16	0.09			
			0.03	0.04	0.01			
K^-,π^-			3.11	1.04	0.75			
			0.41	0.48	0.20			
K^-,K^-			1.33	1.23	1.03			3.19
			0.53	0.70	0.28			0.39
$\bar{p},\pi^-$			3.47	0.78	0.81			
			0.61	0.64	0.23			
$\bar{p},\bar{p}$			3.44	6.03	6.66			9.88
			0.55	1.14	0.60			0.59
π^+,π^-		5.69	2.80	0.84		0.43	0.19	
		0.26	0.13	0.05		0.02	0.02	
π^+K^-		0.71	0.24	0.15		0.04	0.01	
		0.18	0.07	0.02		0.01	0.00	
$\pi^+,\bar{p}$		0.29	0.21	0.06		0.01		
		0.10	0.04	0.01		0.00		
K^+,π^-		3.70	1.99	0.49		0.21		
		0.92	0.53	0.18		0.05		
p,π^-		4.65	1.99	0.42		0.05		
		0.32	0.14	0.04		0.01		
p,K^-		0.42	0.20	0.04				
		0.22	0.10	0.03				
$p,\bar{p}$		0.11						
		0.10						
π^-,π^+			2.83			0.43	0.19	
			0.16			0.02	0.02	

TABLE XV. (*Continued.*)

(c) 100 GeV/c p_T=0.400 GeV/c (*continued*)

x	0.200	0.300	0.500	0.600	0.700	0.880	0.920
π^-,K^+		0.27			0.07	0.02	
		0.08			0.01	0.01	
π^-,p		0.32			0.07		
		0.07			0.01		
K^-,π^+		2.31			0.10		
		0.74			0.06		
$\bar{p},\pi^+$		2.39					
		1.10					

(d) 100 GeV/c p_T=0.500 GeV/c

x	0.200	0.300	0.400	0.500	0.600	0.700	0.800	0.840	0.880	0.920	0.940	0.960
π^+,π^+	4.92	3.58	2.66	1.91	1.58	1.44	1.60	1.85	2.08	2.80		6.04
	0.43	0.15	0.10	0.06	0.04	0.04	0.03	0.04	0.04	0.05		0.09
π^+,K^+	0.49	0.35	0.30	0.20	0.16	0.14	0.07	0.10	0.08	0.07		0.07
	0.36	0.08	0.05	0.03	0.02	0.02	0.01	0.01	0.01	0.01		0.01
π^+,p	0.24	0.43	0.33	0.19	0.14	0.07	0.05	0.03	0.02			
	0.18	0.05	0.03	0.02	0.01	0.01	0.01	0.01	0.01			
K^+,π^+	4.08	2.88	0.92	0.76	0.51	0.20	0.21					
	2.32	0.57	0.29	0.17	0.11	0.11	0.06					
K^+,K^+		1.16	1.79	1.13	0.98	1.03	0.85	1.24	1.61	1.89		4.70
		0.73	0.49	0.23	0.16	0.15	0.10	0.14	0.18	0.21		0.43
p,π^+	3.22	2.44	1.27	0.65	0.35	0.14	0.04	0.01	0.01			
	0.47	0.16	0.09	0.04	0.03	0.02	0.01	0.01	0.01			
p,K^+		0.44	0.22	0.09	0.09	0.04	0.03					
		0.12	0.06	0.03	0.02	0.01	0.01					
p,p	2.17	2.90	3.90	3.79	4.37	4.14	4.13	4.34	4.49	5.17		10.38
	0.46	0.18	0.17	0.12	0.10	0.10	0.06	0.08	0.10	0.10		0.17
π^-,π^-	3.23	2.98	2.27	1.66	1.52		1.66		2.04	2.70		
	0.29	0.13	0.06	0.06	0.05		0.04		0.05	0.06		
π^-,K^-		0.28	0.20	0.15	0.12		0.08		0.06	0.06		
		0.05	0.02	0.02	0.02		0.01		0.02	0.01		
$\pi^-,\bar{p}$	0.36	0.22	0.20	0.13	0.08		0.02					
	0.10	0.04	0.02	0.02	0.01		0.00					
K^-,π^-	4.78	2.14	1.17	0.83	0.26		0.23					
	1.48	0.51	0.24	0.19	0.14		0.11					
K^-,K^-		0.84	1.77	0.97	0.80		1.34		1.50	2.00		
		0.65	0.34	0.25	0.21		0.19		0.32	0.27		
$\bar{p},\pi^-$		2.35	1.59	0.41	0.58							
		0.69	0.32	0.22	0.19							
$\bar{p},\bar{p}$		2.78	3.17	3.48	3.76		3.36		3.54	5.29		
		0.73	0.42	0.49	0.42		0.33		0.39	0.42		
π^+,π^-	2.97	1.76	1.41	0.68	0.35	0.24	0.14	0.10	0.08		0.03	
	0.58	0.11	0.18	0.04	0.05	0.02	0.02	0.02	0.01		0.00	
π^+,K^-		0.15		0.10		0.04	0.01					
		0.06		0.02		0.01	0.01					
$\pi^+,\bar{p}$		0.16	0.26	0.05		0.01	0.01					
		0.04	0.12	0.01		0.01	0.01					
K^+,π^-	6.90	0.96		0.32		0.09	0.19					
	4.13	0.50		0.12		0.08	0.13					
p,π^-	2.95	1.33	0.57	0.23	0.12	0.03	0.01					
	0.83	0.12	0.21	0.03	0.05	0.01	0.01					
π^-,π^+	1.60	1.77	1.03	0.66	0.36	0.22	0.18		0.10			
	0.15	0.12	0.06	0.04	0.02	0.02	0.01		0.01			

TABLE XV. (*Continued.*)

(d) 100 GeV/c p_T=0.500 GeV/c (*continued*)

	x	0.200	0.300	0.400	0.500	0.600	0.700	0.800	0.840	0.880	0.920	0.940	0.960
π^-,K^+		0.30	0.18	0.18	0.12	0.08	0.06	0.02					
		0.09	0.06	0.03	0.02	0.01	0.01	0.01					
π^-,p		0.20	0.26	0.14	0.09	0.06	0.03	0.01					
		0.08	0.05	0.03	0.02	0.01	0.01	0.00					
K^-,π^+		1.68	1.03	1.09	0.34	0.29	0.13						
		0.74	0.57	0.29	0.15	0.08	0.06						
$\bar{p},\pi^-$		3.02	2.06	0.80		0.18							
		1.10	1.02	0.48		0.11							

(e) 100 GeV/c p_T=0.625 GeV/c

	x	0.300	0.500	0.700
π^+,π^-		0.90	0.38	0.12
		0.07	0.03	0.02
π^+,K^-		0.15	0.07	0.01
		0.05	0.02	0.01
$\pi^+,\bar{p}$		0.06	0.04	0.01
		0.03	0.01	0.01
K^+,π^-		0.61	0.17	
		0.40	0.12	
p,π^-		0.80	0.14	0.03
		0.08	0.03	0.01
π^-,π^+		0.77	0.42	0.16
		0.06	0.04	0.01
π^-,K^+		0.10	0.07	0.02
		0.04	0.02	0.01
π^-,p		0.18	0.05	0.02
		0.03	0.02	0.01
K^-,π^+		0.75		
		0.42		
$\bar{p},\pi^+$		1.05		
		0.65		

(g) 100 GeV/c p_T=1.000 GeV/c

	x	0.600	0.800	0.840	0.880	0.920	0.960
π^+,π^+		0.18	0.11	0.14	0.16	0.23	0.46
		0.01	0.01	0.01	0.01	0.01	0.01
π^+,K^+		0.02	0.01	0.01	0.00		
		0.01	0.00	0.00	0.00		
π^+,p		0.03	0.01	0.00	0.00		
		0.01	0.00	0.00	0.00		
K^+,K^+			0.12	0.20	0.16	0.26	0.47
			0.03	0.09	0.06	0.09	0.05
p,π^+		0.04	0.00				
		0.01	0.00				
p,p		0.37	0.23	0.23	0.21	0.25	0.33
		0.02	0.01	0.01	0.01	0.02	0.01

(f) 100 GeV/c p_T=0.750 GeV/c

	x	0.300	0.400	0.500	0.600	0.700	0.800	0.840	0.880	0.920	0.960
π^+,π^+		1.18	0.96	0.73	0.55	0.45	0.48	0.54	0.61	0.83	1.90
		0.11	0.05	0.03	0.02	0.02	0.02	0.02	0.02	0.02	0.03
π^+,K^+		0.12	0.11	0.06	0.08	0.04	0.04	0.03	0.02	0.02	0.01
		0.07	0.03	0.02	0.01	0.01	0.01	0.01	0.01	0.00	0.00
π^+,p		0.11	0.13	0.08	0.07	0.05	0.02	0.02	0.01		
		0.05	0.02	0.01	0.01	0.01	0.00	0.00	0.00		
K^+,π^+			0.40	0.19	0.12	0.09					
			0.21	0.12	0.06	0.06					
K^+,K^+			0.40	0.37	0.43	0.43	0.52	0.37	0.63	0.78	1.65
			0.30	0.17	0.09	0.10	0.07	0.07	0.12	0.11	0.16
p,π^+		0.80	0.48	0.29	0.13	0.05	0.02	0.01			
		0.13	0.04	0.03	0.01	0.01	0.00	0.01			
p,K^+			0.06	0.04	0.04	0.02					
			0.04	0.02	0.01	0.01					
p,p		0.82	1.29	1.47	1.50	1.35	1.01	1.06	1.00	1.15	2.02
		0.14	0.07	0.07	0.05	0.06	0.03	0.03	0.03	0.04	0.05
π^-,π^-		0.95	0.88	0.63	0.53	0.44	0.47			0.76	
		0.07	0.03	0.02	0.02	0.02	0.01			0.03	
π^-,K^-		0.13	0.08	0.05	0.06	0.05	0.03			0.01	
		0.03	0.01	0.01	0.01	0.01	0.01			0.00	

TABLE XV. (*Continued.*)

(f) 100 GeV/c p_T=0.750 GeV/c (*continued*)

	x	0.300	0.400	0.500	0.600	0.700	0.800	0.840	0.880	0.920	0.960
$\pi^-,\bar{p}$		0.07	0.06	0.05	0.04	0.02	0.01				
		0.03	0.01	0.01	0.01	0.00	0.00				
K^-,π^-		0.41	0.39	0.21	0.14	0.12					
		0.31	0.12	0.08	0.08	0.06					
K^-,K^-		0.74	0.46	0.41	0.52	0.26	0.35			0.38	
		0.53	0.16	0.10	0.12	0.09	0.08			0.10	
$\bar{p},\pi^-$		0.88	0.61	0.45	0.12	0.13					
		0.53	0.19	0.12	0.10	0.13					
$\bar{p},\bar{p}$		1.05	1.07	1.28	1.33	1.46	0.68			0.75	
		0.58	0.22	0.20	0.19	0.18	0.13			0.15	

(h) 175 GeV/c p_T=0.150 GeV/c

	x	0.120	0.200	0.300
π^+,π^+		15.08	11.77	8.60
		1.85	0.85	0.37
π^+,K^+		2.10	1.02	0.70
		1.05	0.33	0.15
π^+,p		1.01	1.12	0.82
		0.54	0.29	0.14
K^+,π^+		16.19	4.89	4.58
		5.35	3.56	1.17
K^+,K^+		10.87	3.49	3.70
		9.69	2.28	0.80
p,π^+		22.69	17.02	10.39
		1.32	0.81	0.21
p,K^+		1.22	1.45	0.77
		0.53	0.36	0.08
p,p		2.97	4.34	6.81
		0.51	0.42	0.17
π^-,π^-		16.14	11.50	7.45
		1.35	0.55	0.22
π^-,K^-		1.02	0.99	0.55
		0.53	0.21	0.09
$\pi^-,\bar{p}$		0.81	0.60	0.41
		0.33	0.14	0.06
K^-,π^-			6.52	8.84
			3.69	1.50
K^-,K^-			3.18	6.28
			2.03	1.36
$\bar{p},\pi^-$		64.96	32.35	12.25
		23.04	7.69	2.37
$\bar{p},\bar{p}$			6.68	5.14
			3.88	1.95

(i) 175 GeV/c p_T=0.200 GeV/c

	0.400	0.500	0.600	0.700
π^+,π^-	2.55	1.83	1.47	1.37
	0.17	0.13	0.08	0.07
π^+,K^-	0.29		0.12	0.10
	0.07		0.03	0.02
$\pi^+,\bar{p}$	0.15	0.11	0.08	0.02
	0.05	0.03	0.02	0.01
K^+,π^-	1.28	1.13	1.19	0.58
	0.66	0.45	0.23	0.16
p,π^-	1.76	0.91	0.31	0.09
	0.08	0.05	0.02	0.01
p,K^-	0.10		0.02	
	0.02		0.00	
$p,\bar{p}$		0.01		
		0.01		

(j) 175 GeV/c p_T=0.300 GeV/c

	x	0.120	0.200	0.300	0.400	0.500	0.600
π^+,π^+		13.00	9.68	6.22	4.96	4.54	3.86
		1.15	0.47	0.29	0.16	0.16	0.13
π^+,K^+		1.05	0.98	0.63	0.49	0.27	0.28
		0.82	0.24	0.11	0.06	0.05	0.04
π^+,p		0.74	0.85	0.61	0.42	0.34	0.28
		0.44	0.17	0.10	0.05	0.04	0.03

TABLE XV. (*Continued.*)

(j) 175 GeV/c p_T=0.300 GeV/c (*continued*)

	x	0.120	0.200	0.300	0.400	0.500	0.600
K^+,π^+		8.31	4.42	3.41	2.33	2.25	1.60
		4.23	1.29	0.85	0.38	0.44	0.41
K^+,K^+			3.30	4.01	2.44	1.81	1.97
			1.76	0.84	0.38	0.36	0.31
p,π^+		13.33	9.94	5.11	2.91	1.65	0.96
		0.75	0.35	0.16	0.06	0.05	0.06
p,K^+		1.24	1.33	0.54	0.39	0.23	0.10
		0.50	0.21	0.07	0.03	0.03	0.03
p,p		2.15	3.19	5.24	6.66	7.77	9.39
		0.32	0.21	0.16	0.09	0.10	0.18
π^-,π^-		11.80	9.63	6.20	4.69	4.09	3.89
		0.69	0.27	0.12	0.10	0.09	0.07
π^-,K^-		0.55	0.72	0.61	0.43	0.29	0.28
		0.21	0.10	0.06	0.04	0.03	0.02
$\pi^-,\bar{p}$		0.65	0.48	0.42	0.33	0.17	0.11
		0.20	0.07	0.03	0.03	0.02	0.01
K^-,π^-		11.35	7.61	3.85	3.30	1.25	1.45
		3.51	1.26	0.57	0.48	0.39	0.31
K^-,K^-			3.27	3.00	2.62	1.50	1.98
			1.22	0.62	0.46	0.32	0.24
$\bar{p},\pi^-$			10.85	5.12	2.19	1.78	0.68
			2.56	0.95	0.69	0.37	0.25
$\bar{p},\bar{p}$				5.17	6.04	6.21	9.44
				1.01	0.99	0.76	0.80
π^+,π^-		9.80	7.02	3.86	1.87	1.17	0.83
		0.76	0.43	0.22	0.11	0.08	0.05
π^+,K^-		1.06	0.66	0.29	0.17	0.13	0.10
		0.57	0.23	0.09	0.05	0.03	0.02
$\pi^+,\bar{p}$		0.59	0.39	0.25	0.17	0.10	0.04
		0.22	0.13	0.07	0.04	0.02	0.01
K^+,π^-		7.63	2.83	2.72	1.52	0.74	0.46
		2.48	1.27	0.70	0.27	0.19	0.13
p,π^-		10.79	5.29	2.40	1.22	0.63	0.26
		0.55	0.24	0.11	0.03	0.02	0.01
p,K^-		1.28	0.48	0.24	0.09	0.04	0.01
		0.36	0.11	0.04	0.01	0.01	0.00
$p,\bar{p}$		0.36	0.19	0.10	0.02	0.00	
		0.10	0.06	0.02	0.01	0.00	
π^-,π^+		8.25	6.44	3.21	1.93	1.09	0.91
		0.59	0.25	0.10	0.07	0.06	0.03
π^-,K^+		0.73	0.78	0.54	0.36	0.18	0.10
		0.25	0.13	0.06	0.04	0.03	0.01
π^-,p		0.57	0.57	0.37	0.24	0.15	0.07
		0.22	0.09	0.04	0.02	0.02	0.01
K^-,π^+		11.24	4.54	2.62	1.00	0.61	0.43
		3.46	1.20	0.60	0.33	0.22	0.15
$\bar{p},\pi^+$			5.45	3.17	1.54	0.47	0.47
			2.62	0.95	0.48	0.35	0.15

(k) 175 GeV/c p_T=0.400 GeV/c

	x	0.300	0.500	0.600		0.300	0.500	0.600
π^+,π^-		2.78	0.89	0.54	p,π^-	1.69	0.42	0.17
		0.18	0.06	0.05		0.09	0.01	0.01

TABLE XV. (*Continued.*)

(k) 175 GeV/c p_T=0.400 GeV/c (*continued*)

x	0.300	0.500	0.600		0.300	0.500	0.600
π^+K^-	0.36	0.14	0.14	p,K^-	0.19	0.03	0.01
	0.10	0.03	0.02		0.03	0.00	0.00
$\pi^+,\bar{p}$	0.31	0.08	0.03	$p,\bar{p}$	0.05	0.00	
	0.07	0.02	0.01		0.02	0.00	
K^+,π^-	1.50	0.70	0.34				
	0.71	0.15	0.08				

(l) 175 GeV/c p_T=0.500 GeV/c

x	0.200	0.300	0.400	0.500	0.600	0.700	0.800	0.880	0.895	0.920	0.940
π^+,π^+	5.44	3.70	2.50	1.81	1.53	1.41	1.54		2.10		3.70
	0.37	0.18	0.11	0.07	0.07	0.04	0.05		0.03		0.04
π^+,K^+	0.38	0.39	0.30	0.18	0.19	0.14	0.10		0.08		0.09
	0.22	0.08	0.04	0.03	0.03	0.01	0.02		0.01		0.01
π^+,p	0.30	0.32	0.34	0.25	0.18	0.11	0.08				
	0.14	0.06	0.04	0.03	0.02	0.01	0.01				
K^+,π^+	2.74	2.08	1.23	0.63	0.45	0.23	0.28				
	1.41	0.60	0.22	0.16	0.12	0.08	0.08				
K^+,K^+		1.33	1.39	1.18	1.14	0.92	0.91		1.49		2.97
		0.69	0.26	0.21	0.18	0.12	0.17		0.11		0.19
p,π^+	4.44	2.45	1.40	0.72	0.35	0.14	0.03				
	0.22	0.09	0.04	0.02	0.02	0.01	0.01				
p,K^+	0.72	0.32	0.26	0.15	0.08	0.03	0.01				
	0.14	0.04	0.02	0.02	0.01	0.01	0.00				
p,p	1.58	2.86	3.79	4.21	4.26	4.16	3.93		4.55		7.46
	0.15	0.10	0.06	0.05	0.07	0.04	0.05		0.05		0.08
π^-,π^-	5.10	3.45	2.59	1.60	1.41	1.42	1.48	1.99		2.59	
	0.29	0.07	0.07	0.06	0.04	0.02	0.02	0.03		0.04	
π^-,K^-	0.43	0.33	0.18	0.13	0.14	0.11	0.08	0.07		0.06	
	0.13	0.04	0.02	0.02	0.02	0.01	0.01	0.01		0.01	
$\pi^-,\bar{p}$	0.22	0.29	0.22	0.12	0.08	0.06	0.01				
	0.08	0.02	0.02	0.02	0.01	0.00	0.00				
K^-,π^-	3.90	2.21	1.71	0.67	0.45	0.38	0.18				
	1.72	0.40	0.36	0.22	0.13	0.06	0.06				
K^-,K^-		1.68	2.09	1.26	0.95	0.97	1.02	01.15		1.88	
		0.45	0.38	0.32	0.17	0.08	0.09	0.14		0.16	
$\bar{p},\pi^-$	5.20	3.16	1.14	0.72	0.39	0.12	0.09				
	3.89	0.65	0.48	0.37	0.21	0.07	0.05				
$\bar{p},\bar{p}$		1.46	3.56	4.03	4.05	3.51	3.72	4.41		5.02	
		0.70	0.71	0.87	0.54	0.23	0.22	0.34		0.37	
π^+,π^-	2.70	1.85	1.12	0.57	0.41	0.24					
	0.21	0.15	0.10	0.07	0.04	0.02					
π^+,K^-	0.39	0.29	0.18	0.12	0.09	0.04					
	0.12	0.08	0.04	0.03	0.02	0.01					
$\pi^+,\bar{p}$	0.28	0.18	0.14	0.06	0.02	0.01					
	0.08	0.08	0.04	0.02	0.01	0.01					
K^+,π^-	2.07	2.05	0.85	0.42	0.12	0.10					
	0.67	0.79	0.22	0.16	0.09	0.04					
p,π^-	2.72	1.28	0.67	0.29	0.12	0.03					
	0.12	0.08	0.02	0.02	0.01	0.01					
p,K^-	0.21	0.09	0.04	0.02	0.01						
	0.05	0.03	0.01	0.01	0.00						
$p,\bar{p}$	0.13	0.04	0.01	0.01							
	0.03	0.02	0.00	0.00							

TABLE XV. (*Continued.*)

(m) 175 GeV/c p_T=0.625 GeV/c

x	0.300	0.400	0.500	0.600	0.700
π^+,π^-	0.78	0.58	0.37	0.26	0.13
	0.08	0.07	0.05	0.03	0.02
π^+,K^-	0.16	0.11	0.07	0.05	0.03
	0.05	0.04	0.03	0.01	0.01
$\pi^+,\bar{p}$	0.08	0.07	0.05	0.02	0.01
	0.03	0.05	0.02	0.01	0.01
K^+,π^-	0.87	0.45	0.25	0.08	0.14
	0.48	0.30	0.14	0.05	0.09
p,π^-	0.81	0.43	0.19	0.08	0.02
	0.04	0.03	0.01	0.01	0.01
p,K^-	0.05	0.05	0.01	0.00	
	0.02	0.01	0.00	0.00	
$p,\bar{p}$	0.03		0.01		
	0.01		0.00		

(o) 175 GeV/c p_T=1.000 GeV/c

	0.600	0.895	0.940
π^+,π^+	0.13	0.16	0.35
	0.01	0.01	0.01
π^+,K^+	0.02	0.01	0.00
	0.01	0.00	0.00
π^+,p	0.02		
	0.01		
K^+,π^+	0.05		
	0.04		
K^+,K^+	0.11	0.19	0.33
	0.05	0.07	0.06
p,π^+	0.03		
	0.00		
p,K^+	0.01		
	0.00		
p,p	0.32	0.21	0.30
	0.01	0.00	0.01

(n) 175 GeV/c p_T=0.750 GeV/c

x	0.300	0.400	0.500	0.600	0.700	0.800	0.895	0.920	0.940
π^+,π^+	1.21	0.93	0.73	0.55	0.46	0.43	0.58		1.27
	0.07	0.06	0.04	0.02	0.02	0.02	0.02		0.03
π^+,K^+	0.17	0.08	0.11	0.08	0.05	0.03	0.03		0.02
	0.04	0.03	0.02	0.01	0.01	0.01	0.00		0.01
π^+,p	0.18	0.15	0.08	0.09	0.05	0.02			
	0.03	0.03	0.01	0.01	0.01	0.00			
K^+,π^+	0.68	0.59	0.32	0.17	0.08	0.05			
	0.23	0.17	0.09	0.04	0.04	0.03			
K^+,K^+	0.45	0.61	0.47	0.30	0.31	0.27	0.60		1.26
	0.27	0.20	0.10	0.06	0.07	0.05	0.06		0.14
p,π^+	0.83	0.52	0.29	0.13	0.04	0.01			
	0.03	0.02	0.01	0.00	0.00	0.00			
p,K^+	0.12	0.08	0.05	0.03	0.01	0.01			
	0.02	0.01	0.01	0.00	0.00	0.00			
p,p	0.99	1.36	1.59	1.50	1.29	1.00	1.01		1.67
	0.04	0.03	0.02	0.01	0.02	0.02	0.01		0.03
π^-,π^-	1.14	0.98	0.66	0.43	0.42	0.40		0.73	
	0.04	0.04	0.03	0.03	0.02	0.01		0.02	
π^-,K^-	0.12	0.10	0.06	0.07	0.03	0.02		0.02	
	0.02	0.02	0.01	0.01	0.01	0.00		0.00	
$\pi^-,\bar{p}$	0.12	0.10	0.05	0.03	0.02	0.01			
	0.01	0.01	0.01	0.01	0.00	0.00			
K^-,π^-	0.63		0.13	0.25	0.08	0.05			
	0.22		0.12	0.13	0.05	0.05			
K^-,K^-	0.55	0.54	0.43	0.48	0.25	0.46		0.34	
	0.29	0.23	0.18	0.17	0.09	0.08		0.08	
$\bar{p},\pi^-$	0.68	0.57	0.72						
	0.51	0.43	0.30						
$\bar{p},\bar{p}$	0.74	1.36	1.86	1.08	1.19	0.90		1.05	
	0.47	0.47	0.40	0.51	0.26	0.18		0.18	

p_T sweeps, paralleling in part the data acquisition procedure.

A. Feynman-x dependence

The dependence of the inclusive cross sections on x was investigated[3] for several different values of p_T. In Fig. 11, the x dependence of the data at 100 GeV/c incident momentum is displayed at $p_T=0.3$ GeV/c, for the various incident-particle types. In each case, there is a rather flat cross section with a diffractive peak near $x=1$ for the leading-particle channel, $a+p\rightarrow a+X$. The five other channels, with the outgoing particle different from the incoming one, show a decrease in cross section with increasing x. The falloff tends to be steepest for those channels with the greatest change in quantum numbers between incoming and outgoing particles. The solid curves shown for the nonleading channels are fits to a $(1-x)^n$ parametrization which are discussed below.

Figure 12 shows the same reactions, but for a larger value of the transverse momentum, $p_T=0.75$ GeV/c. The data are very similar in shape to those in Fig. 11, but reduced in magnitude. In fact, separate fits to the form $(1-x)^n$ for the two different values of p_T yield values of n which are consistent within errors. The major difference at larger p_T is a relatively smaller leading-particle peak near $x=1$.

The 175-GeV/c incident-momentum data for $p_T=0.3$ GeV/c are shown in Fig. 13. Within errors, these data are equivalent to those in Fig. 11 from 100 GeV/c, demonstrating Feynman scaling for all the reaction channels at these energies.

All of the x "sweeps" at constant p_T for nonleading reaction channels have been fitted to the functional form $C(1-x)^n$. Here C is a different

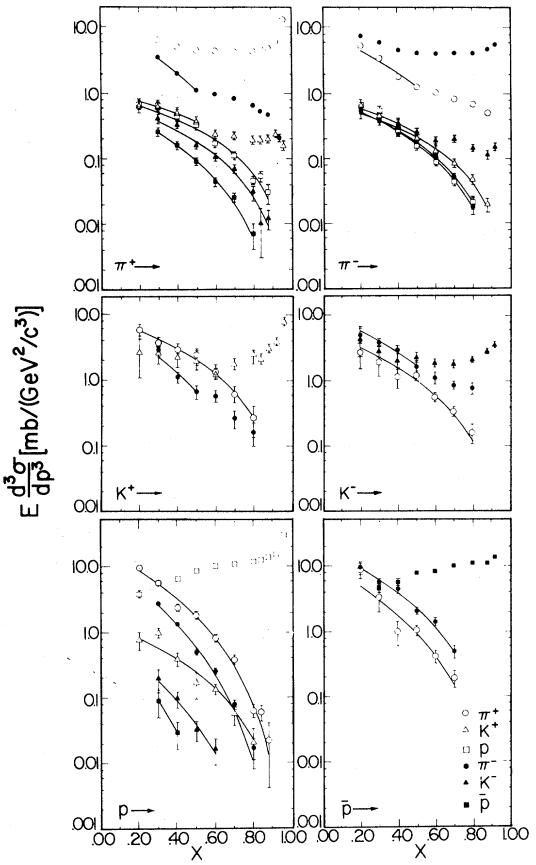

FIG. 11. The invariant differential cross section is shown as a function of x, for an incident energy of 100 GeV and a transverse momentum p_T of 0.3 GeV/c. There is one subfigure for each incident-particle type. Only those data are plotted for which the error was smaller than the value of the cross section. Comparisons to a functional form $C(1-x)^n$ are shown.

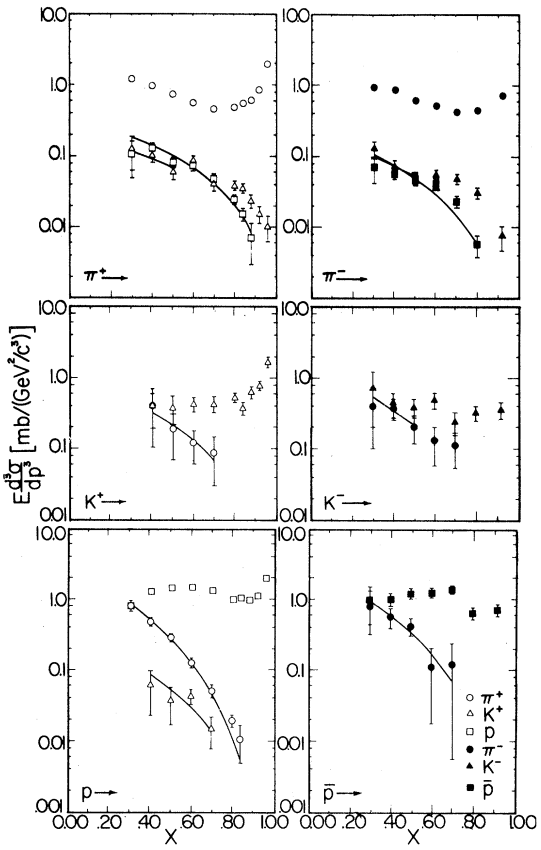

FIG. 12. The invariant differential cross section is shown as a function of x, for an incident energy of 100 GeV and a transverse momentum p_T of 0.75 GeV/c. There is one subfigure for each incident-particle type. Comparisons to a functional form $C(1-x)^n$ are shown.

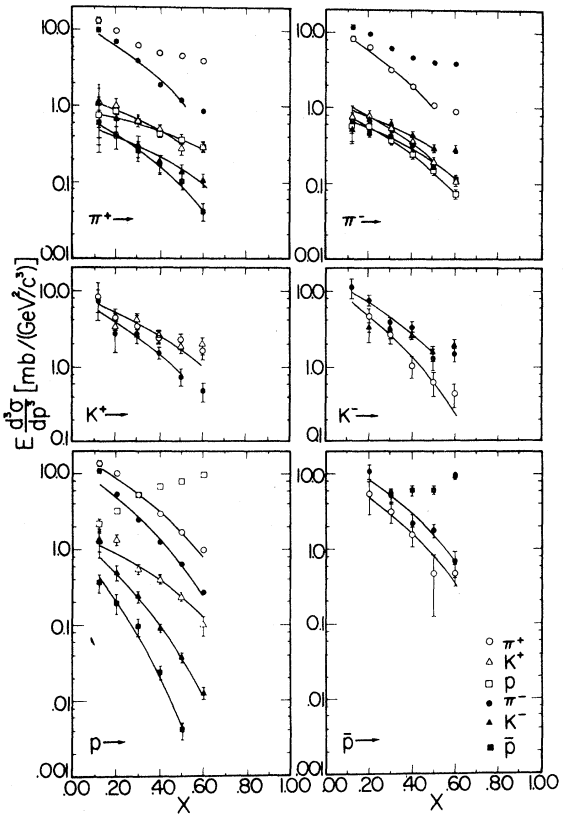

FIG. 13. The invariant differential cross section is shown as a function of x, for an incident energy of 175 GeV and a transverse momentum p_T of 0.3 GeV/c. There is one subfigure for each incident-particle type. Comparisons to a functional form $C(1-x)^n$ are shown.

parameter for each sweep, but the same parameter n is used for all sweeps for a given reaction at a given beam momentum. The results of these fits are given in Table XVI and are shown as the solid curves in Figs. 11–13. In general, this form gives an adequate representation of the data between $0.2<x<0.7$. However, in a few cases noted in the table, the x range of the fit has been limited to avoid contamination from resonance decay products at large x. The exponents n of these fits have been previously related[3] to the quark-parton picture via the quark-counting rules of Brodsky and Gunion.[31]

Since these previous publications, the counting rules have been modified[32] to accommodate the two-particle fragmentation correlation data,[33] which indicated the dominance of gluon rather than quark-exchange graphs. The new general rule is

$$\frac{d\sigma}{dx}\underset{x\to 1}{\approx}(1-x)^{2n_h+n_{PL}-1}, \tag{6}$$

where n_h is the number of quark spectators in the incident hadron not participating in the gluon exchange and n_{PL} is the number of spectators participating in the gluon exchange. The data of Table XVI are compared with these predictions in Fig. 14. Reference 32 contains a more complete comparison of all available fragmentation data with the counting-rule phenomenology. It is to be noted, in addition, that many other processes can occur, specifically, forward resonance production and subsequent decay which may limit the useful kinematic range for the application of this phenomenology. Such behavior has previously been seen[34] at the CERN ISR where the channels $pp\to\pi^{\pm}X$ and $pp\to K^+X$ required a two-component fit in $(1-x)^n$ and where the component dominant at high x was consistent with a single-baryon-exchange-trajectory triple-Regge fit.

B. Transverse-momentum dependence

Figures 15 and 16 show the p_T dependence at several different values of x for reactions with incident 100 GeV/c π^+ and π^-, respectively. It can be seen that the corresponding π^+ and π^- induced reactions have essentially equal cross sections. Figure 17 displays the p_T dependence of reactions with incoming protons at 100 GeV/c.

The functional form of the p_T dependence could be determined at those values of x where detailed p_T sweeps were taken. In general, the data were sufficiently precise to allow discrimination between exponential and Gaussian behavior. However, in most cases, a generalization to the functional form $\exp(-Bp_T{}^n)$, where n is variable could not be justified.

Individual fits to the p_T dependence of each reaction at each x value were made. The resulting χ^2 values indicated a clear separation into regions of Gaussian and exponential transverse-momentum behavior. The reactions in which both the incoming and outgoing particles are mesons show Gaussian behavior for $x\lesssim 0.4$ and exponential behavior at higher x. This is also true for $p\to p$ and $\bar{p}\to\bar{p}$ where the transition in functional form is at a slightly higher value of x. Channels with an incoming proton and an outgoing meson show exponential behavior in p_T over the entire x range where fits could be made. The two channels $\pi^+\to p$ and $\pi^-\to\bar{p}$ show Gaussian transverse-momentum dependence over the entire x range observed. Finally, the two charge exchange channels $\pi^+\to\bar{p}$ and $\pi^-\to p$ had statistics which were inadequate to allow a determination of the func-

TABLE XVI. The differential cross section at several values of p_T and the integrated cross section are fit to the functional form $C(1-x)^n$. The coefficient C is a function of p_T, while the exponent n is constrained to be independent of p_T. The full x range at which data were taken is used for all reactions except those indicated by an asterisk. In those cases, values of x only up to 0.5 are used. Units for $C(p_T)$ are mb/(GeV$^2/c^3$), while units for C_{int} are mb.

	n	$C(0.3)$	$C(0.5)$	$C(0.625)$	$C(0.75)$	C_{int}
			100 GeV/c			
$\pi^+ \to K^+$	1.55±0.40*	1.07±0.10	0.62±0.06		0.20±0.03	1.49±0.06
$\pi^+ \to p$	1.73±0.06	0.94±0.05	0.71±0.03		0.33±0.02	1.69±0.04
$\pi^+ \to \pi^-$	3.37±0.09*	11.47±0.25	6.45±0.25			12.80±0.14
$\pi^+ \to K^-$	2.10±0.12	0.78±0.05	0.40±0.06			1.12±0.04
$\pi^+ \to \bar{p}$	2.98±0.18	0.74±0.05	0.44±0.07			
$K^+ \to \pi^+$	2.16±0.19	9.03±0.69	3.82±0.41		0.97±0.28	9.73±0.44
$K^+ \to \pi^-$	2.29±0.25	4.17±0.39	1.74±0.47			4.91±0.26
$p \to \pi^+$	3.39±0.05	18.09±0.44	7.52±0.23		2.91±0.14	23.18±0.28
$p \to K^+$	2.56±0.20	1.41±0.14	0.82±0.09		0.32±0.06	2.56±0.14
$p \to \pi^-$	4.39±0.10	12.17±0.40	5.98±0.40	3.59±0.33		18.57±0.32
$p \to K^-$	4.59±0.92	0.92±0.16				
$\pi^- \to \pi^+$	2.65±0.11*	8.08±0.19	3.90±0.13	2.18±0.14		8.87±0.13
$\pi^- \to K^+$	1.76±0.10	0.72±0.04	0.41±0.03	0.21±0.04		1.08±0.04
$\pi^- \to p$	2.43±0.11	0.89±0.04	0.52±0.04	0.36±0.05		
$\pi^- \to K^-$	1.84±0.30*	0.88±0.06	0.53±0.04		0.19±0.02	1.26±0.04
$\pi^- \to \bar{p}$	2.29±0.08	0.86±0.03	0.62±0.03		0.25±0.02	1.34±0.03
$K^- \to \pi^+$	2.31±0.25	5.27±0.45	2.39±0.37			6.19±0.41
$K^- \to \pi^-$	2.58±0.37*	10.19±0.78	4.97±0.59		1.32±0.30	11.27±0.50
$\bar{p} \to \pi^+$	3.56±0.43	10.72±1.22	5.84±1.43			18.0 ±1.8
$\bar{p} \to \pi^-$	3.00±0.19	17.7 ±1.1	6.3±0.9		2.95±0.50	21.81±0.93
			175 GeV/c			
$\pi^+ \to K^+$	2.11±0.38*	1.37±0.11	0.83±0.07		0.37±0.05	2.01±0.08
$\pi^+ \to p$	1.36±0.09	0.92±0.06	0.62±0.03		0.26±0.02	1.33±0.04
$\pi^+ \to \pi^-$	3.56±0.12*	13.48±0.38	6.44±0.28	3.17±0.22		13.88±0.22
$\pi^+ \to K^-$	2.07±0.20	0.61±0.07	0.53±0.05	0.32±0.05		1.04±0.05
$\pi^+ \to \bar{p}$	3.28±0.25	0.87±0.10	0.57±0.09	0.33±0.08		
$K^+ \to \pi^+$	2.37±0.25	8.77±0.85	4.02±0.43		1.65±0.22	11.06±0.53
$K^+ \to \pi^-$	2.84±0.31	6.34±0.69	3.23±0.50	1.64±0.49		8.21±0.46
$p \to \pi^+$	3.50±0.03	18.49±0.25	8.54±0.14		3.15±0.05	24.7 ±0.2
$p \to K^+$	2.77±0.10	1.59±0.09	1.00±0.05		0.33±0.02	2.38±0.06
$p \to \pi^-$	4.36±0.05	12.50±0.18	6.36±0.14	3.96±0.13		16.77±0.14
$p \to K^-$	5.48±0.24	1.60±0.10	0.67±0.08	0.43±0.07		2.21±0.09
$p \to \bar{p}$	8.03±0.44	1.19±0.14	0.71±0.12	0.58±0.21		1.70±0.12
$\pi^- \to \pi^+$	3.75±0.13*	13.25±0.24				
$\pi^- \to K^+$	2.85±0.22	1.44±0.08				
$\pi^- \to p$	2.87±0.22	1.04±0.05				
$\pi^- \to K^-$	2.06±0.25*	1.20±0.06	0.58±0.04		0.26±0.03	1.52±0.04
$\pi^- \to \bar{p}$	2.21±0.07	0.88±0.04	0.64±0.02		0.27±0.02	1.37±0.03
$K^- \to \pi^+$	4.33±0.77	12.3 ±1.5				
$K^- \to \pi^-$	3.32±0.45*	14.7 ±1.2	7.7 ±0.9		1.85±0.62	16.96±0.86
$\bar{p} \to \pi^+$	3.72±0.87	10.9 ±1.8				
$\bar{p} \to \pi^-$	3.59±0.37	18.9 ±2.0	9.8 ±1.5		3.7 ±1.4	28.8 ±1.9

tional form.

The fits also indicated that all channels have an average transverse momentum squared which is typically between 0.25 and 0.30 (GeV/c)^2. The only exceptions are the baryon-induced leading-particle channels at high x, namely, $p \to p$ and $\bar{p} \to \bar{p}$. Here the average transverse momentum squared shrinks to about 0.15 (GeV/c)^2.

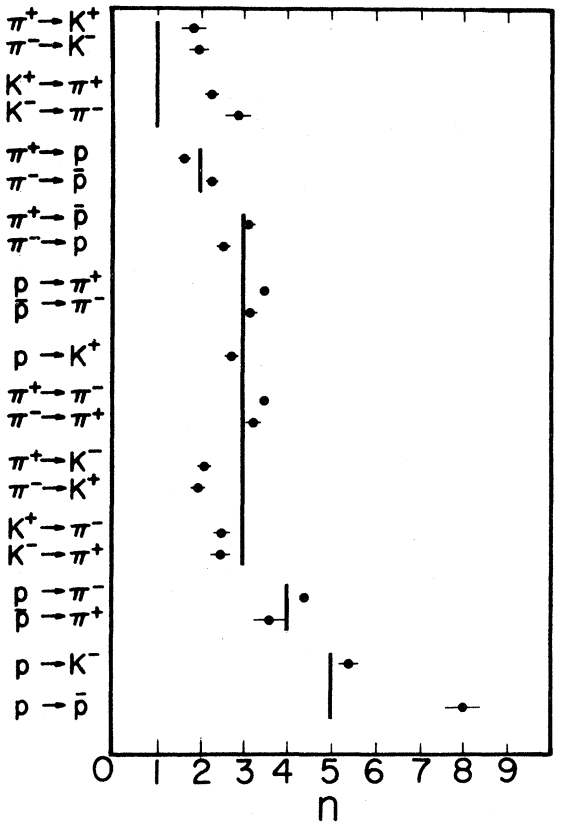

FIG. 14. The fitted exponent n for the differential cross sections fitted to the form $x\,d\sigma/dx = C(1-x)^n$. The plotted value of n represents the average for 100- and 175-GeV data runs. The vertical bars represent the values predicted by quark counting rules; see Ref. 32.

C. p_T-integrated cross sections

The determination of the functional form of the transverse momentum dependence of the invariant cross section allows computation of the integrated cross section

$$x\frac{d\sigma}{dx} = E\frac{d\sigma}{dp_l} = 2\pi \int_0^\infty E\frac{d^3\sigma}{dp^3} p_T dp_T \ . \tag{7}$$

In the x region where exponential p_T behavior was observed the functional form used was

$$E\frac{d^3\sigma}{dp^3} = \frac{A}{2\pi B^2} e^{-Bp_T} \ . \tag{8}$$

In the x region where behavior was Gaussian in p_T the form used was

$$E\frac{d^3\sigma}{dp^3} = \frac{A}{\pi B} e^{-Bp_T{}^2} \ . \tag{9}$$

The powers of B in the denominators normalize

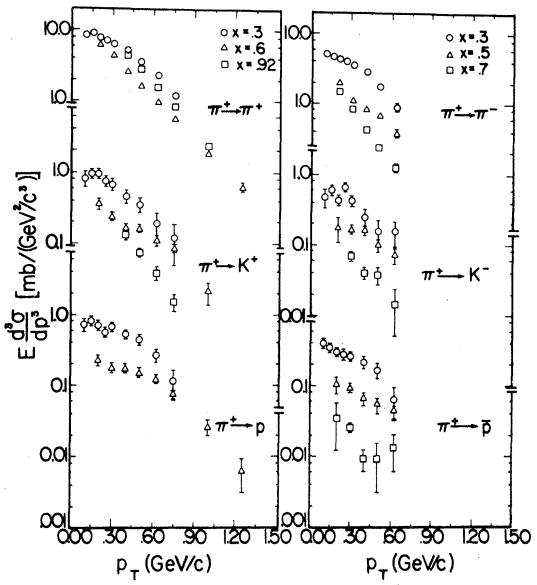

FIG. 15. The invariant differential cross section for π^+-induced reactions is shown as a function of transverse momentum p_T. The incident energy is 100 GeV. The values of x for which the transverse-momentum dependence is shown are those at which the most thorough p_T sweeps were made.

the functional forms of the differential cross sections so that the integrated cross section is A for both functional forms. Since the data were centered around the average value of the transverse momentum, $p_T \simeq 0.5$ GeV/c, the fitted parameters

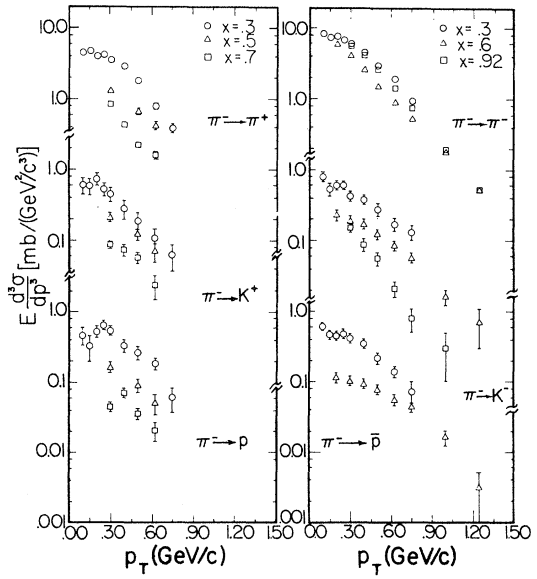

FIG. 16. The invariant differential cross section for π^--induced reactions is shown as a function of transverse momentum p_T. The incident energy is 100 GeV.

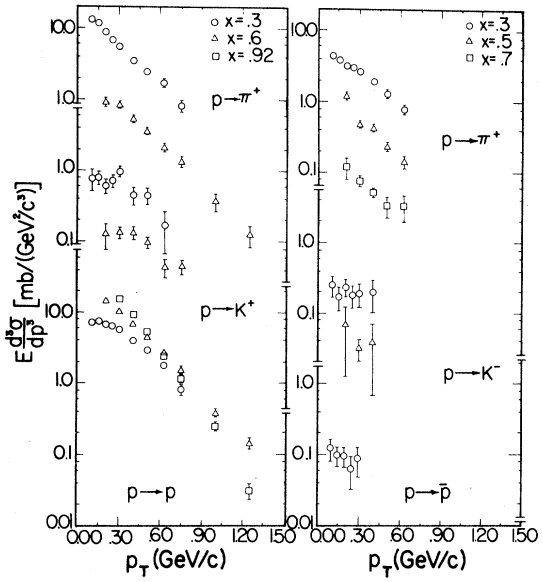

FIG. 17. The invariant differential cross section for proton-induced reactions is shown as a function of transverse momentum p_T. The incident energy is 100 GeV.

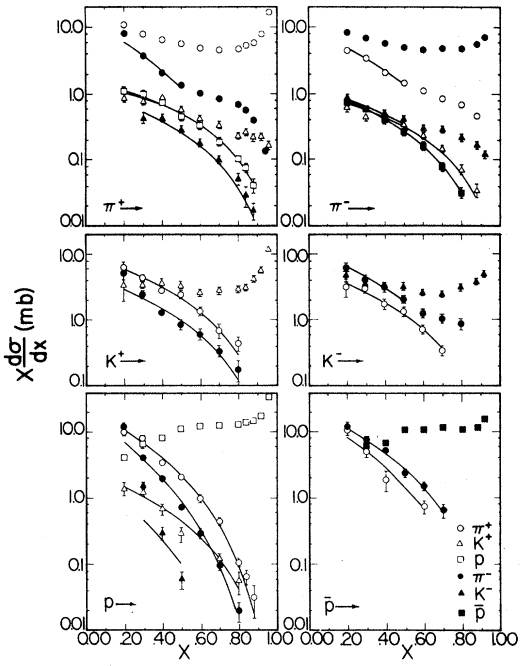

FIG. 18. The single differential cross section $x\,d\sigma/dx$ is shown as a function of x. It is obtained by integrating the invariant cross section over transverse momentum. The incident energy is 100 GeV. There is one subfigure for each incident-particle type.

A and B were essentially uncorrelated.

A global fit was made for each reaction in those regions where the cross section showed a particular functional form. Thus, for reactions with both Gaussian and exponential regions, two fits were made. If, within a given region, there existed two or more values of x at which a detailed p_T sweep was made, the value of B was allowed to vary linearly with x in that region. Thus, the p_T dependence from the detailed sweep could be used to interpolate the B values at other points. Reactions which supplied enough data to allow a linear variation of B with x were the leading-particle channels and $\pi^+ \rightarrow K^+$ in the higher-x region, and proton$\rightarrow$ meson$^{\pm}$ for all x. For other channels, B was taken to be a constant, independent of x.

The coefficients A were then obtained separately for each value of x. The integrals and their errors are listed in Table XVII and are shown in Figs. 18 and 19 at 100 and 175 GeV/c, respectively. The curves shown have the functional form $C(1-x)^n$. The value of n used is that obtained in the global fit of the differential cross sections. The value of C was detemined by a one-parameter fit to the integrated cross sections. For a given reaction, the fit was made over the same x range as was the global fit to the differential cross sections. The parameter C for the integrated cross sections is also shown in Table XVI for all cases where the

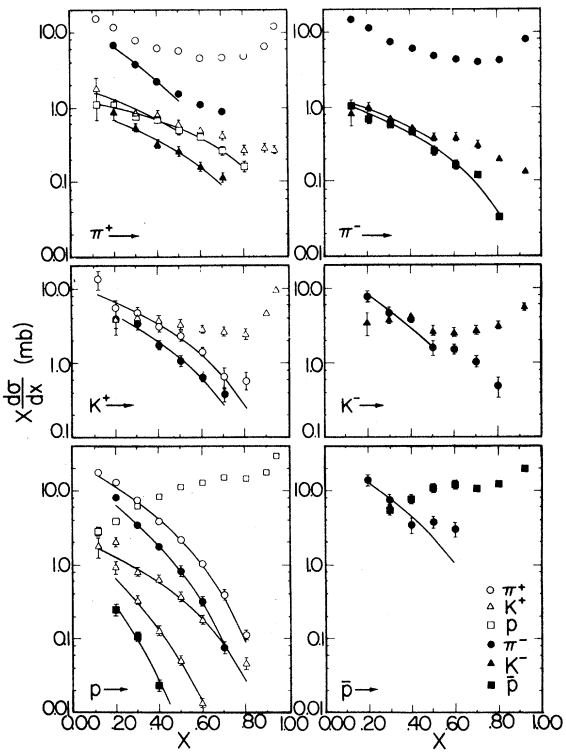

FIG. 19. The integrated cross section $x\,d\sigma/dx$ as a function of x for incident energy of 175 GeV.

TABLE XVII. Cross sections $x\,d\sigma/dx$ in millibarns integrated over p_T. The errors shown below each entry include both statistical and estimated systematic errors in quadrature. In addition, there is an overall 7% absolute normalization uncertainty. The notation for reactions is $a,c \equiv a+p \to c+X$.

						100 GeV/c					
x	0.200	0.300	0.400	0.500	0.600	0.700	0.800	0.840	0.880	0.920	0.940	0.960
π^+,π^+	10.91	7.91	6.56	5.71	4.89	4.64	4.79	5.39	5.92	7.87		16.97
	0.24	0.10	0.11	0.12	0.05	0.08	0.05	0.07	0.08	0.08		0.15
π^+,K^+	0.89	0.79	0.80	0.58	0.42	0.33	0.23	0.26	0.22	0.23		0.17
	0.13	0.05	0.06	0.06	0.02	0.03	0.01	0.02	0.02	0.02		0.02
π^+,p	1.11	0.99	0.74	0.46	0.34	0.19	0.11	0.08	0.04			
	0.12	0.05	0.05	0.03	0.01	0.01	0.01	0.01	0.01			
K^+,π^+	6.38	4.40	2.87	2.48	1.37	0.69	0.45					
	0.72	0.33	0.35	0.38	0.15	0.17	0.11					
K^+,K^+	3.44	3.49	3.65	3.29	2.61	2.82	3.00	3.14	4.29	5.73		11.73
	1.45	0.41	0.53	0.52	0.22	0.27	0.19	0.25	0.32	0.30		0.62
p,π^+	10.83	7.32	3.42	2.06	0.98	0.44	0.11	0.06	0.03			
	0.30	0.13	0.16	0.10	0.03	0.03	0.01	0.02	0.02			
p,K^+	1.37	1.20	0.68	0.29	0.26	0.12	0.05					
	0.28	0.11	0.12	0.07	0.02	0.02	0.02					
p,p	4.09	6.56	8.20	11.15	12.23	12.47	12.86	13.87	14.66	17.18		32.93
	0.22	0.13	0.23	0.26	0.13	0.18	0.13	0.17	0.20	0.18		0.32
π^-,π^-	8.48	7.00	5.82	5.09	4.72	4.94	4.87		5.73	7.26		
	0.25	0.07	0.07	0.07	0.05	0.05	0.06		0.08	0.07		
π^-,K^-	0.84	0.63	0.50	0.38	0.31	0.30	0.22		0.17	0.12		
	0.14	0.03	0.03	0.03	0.02	0.02	0.02		0.02	0.01		
$\pi^-,\bar{p}$	0.73	0.60	0.43	0.27	0.17	0.08	0.03					
	0.09	0.02	0.03	0.02	0.01	0.01	0.01					
K^-,π^-	6.35	4.19	3.26	2.08	1.26	1.05	0.88					
	0.89	0.27	0.26	0.25	0.18	0.15	0.17					
K^-,K^-	5.65	3.46	3.47	3.18	2.63	2.44	3.10		3.83	5.02		
	1.76	0.34	0.36	0.32	0.22	0.23	0.28		0.33	0.29		
$\bar{p},\pi^-$	11.60	7.39	5.17	2.37	1.49	0.65						
	1.88	0.43	0.59	0.31	0.18	0.14						
$\bar{p},\bar{p}$		6.16	6.84	10.77	10.73	11.69	10.85		11.52	15.49		
		0.42	0.62	0.59	0.42	0.46	0.58		0.53	0.51		
π^+,π^-	8.11	3.77	2.14	1.37	1.02	0.85	0.69	0.57	0.40		0.14	
	0.36	0.06	0.05	0.03	0.03	0.02	0.02	0.02	0.02		0.01	
π^+,K^-		0.43	0.43	0.29	0.18	0.10	0.05	0.03	0.02			
		0.03	0.04	0.02	0.02	0.01	0.01	0.01	0.00			
K^+,π^-	5.44	2.45	1.31	0.86	0.62	0.34	0.18					
	1.29	0.20	0.14	0.13	0.10	0.06	0.07					
p,π^-	11.53	4.06	1.97	0.72	0.29	0.09	0.02					
	0.78	0.09	0.09	0.03	0.02	0.01	0.01					
p,K^-		1.54	0.29	0.06								
		0.22	0.07	0.02								
$p,\bar{p}$		0.06										
		0.01										
π^-,π^+	4.52	3.52	2.16	1.50	1.15	0.86	0.70		0.47			
	0.23	0.08	0.06	0.04	0.03	0.02	0.02		0.02			
π^-,K^+	0.66	0.46	0.45	0.35	0.24	0.15	0.07		0.03			
	0.12	0.04	0.04	0.03	0.02	0.01	0.01		0.01			
K^-,π^+	3.29	3.09	1.78	1.38	0.72	0.35						
	1.04	0.44	0.28	0.21	0.10	0.06						
$\bar{p},\pi^+$	11.24	5.27	1.88		0.74							
	2.57	0.72	0.65		0.16							

TABLE XVII. (*Continued.*)

	175 GeV/c										
x	0.120	0.200	0.300	0.400	0.500	0.600	0.700	0.800	0.895	0.920	0.940
π^+,π^+	15.21	11.58	7.79	6.01	5.56	4.47	4.53	4.66	6.21		11.64
	1.09	0.40	0.14	0.10	0.13	0.08	0.11	0.12	0.08		0.11
π^+,K^+	1.72	1.09	0.82	0.76	0.57	0.47	0.40	0.25	0.27		0.25
	0.74	0.20	0.06	0.05	0.06	0.03	0.03	0.03	0.02		0.02
π^+,p	1.09	1.07	0.80	0.67	0.51	0.39	0.26	0.15			
	0.44	0.16	0.05	0.05	0.04	0.02	0.02	0.02			
K^+,π^+	13.26	5.52	4.66	3.08	2.29	1.40	0.65	0.57			
	3.76	1.32	0.45	0.24	0.32	0.16	0.20	0.16			
K^+,K^+		4.04	3.96	3.60	3.10	2.75	2.57	2.35	4.53		9.18
		1.68	0.44	0.29	0.36	0.20	0.29	0.30	0.27		0.45
p,π^+	17.48	12.87	7.00	3.90	2.18	1.04	0.39	0.11			
	0.71	0.32	0.08	0.06	0.04	0.02	0.02	0.01			
p,K^+	1.77	2.04	0.80	0.62	0.37	0.18	0.08	0.05			
	0.54	0.23	0.04	0.03	0.02	0.01	0.01	0.01			
p,p	2.77	3.86	6.35	8.32	11.29	12.81	15.18	14.58	17.64		29.35
	0.31	0.18	0.08	0.08	0.09	0.07	0.12	0.15	0.12		0.23
π^-,π^-	15.00	11.64	7.53	6.30	5.04	4.51	4.21	4.45		8.39	
	0.72	0.26	0.07	0.07	0.09	0.05	0.05	0.05		0.08	
π^-,K^-	0.82	1.00	0.71	0.54	0.40	0.40	0.32	0.21		0.14	
	0.26	0.11	0.03	0.03	0.03	0.02	0.02	0.02		0.01	
$\pi^-,\bar{p}$	1.02	0.70	0.61	0.51	0.27	0.17	0.13	0.03			
	0.25	0.08	0.02	0.03	0.02	0.01	0.01	0.00			
K^-,π^-		7.89	4.75	3.96	1.62	1.57	1.06	0.51			
		1.19	0.34	0.34	0.36	0.17	0.17	0.15			
K^-,K^-		3.49	3.78	4.30	2.67	2.60	2.75	3.18		5.77	
		1.13	0.36	0.38	0.41	0.21	0.23	0.25		0.39	
$\bar{p},\pi^-$		13.98	7.58	3.48	3.78	3.02					
		2.32	0.65	0.83	0.67	0.65					
$\bar{p},\bar{p}$			5.46	7.73	10.72	12.07	10.66	12.27		19.90	
			0.57	0.92	1.03	0.66	0.67	0.68		1.18	
π^+,π^-		6.58	3.66	2.17	1.49	1.06	0.86				
		0.32	0.09	0.06	0.05	0.03	0.04				
π^+,K^-		0.86	0.52	0.31	0.25	0.16	0.11				
		0.20	0.05	0.03	0.03	0.02	0.01				
K^+,π^-		3.96	3.43	1.74	1.06	0.64	0.38				
		1.05	0.38	0.18	0.15	0.08	0.08				
p,π^-		8.11	3.41	1.76	0.84	0.32	0.08				
		0.26	0.05	0.03	0.02	0.01	0.01				
p,K^-		0.92	0.32	0.13	0.05	0.01					
		0.16	0.02	0.01	0.00	0.00					
$p,\bar{p}$		0.25	0.11	0.02	0.83						
		0.05	0.01	0.00	0.15						
π^-,π^+			3.56								
			0.05								
π^-,K^+			0.63								
			0.03								
K^-,π^+			2.93								
			0.25								
$\bar{p},\pi^+$			4.54								
			0.60								

data were sufficiently good to derive such a parameter.

D. Triple-Regge parametrizations

The cross section for the reaction channel $ap \to cX$ in the kinematic range $s/M_X^2 \gg 1$ and large M_X^2 can be described by triple-Regge phenomenology[35,36] as shown schematically by the Feynman diagram in Fig. 20. The form of the invariant cross section is given by the sum over the exchanged trajectories,

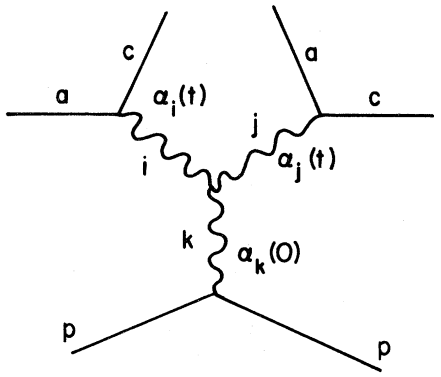

FIG. 20. Triple-Regge-exchange diagram for the process $a+p \to c+X$ for $s/M_X^2 \gg 1$ and $s \to \infty$.

$$E\frac{d^3\sigma}{dp^3} = \frac{s}{\pi}\frac{d^3\sigma}{dt\,dM_X^2} = \sum_{ijk} G_{ijk}(t)(1-x)^{a_k(0)-\alpha_i(t)-\alpha_j(t)} s^{\alpha_k(0)-1} , \tag{10}$$

where $\alpha_i(t)$ is the Regge trajectory of the exchanged particle and where $G_{ijk}(t)$ is the product residue functions at the four vertices. In this simplified formulation G_{ijk} also includes the effect of the signatures of the exchanged trajectories. The invariant momentum transfer t and the missing mass squared M_X^2 are defined, along with their high-energy approximations, by

$$t=(p_a-p_c)^2$$
$$=M_a^2(1-x)+M_c^2\left[1-\frac{1}{x}\right]-\frac{p_T^2}{x} \tag{11}$$

and

$$M_X^2=(p_a+p_b-p_c)^2=s(1-x) . \tag{12}$$

In addition to the 100 and 175 GeV/c data, runs were also made at 70 GeV/c with positive beam to cover the kinematic range $0.75<x<0.97$ and $0.2<p_T<1.25$ GeV/c^2. The data for the reactions $\pi^+p \to \pi^+X$, $\pi^-p \to \pi^-X$, and $pp \to pX$ were further broken down into seven Feynman-x bins for each spectrometer setting. The lower-statistics data accummulated for the $K^\pm$ and $\bar{p}$ leading-particle reactions were left in a single bin per setting.

For these leading-particle reactions, the invariant cross section data were fit using a triple-Pomeron (PPP) and the leading Reggeon-Reggeon-Pomeron (RRP) terms. The Reggeon form incorporates a linear combination of ρ, f, ω, and A_2 exchanges, which share a common trajectory $\alpha_R(t)=\frac{1}{2}+t$, where t is in GeV^2. In addition, for the $pp \to pX$ channel, $\pi\pi P$ and $\pi\pi R$ contributions were added. The strength and form of the $\pi\pi P$ and $\pi\pi R$ terms were taken from the analysis by Field and Fox.[36] The t slope for the Pomeron was taken as a free parameter, except for the lower-statistics $K^\pm p$

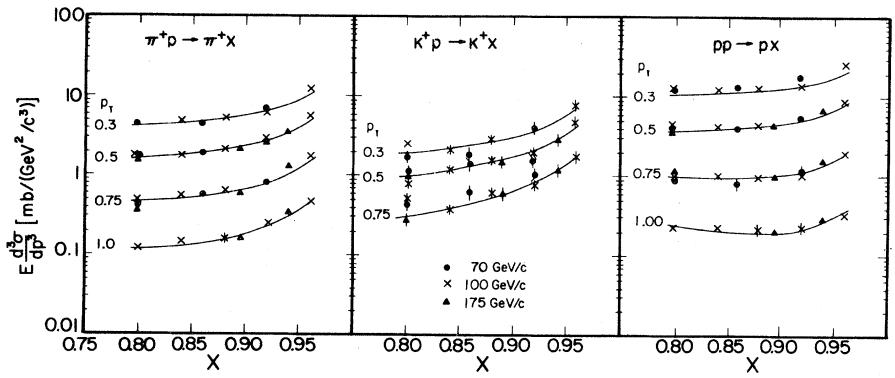

FIG. 21. Data and triple-Regge fits to $\pi^+p \to \pi^+X$, $K^+p \to K^+X$, and $pp \to pX$ at 70, 100, and 175 GeV.

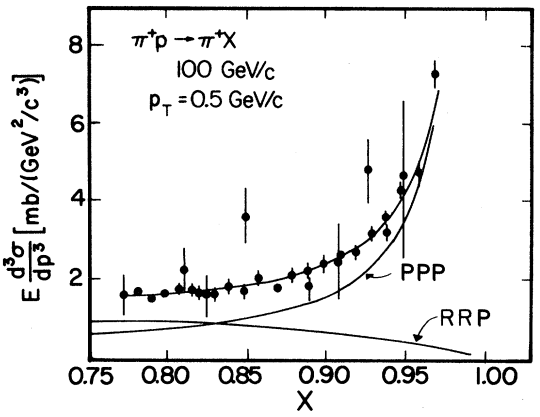

FIG. 22. Fine-binned data for $\pi^+p \to \pi^+X$ at 100 GeV/c and p_T=0.5 GeV/c with *PPP* and *RRP* contributions to the triple-Regge fit.

$\to K^{\pm}X$ and $\bar{p}p \to \bar{p}X$ channels where it was constrained to zero. This simplified form of the cross section was thus

$$E\frac{d^3\sigma}{dp^3}(x,t,s) = G_{PPP}(t)(1-x)^{-1-2\alpha'_P t} + G_{RRP}(t)(1-x)^{-2t} + (\pi\pi P + \pi\pi R)\,. \quad (13)$$

A single triple-Regge fit was made for all x, t, and s values simultaneously for each reaction channel. Residue functions of the form $G(t)=Ae^{bt}+Ce^{dt}$ were used. The leading-particle reaction data, along with the triple-Regge fits are presented in Fig. 21. The contribution of the *PPP* and *RRP* terms are shown for the fine-bin data for $\pi^+p \to \pi^+X$ in Fig. 22. The parameters of the fits are summarized in Table XVIII; complete tables of the parameters and their error matrix can be found in Ref. 5.

To permit comparison between reaction channels without the complication of residue functions, the contributions of both the *PPP* and *RRP* terms were integrated over the t range covered by the data. Integration over this t range is estimated to contain 80–90% of the cross section at a given x. These integrated cross sections are listed in Table XIX.

The leading-particle cross sections change by less than 12% over the 70–175 GeV/c beam momentum range studied. Good fits are obtained without the use of nonscaling *PPR* terms. To check the sensitivity of the data to a nonscaling *PRR* interference term, the leading-particle data for particle and antiparticle beams were simultaneously fit to a form $PPP+RRP+PRR$ since only the *PRR* term changes sign between $a^+p \to a^+X$ and $a^-p \to a^-X$ interactions. The contributions of the t-integrated nonscaling terms for $\pi^{\pm}$,$K^{\pm}$, and $p^{\pm}$ beams at $x=0.88$ are (3±1)%, (10±5)%, and (3±2)%, respectively.

Using these data, two simple tests of factorization may be performed. Neglecting kinematic terms, the cross section for leading-particle inelastic reactions $a^{\pm}p \to a^{\pm}X$ at high x may be written as a product of vertex functions:

TABLE XVIII. Triple-Regge fits to $ap \to aX$.

$$\frac{E\,d^3\sigma}{dp^3} = [(C_2e^{C_3t}+C_4e^{C_5t})(1-x)^{-1-2\alpha'_P t}+(C_6e^{C_7t}+C_8e^{C_9t})(1-x)^{-2t}$$

$$+(\text{Field and Fox } \pi\pi P \text{ and } \pi\pi R \text{ for } pp \to pX \text{ only})]$$

$$= PPP + RRP + (\pi\pi P + \pi\pi R)\,.$$

Parameter	π^+	K^+	p	π^-	K^-	$\bar{p}$
α'_p (GeV^{-2})	0.01±0.03	0	0.14±0.03	0.40±0.04	0	0
C_2 (mb/GeV^2)	0.36±0.04	0.32±0.02	1.00±0.04	0.32±0.08	0.42±0.05	1.11±0.14
C_3 (GeV^{-2})	4.52±0.67	2.57±0.11	4.53±0.40	2.26±1.10	4.47±0.38	4.77±0.34
C_4 (mb/GeV^2)	0.10±0.05		0.10±0.05	0.11±0.09		
C_5 (GeV^{-2})	1.73±0.40		1.29±0.35	−0.03±0.57		
C_6 (mb/GeV^2)	4.93±0.67	1.41±0.41	7.46±6.38	5.37±0.52	0.84±0.28	2.87±1.05
C_7 (GeV^{-2})	7.16±1.94	1.50±1.01	12.44±6.75	3.65±0.44	1.95±0.60	−0.61±0.76
C_8 (mb/GeV^2)	1.62±0.35		2.83±0.26			
C_9 (GeV^{-2})	−0.54±0.26		−1.02±0.10			

TABLE XIX. Integrated cross sections $d\sigma/dM^2$ (10^{-2} mb/GeV^2) (t integrated from -0.1 to -1.0 GeV/c^2).

Reaction	Term \ x	0.8	0.84	0.88	0.92	0.96
$p\to p$	*PPP*	1.191±0.08	1.485±0.11	1.970±0.16	2.920±0.25	5.618±0.50
	RRP	1.804±0.18	1.524±0.10	1.246±0.05	0.961±0.02	0.652±0.004
$\pi^+\to\pi^+$	*PPP*	0.721±0.05	0.901±0.07	1.199±0.09	1.796±0.13	3.580±0.26
	RRP	0.984±0.05	0.853±0.03	0.718±0.02	0.574±0.006	0.409±0.001
$K^+\to K^+$	*PPP*	0.717±0.03	0.896±0.04	1.195±0.05	1.792±0.07	
	RRP	0.312±0.06	0.273±0.06	0.232±0.05	0.188±0.04	
$\bar{p}\to\bar{p}$	*PPP*	1.188±0.08	1.486±0.11	1.981±0.14	2.971±0.21	
	RRP	1.284±0.22	1.085±0.18	0.886±0.15	0.682±0.12	
$\pi^-\to\pi^-$	*PPP*	0.962±0.06	1.120±0.07	1.367±0.08	1.818±0.11	2.944±0.18
	RRP	0.658±0.04	0.591±0.04	0.517±0.03	0.433±0.03	0.325±0.02
$K^-\to K^-$	*PPP*	0.491±0.04	0.614±0.05	0.819±0.06	1.228±0.10	
	RRP	0.666±0.27	0.544±0.20	0.427±0.11	0.312±0.05	

$$\left.\frac{d^2\sigma(t)}{dM_X{}^2dt}\right|_{\text{inelastic}} \propto \beta_{aaP}{}^2(t)\beta_{PPP}(t)\beta_{ppP}(0)\ . \quad (14)$$

In the same spirit of neglecting all exchanges except for the Pomeron, the coupling for the elastic cross section $a^{\pm}p\to a^{\pm}p$ can be expressed at the same t value as

$$\left.\frac{d\sigma(t)}{dt}\right|_{\text{elastic}} \propto \beta_{aaP}{}^2(t)\beta_{ppP}{}^2(t)\ . \quad (15)$$

Dividing these terms and canceling the beam-dependent $\beta_{aaP}{}^2(t)$ coupling, the ratio

$$\frac{\left.\frac{d^2\sigma(t)}{dM_X{}^2dt}\right|_{\text{inelastic}}}{\left.\frac{d\sigma(t)}{dt}\right|_{\text{elastic}}} \propto \frac{\beta_{PPP}(t)\beta_{ppP}(0)}{\beta_{ppP}{}^2(t)} \quad (16)$$

is independent of the beam particle species. The inelastic data for 100 GeV, $p_T=0.3$ GeV/c, $x=0.92$, $t=-0.098$ GeV^2 is divided for each leading-particle channel by the corresponding elastic cross section as parametrized in Ref. 1. The ratios are presented in Table XX. Although the data still contain substantial non-Pomeron contributions at $x=0.92$, the constancy of the ratios indicates that factorization holds to better than 10% for this test.

Although the particle-changing data are somewhat sparser, a similar factorization test can be demonstrated for the reactions $\pi^+p\to K^+X$ ($\pi^-p\to K^-X$). The cross sections may be expressed as products of the $\pi^+K^+\bar{K}^{*0}$ ($\pi^-K^-K^{*0}$) coupling constants squared times the exchanged $\bar{K}^{*0}{}_p$ ($K^{*0}p$) total cross section, and thus

$$\frac{\frac{d^2\sigma}{dt\,dM_X{}^2}(\pi^-p\to K^-X)}{\frac{d^2\sigma}{dt\,dM_X{}^2}(\pi^+p\to K^+X)} \propto \frac{|\beta_{\pi^-K^-K^*}(t)|^2\sigma_{\text{tot}}^{K^*p}[E_{\text{eff}}=(1-x)E\pi^-]}{|\beta_{\pi^+K^+\bar{K}^*}(t)|^2\sigma_{\text{tot}}^{\bar{K}^*p}[E_{\text{eff}}=(1-x)E\pi^+]}\ . \quad (17)$$

The coupling constants cancel by charge symmetry and the $K^{*0}p$ to $\bar{K}^{*0}p$ cross-section ratio should be the same as the K^+p to K^-p total-cross-section ratio at equivalent energy. The inelastic $\pi^{\pm}p\to K^{\pm}X$ data at 100 GeV, $p_T=0.3$ GeV/c, and $x=0.92$, 0.88, and 0.80 are used to find the ratio of $\sigma_t(K^{*0}p)/\sigma_t(\bar{K}^{*0}p)$ and compared in Fig. 23 with the ratio of $\sigma_t(K^+p)/\sigma_t(K^-p)$ as measured in Ref. 37. The agreement of the cross-section ratios again indicates agreement with the factorization hypothesis.

Because of limited statistics or contamination from forward resonance production[2,38] other particle-changing reaction channels at high x in the data set are inadequate for further application of triple-Regge phenomenology.

TABLE XX. Ratio of inelastic cross section for $a+p\to a+X$ at $x=0.92$ and elastic cross section (Ref. 1) for $a+p\to a+p$ for a common beam momentum of 100 GeV/c and $t=-0.098$ GeV^2.

a	$\left.\frac{d^2\sigma}{dt\,dM_X^2}\right\|_{\text{inelastic}} \Big/ \left.\frac{d\sigma}{dt}\right\|_{\text{elastic}}$
p	0.57±0.02
$\bar{p}$	0.46±0.03
K^+	0.45±0.05
K^-	0.42±0.04
π^+	0.52±0.02
π^-	0.49±0.02
Weighted average	0.51±0.01

VI. ASSOCIATED-MULTIPLICITY RESULTS

In addition to the behavior of single-particle inclusive cross sections for the process $a+p\to c+X$, this experiment also studied the charged-particle multiplicity and pseudorapidity distributions of the charged-particle secondaries which comprise the recoil state X. Such additional information can shed new insight into the systematics of multiparticle production by correlating the measured distributions with the identities and kinematics of the trigger particles.

Data for this experiment were taken in sweeps of transverse momenta p_T and Feynman x. The natural variable for the study of multiplicities is the missing mass squared of the recoiling system $M_X^2=(1-x)s$. Since the longitudinal phase space available for particle production varies as $\ln M_X^2$, it is to be expected that the produced particle multiplicity should vary as $\langle n(x)\rangle=A+B\ln M_X^2$. Here the coefficient A represents the multiplicity of the two fragmentation regions and B represents the height of the central plateau in rapidity space. In models where the central region is uncorrelated with the fragmentation region production, the coefficient B is expected to be independent of the participating particle identities.

This experiment can also investigate whether the associated multiplicities further depend on the p_T or the invariant momentum transfer t between the particles a and c. It might be expected that as p_T or t increases, the interaction involves scattering at shorter distances. This is possibly associated with an increase in the multiplicities.

The average charged-particle multiplicities as a function of Feynman x and p_T are listed in Table XXI. Complete tables of the charged-prong distributions and pseudorapidity distributions are available in Ref. 7.

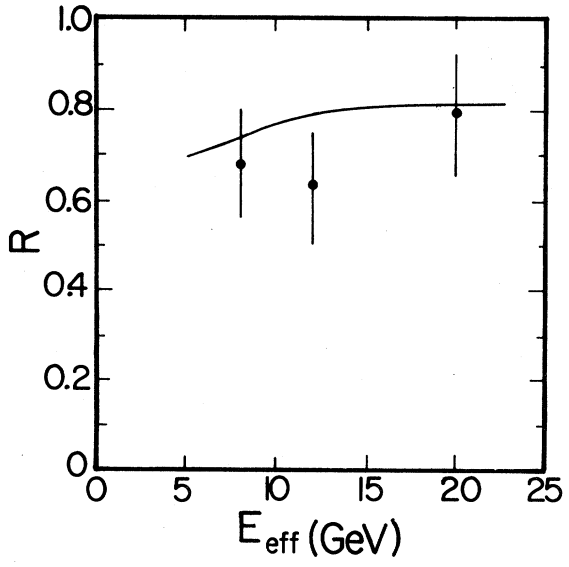

FIG. 23. The ratio R of $\sigma_{\text{tot}}(K^{*0}p)/\sigma_{\text{tot}}(\bar{K}^{*0}p)$ as calculated from $\pi^{\pm}p\to K^{\pm}X$-inclusive scattering. The curve is the $\sigma_{\text{tot}}(K^+p)/\sigma_{\text{tot}}(K^-p)$ ratio from data of Ref. 37.

A. Associated charged-particle multiplicities

The average charged-particle multiplicities for the reactions $a+p\to c+X$ are shown as a function of x at constant p_T in Fig. 24. The multiplicity for each beam species a is nearly independent of the detected spectrometer species c. An exception to this rule is evident in comparing $pp\to pX$ and $pp\to\pi^+X$ associated multiplicities. The pion production channel multiplicities are systematically lower than the multiplicities for the leading proton channel. Production of π^+ at high x may be due to decays of forward nucleon resonances. In the decays of charged resonances, often most of the incident momentum is carried away by undetected neutrons, thereby lowering the energy available for charged-particle production. Leading protons, on the other hand, are often associated with inelastic target fragmentation leading to relatively higher charged-secondary-particle multiplicities.

The dependence of the individual charged-prong cross sections as a function of x are displayed in Fig. 25, for the leading-particle $\pi^+p\to\pi^+X$ and $pp\to pX$ channels and for the charge-changing reactions $\pi^+p\to\pi^-X$ and $pp\to\pi^-X$. The leading particle enhancement at high x is observed to con-

TABLE XXI. Average associated multiplicity as a function of Feynman x and p_T for all reaction channels. The errors shown below each entry are statistical only. There is an overall systematic error estimated to be ± 0.17 not included in the listed errors. The notation for reactions is $ac \equiv a + p \to c + X$.

(a) 100 GeV/c $a^- + p \to c^- + X$

x	p_T (GeV/c)	$\pi\pi$	πK	πp	$K\pi$	KK	Kp	$p\pi$	pp
0.920	0.300	3.21	3.11			3.05			3.40
		0.05	0.41			0.23			0.27
0.920	0.400	3.22	3.22		2.81	3.44			3.39
		0.06	0.29		0.46	0.20			0.13
0.920	0.500	3.23	3.38			3.87			3.67
		0.08	0.34			0.26			0.20
0.920	0.625	3.22	2.25			3.76			3.38
		0.05	0.74			0.28			0.24
0.920	0.750	3.23	3.19			3.66	3.72		3.24
		0.10	0.53			0.42	0.36		0.30
0.920	1.000	3.24				3.31			4.04
		0.12				0.36			0.43
0.920	1.250	2.96							
		0.20							
0.880	0.300	3.67	3.20		3.41	4.50			3.93
		0.08	0.44		0.50	0.24			0.19
0.800	0.500	4.52		3.78			5.10		5.21
		0.10		0.42			0.55		0.33
0.800	0.750	4.56		4.15			5.35		4.89
		0.10		0.33			0.63		0.62
0.700	0.300	4.33	4.55	3.33	3.83	4.57		5.40	4.38
		0.05	0.28	0.36	0.41	0.30		1.21	0.15
0.700	0.500	4.76	4.62	4.00	3.87	5.21			4.90
		0.10	0.52	0.28	0.54	0.68			0.20
0.700	0.750	5.10	5.34	4.49	4.66	4.70			5.08
		0.13	0.50	0.42	0.88	0.57			0.28
0.600	0.200	4.47	5.31	4.98		5.97		4.82	4.38
		0.09	0.34	0.49		0.83		0.59	0.26
0.600	0.300	4.67	5.28	4.57	4.89	4.07		4.55	5.08
		0.07	0.22	0.23	0.42	0.28		0.59	0.20
0.600	0.400	4.70	5.20	4.96	3.84	4.70		4.39	5.59
		0.08	0.31	0.39	0.58	0.52		0.93	0.31
0.600	0.500	5.09	5.25	5.20	4.52	5.21		3.39	5.44
		0.14	0.41	0.42	1.17	0.66		1.04	0.36
0.600	0.625	5.28	5.81	3.94	4.81	4.76			4.41
		0.14	0.47	0.50	0.74	0.71			0.31
0.600	0.750	5.21	5.10	4.79	6.38	4.83			5.77
		0.15	0.42	0.37	1.66	0.47			0.42
0.600	1.000	5.48	6.32	5.94		5.80			5.45
		0.22	0.75	0.71		0.84			0.58
0.600	1.200	5.38	6.03						
		0.23	1.52						
0.500	0.300	4.92	4.98	5.44	3.60	5.85		4.08	5.69
		0.07	0.18	0.27	0.28	0.45		0.77	0.24
0.500	0.400	5.17	4.92	4.67					4.92
		0.20	0.85	0.69					0.51
0.500	0.500	5.46	5.25	4.69	4.84	6.90		3.55	5.47
		0.14	0.48	0.28	0.91	0.94		2.34	0.43
0.500	0.750	5.48	5.68	5.67	4.93	7.35		4.38	6.46
		0.18	0.45	0.38	0.72	0.86		0.58	0.39

TABLE XXI. (*Continued.*)

(a) 100 GeV/c $a^- + p \to c^- + X$ (*continued*)

x	p_T (GeV/c)	$\pi\pi$	πK	πp	$K\pi$	KK	Kp	$p\pi$	pp
0.400	0.300	5.20	5.39	5.52	4.56	6.11	6.34	6.20	5.94
		0.08	0.28	0.26	0.50	0.73	0.82	0.53	0.33
0.400	0.500	5.76	6.31	5.46	5.67	7.04		4.43	6.91
		0.11	0.40	0.26	0.59	0.69		0.53	0.51
0.400	0.750	5.94	6.91	5.87	8.18			3.75	5.48
		0.15	0.55	0.89	2.27			1.58	0.59
0.300	0.100	5.46	6.84	6.37	5.73	4.16		5.19	6.44
		0.22	0.83	0.56	2.35	1.00		0.84	0.93
0.300	0.150	5.46	6.16	5.27	4.36	4.69		4.69	6.85
		0.11	0.58	0.30	0.44	0.83		0.33	0.89
0.300	0.200	5.57	6.37	5.96	4.32	7.62		5.20	5.97
		0.10	0.43	0.32	0.44	1.42		0.32	0.51
0.300	0.250	5.74	6.14	5.32	4.47	5.71		5.75	6.68
		0.14	0.35	0.23	0.67	0.51		0.45	0.52
0.300	0.300	5.61	6.34	6.66	5.22	7.06		5.71	6.36
		0.10	0.34	0.41	0.46	0.86		0.62	0.59
0.300	0.400	5.82	5.74	6.23	6.52	5.70		6.12	7.10
		0.10	0.44	0.35	0.51	0.62		0.82	0.66
0.300	0.500	5.79	5.48	6.82	5.86			5.66	6.50
		0.19	0.81	0.50	0.70			1.21	0.69
0.300	0.625	6.23	5.41	6.66	5.75	7.00		6.71	8.19
		0.17	1.12	0.78	1.23	0.93		1.13	1.24
0.300	0.750	6.28	5.95	6.88					
		0.24	0.57	1.69					
0.200	0.100	6.77							
		0.91							
0.200	0.200	6.28	8.83	6.75	4.31				
		0.22	1.50	1.17	1.98				
0.200	0.300	6.36	8.72	7.05	7.66			5.99	
		0.15	1.00	0.55	0.94			0.99	
0.200	0.500	7.32							
		0.39							

(b) 100 GeV/c $a^- + p \to c^+ + X$

x	p_T (Gev/c)	$\pi\pi$	πK	πp	$K\pi$	$p\pi$
0.880	0.300	3.05	3.55	3.24		
		0.06	0.35	0.40		
0.880	0.400	2.96		3.68		
		0.17		0.39		
0.880	0.500	2.64				
		0.22				
0.800	0.300	3.92	3.98	4.67	1.96	
		0.10	0.32	0.32	0.29	
0.800	0.500	3.71	4.00	4.45		
		0.13	0.39	0.59		
0.700	0.300	4.21	4.46	5.01	3.89	4.15
		0.10	0.17	0.25	0.38	0.52
0.700	0.400	4.22	4.60	4.93		
		0.13	0.52	0.29		
0.700	0.500	4.07	4.83	5.54		
		0.18	0.43	0.61		
0.700	0.625	4.22	5.06	5.21		

TABLE XXI. (*Continued.*)

(b) 100 GeV/c $a^- + p \to c^+ + X$ (*continued*)

x	p_T (GeV/c)	$\pi\pi$	πK	πp	$K\pi$	$p\pi$
		0.22	0.56	0.84		
0.600	0.300	4.72	4.99	5.52	4.38	5.21
		0.09	0.20	0.21	0.40	0.55
0.600	0.500	4.62	4.98	5.55	4.09	
		0.14	0.38	0.42	0.55	
0.500	0.300	5.29	5.58	6.33	4.53	5.67
		0.11	0.35	0.32	0.30	0.70
0.500	0.500	5.40	6.18	4.78	3.97	
		0.21	0.51	0.93	0.65	
0.500	0.625	4.87				
		0.28				
0.400	0.300	5.51	5.09	6.39	4.93	6.81
		0.11	0.24	0.29	0.54	1.20
0.400	0.500	5.10	5.97	5.21	4.81	
		0.16	0.55	0.87	0.51	
0.300	0.100	5.28	8.06	7.86		
		0.24	1.51	1.31		
0.300	0.150	6.01	5.96	6.54	5.05	4.71
		0.25	1.23	1.34	1.93	0.92
0.300	0.200	6.11	5.56	7.87	3.89	
		0.26	0.65	0.92	1.67	
0.300	0.250	6.22	7.10	6.88	4.71	
		0.20	1.18	0.49	2.49	
0.300	0.300	5.92	6.72	7.58		6.47
		0.17	0.67	0.55		1.13
0.300	0.400	5.92	7.28	6.63	6.39	
		0.17	0.83	0.77	1.08	
0.300	0.500	6.19	6.79	7.21		
		0.21	1.16	0.64		
0.300	0.625	6.32	6.58	7.70		
		0.23	1.68	0.68		
0.300	0.750	9.08				
		0.47				
0.200	0.300	6.60	7.04	7.15	4.33	
		0.19	0.90	0.86	2.56	
0.200	0.500	6.66		5.84		
		0.27		1.84		

(c) 100 GeV/c $a^+ + p \to c^- + X$

x	p_T (GeV/c)	$\pi\pi$	πK	πp	$K\pi$	$p\pi$	pK	pp
0.880	0.300	3.82	3.97					
		0.09	0.75					
0.880	0.400	3.38						
		0.14						
0.880	0.500	4.20						
		0.26						
0.840	0.300	3.93	4.40		3.89			
		0.10	0.58		0.48			
0.800	0.300	3.88	4.70		2.23			
		0.13	0.81		0.43			
0.700	0.300	4.51	4.56	4.76	3.91	4.65		
		0.12	0.53	0.48	0.56	0.55		

TABLE XXI. (*Continued.*)

(c) 100 GeV/c $a^+ + p \to c^- + X$ (*continued*)

x	p_T (GeV/c)	$\pi\pi$	πK	πp	$K\pi$	$p\pi$	pK	pp
0.700	0.400	4.44	4.64		3.98	4.55		
		0.12	0.34		0.40	0.40		
0.700	0.500	4.66	4.63					
		0.25	0.38					
0.700	0.625	4.45				4.41		
		0.24				0.47		
0.600	0.300	5.01	4.90	5.29	5.05	4.59		
		0.11	0.39	0.37	0.51	0.20		
0.600	0.500	5.05						
		0.47						
0.500	0.300	5.36	4.65	5.23	4.51	5.46	6.36	
		0.11	0.27	0.35	0.34	0.22	0.86	
0.500	0.400	5.30	6.20	6.07	4.86	4.71		
		0.19	0.52	0.78	1.50	0.24		
0.500	0.500	5.31	6.18	4.40		4.82		
		0.16	0.49	0.33		0.33		
0.500	0.625	4.91	4.92	4.06		4.92		
		0.23	0.59	0.36		0.71		
0.400	0.300	5.68	5.55	6.12	4.58	5.64	4.78	
		0.13	0.34	0.42	0.50	0.19	0.46	
0.400	0.500	5.59						
		0.46						
0.300	0.100	6.35	6.27	6.25	8.75	5.64	6.12	
		0.28	1.18	0.73	3.62	0.32	0.82	
0.300	0.150	6.06	7.82	6.92	5.21	6.26		
		0.15	0.91	0.43	0.56	0.67		
0.300	0.200	6.45	6.09	5.53	6.57	5.67	6.77	6.87
		0.14	0.42	0.32	0.76	0.17	1.34	1.14
0.300	0.250	6.06	5.96	6.24	6.01	5.90		
		0.15	0.41	0.47	0.72	0.21		
0.300	0.300	6.23	7.21	6.44	5.55	6.01		
		0.15	0.43	0.45	0.52	0.21		
0.300	0.400	6.15	8.29	7.44	6.09	5.71		
		0.17	1.11	0.64	0.62	0.15		
0.300	0.625	6.69	5.60	6.71		6.32		
		0.28	0.68	0.72		0.37		
0.200	0.400	7.00	6.94	6.92	8.62	6.81	8.37	
		0.20	0.55	0.66	1.74	0.34	1.12	

(d) 100 GeV/c $a^+ + p \to c^+ + X$

x	p_T (GeV/c)	$\pi\pi$	πK	πp	$K\pi$	KK	$p\pi$	pK	pp
0.960	0.300	2.24	2.61			2.12	2.18		2.27
		0.08	0.24			0.21	0.31		0.06
0.960	0.500	2.18	2.15			2.52			2.21
		0.09	0.46			0.29			0.11
0.960	0.750	2.15				2.20			2.20
		0.06				0.17			0.06
0.960	1.000	2.10				2.19			2.21
		0.08				0.32			0.16
0.920	0.300	3.23	3.24			3.08		3.58	3.17
		0.07	0.33			0.48		0.42	0.05

TABLE XXI. (*Continued.*)

(d) 100 GeV/c $a^+ + p \to c^+ + X$ (*continued*)

x	p_T (GeV/c)	$\pi\pi$	πK	πp	$K\pi$	KK	$p\pi$	pK	pp
0.920	0.400	3.23	3.45			3.01			3.18
		0.11	0.44			0.34			0.07
0.920	0.500	3.18	3.72			3.34			3.24
		0.06	0.33			0.29			0.05
0.920	0.625	3.23	3.85			3.48			3.22
		0.07	0.69			0.30			0.07
0.920	0.750	3.11	3.61			2.53			3.25
		0.10	0.80			0.30			0.10
0.920	1.000	3.35				2.82			3.18
		0.15				0.35			0.21
0.920	1.250	3.20				0.00			2.80
		0.27				0.00			0.33
0.880	0.300	3.43	3.03			3.91			3.52
		0.10	0.30			0.32			0.09
0.880	0.500	3.54	3.24			3.83			3.54
		0.11	0.30			0.32			0.12
0.880	0.750	3.47	2.79			2.52			3.51
		0.10	0.30			0.54			0.11
0.880	1.000	3.82				3.37			3.76
		0.22				0.47			0.22
0.840	0.300	3.89	4.01		4.48	3.74	3.12	3.24	3.93
		0.11	0.34		0.64	0.49	0.76	0.87	0.15
0.840	0.500	4.30	4.06	5.29		4.38	3.07	4.47	4.11
		0.08	0.37	0.62		0.43	0.53	1.02	0.07
0.840	0.750	4.43	3.67	4.42		4.58			4.41
		0.16	0.30	0.56		0.39			0.10
0.840	1.000	4.72	5.19			4.51			4.32
		0.10	0.75			0.82			0.19
0.800	0.300	4.14	4.52	4.63	0.00	5.02			4.30
		0.11	0.37	1.15	0.00	0.48			0.09
0.800	0.500	4.49	4.74	4.80	3.67	4.46	3.91	4.28	4.47
		0.07	0.21	0.32	0.45	0.25	0.40	0.80	0.06
0.800	0.750	4.52	5.42	4.33	4.43	5.39	3.26		4.55
		0.08	0.25	0.35	0.58	0.27	0.47		0.10
0.800	1.000	4.72	4.68	4.30		5.73			4.63
		0.13	0.41	0.53		0.49			0.11
0.700	0.300	4.38	4.32	5.02	4.71	4.22	3.58		4.64
		0.10	0.34	0.74	1.12	1.10	0.32		0.09
0.700	0.500	4.60	4.87	5.04	4.56	4.14	4.00	4.47	4.75
		0.08	0.21	0.35	1.21	0.37	0.30	0.41	0.07
0.700	0.750	4.79	4.86	5.20	0.00	0.00	4.37		4.74
		0.20	0.40	0.56	0.00	0.00	0.53		0.10
0.600	0.200	4.59	5.26	5.94		5.53	3.07	6.46	4.86
		0.10	0.38	0.51		0.90	0.27	1.06	0.12
0.600	0.300	4.69	4.94	5.04	3.50	5.36	3.66	4.87	5.15
		0.14	0.21	0.22	0.30	0.77	0.15	1.14	0.10
0.600	0.400	4.97	4.90	5.05	5.87	6.09	3.67	5.72	5.17
		0.10	0.28	0.41	1.00	0.88	0.22	0.64	0.09

TABLE XXI. (*Continued.*)

(d) 100 GeV/c $a^+ + p \to c^+ + X$ (*continued*)

x	p_T (GeV/c)	$\pi\pi$	πK	πp	$K\pi$	KK	$p\pi$	pK	pp
0.600	0.500	5.09	4.65	4.75	5.50	4.71	4.27	4.88	5.42
		0.11	0.23	0.21	0.64	0.64	0.19	0.51	0.09
0.600	0.625	5.34	5.43	5.11	5.12	5.70	3.67	5.94	5.48
		0.12	0.44	0.27	0.86	0.60	0.25	0.50	0.10
0.600	0.750	5.22	5.36	4.63	4.91	6.28	4.49	5.19	5.33
		0.18	0.36	0.29	0.71	0.67	0.30	0.52	0.11
0.600	1.000	5.26	5.44	5.53			4.25		5.29
		0.15	0.71	0.75			0.59		0.19
0.600	1.200	5.42	0.00	6.44			5.06		6.11
		0.28	0.00	1.20			0.54		0.23
0.500	0.300	4.98	6.12	6.11	4.14	5.15	4.07		5.88
		0.14	0.53	0.40	0.52	1.09	0.32		0.15
0.500	0.500	5.45	5.70	5.89	6.34	5.31	4.66	6.62	6.00
		0.15	0.38	0.37	0.68	0.59	0.24	1.01	1.11
0.500	0.750	5.59	5.38	6.45		5.56	5.55		5.97
		0.16	0.50	0.55		0.85	0.54		0.15
0.400	0.300	5.29	5.28	5.49	4.23	6.19	4.60	5.43	6.29
		0.16	0.60	0.57	0.48	1.30	0.25	0.67	0.17
0.400	0.500	5.62	6.14	6.20	5.40	5.95	5.18	5.02	6.20
		0.13	0.52	0.34	0.74	0.82	0.29	0.66	0.16
0.400	0.750	6.09	5.61	6.62			4.58		6.35
		0.16	0.64	0.52			0.24		0.17
0.300	0.100	5.74	5.27	5.96	4.89		4.79		8.16
		0.30	1.13	0.99	1.40		0.25		0.68
0.300	0.150	5.91	5.68	7.06	6.22	6.25	4.93	3.85	7.02
		0.19	0.72	0.52	1.28	0.97	0.19	0.72	0.20
0.300	0.200	5.59	5.69	6.58	7.68	4.26	5.04	6.78	6.71
		0.18	0.46	0.45	3.23	0.51	0.19	0.93	0.19
0.300	0.250	5.81	7.26	6.60	4.59		5.13	7.12	7.23
		0.13	0.72	0.68	0.42		0.18	1.03	0.22
0.300	0.300	5.99	6.95	6.63	6.68	5.27	5.69	7.61	7.47
		0.14	0.62	0.45	1.09	1.04	0.19	0.71	0.20
0.300	0.400	5.94	6.66	7.39	5.99		5.57	7.89	7.33
		0.20	0.86	0.54	0.86		0.22	1.07	0.30
0.300	0.500	6.23	6.59	7.27	6.16		5.84	7.40	7.11
		0.18	0.63	0.41	0.91		0.29	0.89	0.22
0.300	0.625	6.03		5.77			5.34		6.86
		0.20		0.64			0.25		0.29
0.300	0.750	6.36					5.41		6.84
		0.33					0.46		0.61
0.200	0.100	6.16		9.73	7.44		5.24		8.83
		0.30		3.20	2.67		0.31		1.43
0.200	0.200	6.66	6.38	8.62	5.62		5.83		7.03
		0.20	0.66	0.83	0.84		0.17		0.32
0.200	0.300	6.19	6.48	6.37	6.78		6.16	6.65	7.67
		0.16	0.55	0.77	0.70		0.18	0.99	0.24
0.200	0.500	9.64					8.07		10.58
		0.42					0.70		0.74

TABLE XXI. (*Continued.*)

(e) 175 GeV/c $a^- + p \to c^- + X$

x	p_T (GeV/c)	$\pi\pi$	πK	πp	$K\pi$	KK	Kp	$p\pi$	pp
0.920	0.500	3.86				3.74			3.86
		0.12				0.31			0.30
0.920	0.625	3.87				3.85			4.41
		0.11				0.38			0.32
0.800	0.500	4.88	4.78	4.12	4.64	4.98			4.91
		0.10	0.18	0.46	0.55	0.34			0.32
0.800	0.750	4.60	4.48	3.27	0.00	5.15			0.00
		0.09	0.29	0.67	0.00	0.40			0.00
0.700	0.500	5.50	5.26	3.55	4.52	5.28			5.35
		0.10	0.26	0.65	0.59	0.36			0.48
0.600	0.300	5.26	5.54	4.99	5.35	5.26			5.85
		0.12	0.22	0.43	1.19	0.42			0.52
0.600	0.400	5.26	5.93	5.84	6.85	5.56			6.71
		0.11	0.31	0.39	0.80	0.44			0.34
0.300	0.150	6.10	6.97	6.63	4.72	7.33		5.49	7.89
		0.14	0.56	0.46	0.72	1.08		0.56	0.92
0.300	0.225	6.28	6.19	6.66	6.61	7.88		4.68	6.79
		0.14	0.57	0.45	0.91	1.25		1.06	1.00
0.300	0.300	6.44	6.05	6.89	5.82	6.91		7.50	9.07
		0.10	0.22	0.33	0.53	0.75		0.85	0.52
0.300	0.400	6.41	7.22	6.94	6.26	7.75		5.23	8.64
		0.12	0.32	0.26	0.47	1.03		0.67	0.84
0.300	0.500	6.70	6.87	7.23	6.98	6.54		7.32	8.24
		0.11	0.32	0.24	0.66	0.98		0.89	2.42
0.300	0.625	7.11	7.22	6.69	7.06	6.22	7.87	6.18	7.63
		0.11	0.41	0.23	0.82	1.19	1.13	0.63	0.81
0.300	0.750	7.45	7.55	8.40	8.27				
		0.15	0.81	0.52	0.94				
0.200	0.150	6.87	6.66	7.35	4.10			6.93	
		0.21	0.84	1.15	1.11			0.92	
0.200	0.300	6.99	7.79	9.00	6.60	7.16		6.85	
		0.20	0.41	0.48	0.89	1.01		1.09	
0.200	0.500	7.13	5.22	9.01					
		0.15	1.10	1.36					

(f) 175 GeV/c $a^- + p \to c^+ + X$

x	p_T (GeV/c)	$\pi\pi$	πK	πp	$K\pi$	$p\pi$
0.300	0.150	6.59	6.35	8.35	6.77	7.98
		0.16	0.62	0.69	0.99	1.24
0.300	0.225	6.62	6.59	8.03	7.23	
		0.17	0.43	0.63	1.50	
0.300	0.400	6.48	6.95	8.35	6.14	6.24
		0.11	0.37	0.36	0.59	0.98
0.300	0.500	6.71	6.81	7.53	6.67	
		0.12	0.44	0.32	0.65	
0.300	0.625	7.28	6.35	7.54	6.49	5.52
		0.15	0.49	0.35	0.81	0.62
0.300	0.750	7.63	7.50	8.44	7.94	7.62
		0.20	0.46	0.49	0.91	1.30
0.200	0.300	7.75	9.50	8.92	7.67	
		0.18	0.75	0.74	0.94	

TABLE XXI. (*Continued.*)

(g) 175 GeV/c $a^+p \to c^- + X$

x	p_T (GeV/c)	$\pi\pi$	πK	πp	$K\pi$	$p\pi$	pK	pp
0.700	0.500	4.89	4.51	4.62		5.14		
		0.20	0.42	0.95		0.37		
0.600	0.300	5.21	5.24	5.36	4.91	5.07	4.13	
		0.17	0.52	0.79	0.72	0.14	0.38	
0.600	0.400	5.37	6.30	5.88	5.09	5.24	4.50	
		0.25	0.55	0.92	0.68	0.13	0.49	
0.600	0.400	5.00	6.02		5.35	5.24	4.07	
		0.20	0.54		0.67	0.16	0.62	
0.600	0.500	5.06	5.42			5.51		
		0.27	0.65			0.20		
0.600	0.625	5.75				5.77		
		0.41				0.31		
0.500	0.300	5.85	6.01		5.38	5.69	5.51	
		0.15	0.48		0.74	0.12	0.29	
0.500	0.400	6.01	6.55		5.16	6.02	6.05	
		0.22	0.52		0.45	0.12	0.40	
0.500	0.500	5.19	7.26		5.74	5.64	6.29	
		0.25	1.02		0.93	0.16	0.58	
0.500	0.625	6.04				6.21		
		0.42				0.25		
0.400	0.300	6.38	6.67	6.40	6.86	6.57	6.27	6.54
		0.19	0.47	0.50	0.83	0.10	0.26	0.81
0.400	0.500	6.40	7.39	4.71	5.66	6.69	8.05	
		0.28	0.69	1.20	0.58	0.14	0.58	
0.300	0.150	6.67	7.73		6.71	6.38	7.00	
		0.22	1.08		0.70	0.12	0.42	
0.300	0.225	6.52	6.96		7.50	6.64	6.94	
		0.15	0.78		0.65	0.13	0.41	
0.300	0.300	6.60	6.28		6.62	6.87	5.50	
		0.15	1.13		0.96	0.15	0.95	
0.300	0.400	6.15	7.13		6.11	6.90	7.56	
		0.19	0.71		1.66	0.19	0.50	
0.300	0.500	6.69	5.14			6.36	6.91	
		0.37	0.83			0.18	0.95	
0.300	0.625	6.64				7.82	5.35	
		0.39				0.29	0.92	
0.300	0.750	8.52				8.37		
		0.50				0.40		
0.300	0.850	8.71				9.63		
		0.49				0.58		
0.200	0.300	7.51	7.72	8.65	10.73	7.83	4.41	8.17
		0.27	0.85	1.36	2.43	0.20	1.99	1.26
0.200	0.500	7.83	10.80	8.72	6.24	7.85	8.43	6.32
		0.32	1.23	0.83	0.74	0.23	0.94	0.64
0.120	0.300	8.03	9.18		8.94	8.73	9.75	7.23
		0.35	1.52		0.91	0.30	1.38	1.92

TABLE XXI. (*Continued.*)

(h) 175 GeV/c $a^+ + p \to c^+ + X$

x	p_T (GeV/c)	$\pi\pi$	πK	πp	$K\pi$	KK	Kp	$p\pi$	pK	pp
0.940	0.500	3.53	3.32	3.73	3.43	3.70	3.48		4.48	3.61
		0.05	0.38	0.31	0.48	0.18	0.48		0.79	0.09
0.940	0.625	3.42	3.63	2.99		3.79			3.38	3.58
		0.06	0.34	0.28		0.24			0.34	0.04
0.940	0.750	3.46	3.38	3.60		3.48			3.30	3.57
		0.06	0.57	0.37		0.19			0.32	0.07
0.940	1.000	3.53				3.71				3.65
		0.10				0.24				0.09
0.940	1.250	3.48				5.07				3.90
		0.20				0.67				0.17
0.895	0.500	4.44	4.98	5.33	3.86	4.66			5.51	4.63
		0.06	0.30	0.41	0.52	0.16			0.88	0.07
0.895	0.750	4.49	4.59	4.92	5.39	4.28		1.70	4.30	4.66
		0.05	0.28	0.62	0.76	0.20		0.70	0.46	0.04
0.895	1.000	4.68	4.51			5.08				4.74
		0.11	0.43			0.31				0.08
0.800	0.500	5.36	5.78	5.39	4.49	5.81		4.74	6.09	5.41
		0.06	0.36	0.31	0.52	0.28		0.24	0.61	0.07
0.800	0.750	5.23	5.20	5.12	5.18	5.06		4.04	4.25	5.28
		0.13	0.31	0.40	0.55	0.31		0.55	0.40	0.07
0.700	0.500	5.61	5.25	6.23	5.71	6.50		4.55	6.46	5.80
		0.16	0.50	0.54	0.63	0.63		0.18	0.57	0.09
0.700	0.750	5.91	6.34	5.99	5.39	5.75		4.96	4.96	5.94
		0.14	0.58	0.71	0.78	0.45		0.24	0.95	0.08
0.600	0.300	5.21	5.65	6.21	5.14	4.83	4.87	4.54	6.27	5.76
		0.13	0.34	0.41	1.02	0.36	1.19	0.27	0.60	0.11
0.600	0.400	5.46	6.03	5.56	6.24	6.48		4.84	5.91	5.96
		0.12	0.43	0.34	0.74	0.52		0.14	0.25	0.07
0.600	0.500	5.67	5.61	6.19	5.88	5.75		5.00	5.79	6.12
		0.13	0.39	0.49	0.79	0.38		0.21	0.33	0.07
0.600	0.625	5.88	6.70	6.54	6.85	5.47	7.62	5.23	6.03	6.17
		0.14	0.51	0.47	0.68	0.50	0.89	0.14	0.28	0.06
0.600	0.750	5.98	5.53	5.83	6.91	5.20		5.28	6.30	6.26
		0.19	0.62	0.33	0.68	0.57		0.14	0.24	0.05
0.600	0.900	6.38	5.84	4.94	6.15	7.20		5.16	5.96	6.50
		0.28	0.59	1.16	0.88	0.82		0.16	0.59	0.06
0.600	1.050	6.75	6.40	5.54				5.67	6.76	6.81
		0.40	0.86	0.80				0.23	0.89	0.11
0.600	1.200	6.50						5.48	6.85	6.84
		0.49						0.48	0.60	0.12
0.500	0.300	5.46	6.29	7.26	5.55	5.25	4.63	5.12	6.20	6.53
		0.16	0.44	0.41	0.71	0.54	0.83	0.20	0.18	0.09
0.500	0.500	6.20	6.49	5.89	6.08	5.73		5.78	6.26	6.76
		0.14	0.46	0.40	0.77	0.47		0.17	0.28	0.09
0.500	0.750	6.64	5.99	6.15	8.77	6.61		5.62	6.92	6.96
		0.25	0.47	0.52	1.89	0.73		0.16	0.25	0.08
0.400	0.300	6.14	7.01	7.35	6.12	5.43	9.63	6.06	6.63	7.30
		0.12	0.45	0.40	0.60	0.37	1.93	0.21	0.21	0.10
0.400	0.500	6.43	7.71	8.04	6.87	6.90		6.23	6.86	7.44
		0.17	0.64	0.43	0.69	0.64		0.12	0.25	0.09

TABLE XXI. (*Continued.*)

(h) 175 GeV/c $a^+ + p \to c^+ + X$ (*continued*)

x	p_T (GeV/c)	$\pi\pi$	πK	πp	$K\pi$	KK	Kp	$p\pi$	pK	pp
0.400	0.750	7.04						5.90	7.59	7.75
		0.34						0.20	0.70	0.13
0.300	0.150	6.34	6.04	7.72	6.55	6.30		5.56	7.03	7.46
		0.21	0.82	0.57	1.25	0.87		0.14	0.38	0.14
0.300	0.225	6.27	7.69	6.94	6.14	5.44		5.68	6.69	7.84
		0.21	0.60	0.45	1.12	0.76		0.13	0.29	0.11
0.300	0.300	6.21	6.94	7.32	5.66	7.12		6.14	6.67	7.69
		0.18	0.55	0.63	0.61	1.20		0.19	0.39	0.13
0.300	0.400	6.46	6.49	7.19	6.27			6.59	7.76	8.09
		0.23	0.63	0.91	0.62			0.21	0.81	0.19
0.300	0.500	6.88	8.41	6.43	6.78			6.75	6.54	8.06
		0.19	0.87	0.61	1.02			0.17	0.65	0.15
0.300	0.625	6.42	7.17	7.88	7.54	5.12		6.82	7.13	8.43
		0.22	0.64	1.41	0.78	0.67		0.18	0.55	0.16
0.300	0.750	6.59	11.28	11.19	10.71			6.78	7.97	10.48
		0.21	1.37	1.01	1.27			0.20	0.83	0.21
0.300	0.850	6.97		7.25				7.05	8.31	8.46
		0.42		0.84				0.26	2.13	0.26
0.200	0.150	6.65	8.17	11.94	7.47			6.79	8.18	8.33
		0.28	0.88	3.04	1.87			0.23	1.07	0.46
0.200	0.300	7.09	8.81	7.81	5.68			7.14	8.21	8.46
		0.18	0.82	0.66	0.68			0.17	0.55	0.32
0.200	0.500	7.73	7.40	7.75				7.07	7.66	9.82
		0.33	1.27	0.89				0.19	0.76	0.44
0.120	0.150	7.24						6.94	0.00	9.36
		0.60						0.32	0.00	1.25
0.120	0.300	8.06						7.23	8.03	7.95
		0.51						0.25	1.19	0.58

sist almost entirely of one- and three-prong contributions suggesting the diffractive nature of these topological cross sections in the low-mass region. The contributions of five-, seven-, and nine-prong processes for $pp \to \pi^- X$ and $\pi^+ p \to \pi^- X$ are similar, falling steeply with increasing x. The one-pion-exchange[2] high-x shoulder in $\pi^+ p \to \pi^- X$ is due predominantly to an x-independent associated three-prong contribution where one associated prong arises from the decay of a forward-produced vector meson, and where the low effective energy $\pi^+ p$ vertex produces predominantly two-prong states.

The associated-charged-particle multiplicities for leading-particle reactions are displayed in Fig. 26 as a function of invariant momentum transfer t at fixed x or $M_X{}^2$. Similar multiplicities for high-statistics particle-exchange reactions are displayed in Fig. 27 as a function of transverse momentum p_T at fixed x. There is a definite increase of the associated multiplicities with increasing $|t|$ or p_T for $x < 0.8$ for all channels with sufficient statistics.

The leading-particle data have been fit to the form

$$\langle n(x, |t|) \rangle = \alpha(x) + \beta(x)|t| \tag{18}$$

at a constant x or $M_X{}^2$. Results of this fit are displayed in Fig. 26. For the high-statistics channels the term $\beta(x)$, shown in Fig. 28, is positive, indicating an increase in the average multiplicity with increasing scattering angle. $\beta(x)$ is independent of x except for $x > 0.8$, where it falls to zero as $x \to 1$.

Both bubble-chamber[39,40] and counter[41,42] experiments have also studied the $M_X{}^2$ and t dependences of associated multiplicities for leading-particle reactions. Most of the $pp \to pX$ experiments find very little dependence of the multiplicity on the

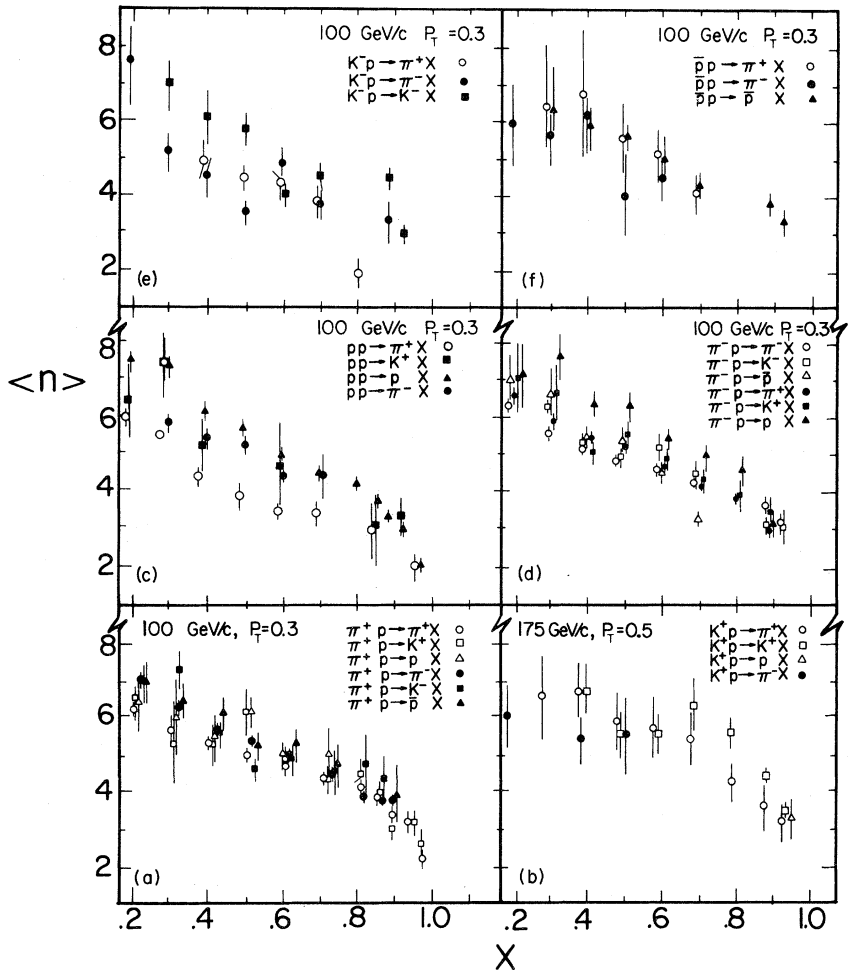

FIG. 24. Average associated-charged-particle multiplicities for $a+p \to c+X$ as a function of x for fixed p_T.

momentum transfer t. However, the ARGO spectrometer group[42] found a definite increase in the associated multiplicity with increasing t with a form

$$n=\alpha(x)+\beta(M_X-M_p)^2|t| \ . \tag{19}$$

This functional form is consistent with the behavior of the presently fitted $\beta(x)$ at comparable $M_X{}^2$ for $x>0.8$. The Fermilab Proportional Hybrid System Consortium[40,43] has also found a form $n=\alpha(x)+\beta|t|$ for the reaction $\pi^-p \to \pi^-X$ with the t coefficient, $\beta=1.2\pm0.2$, independent of x or $M_X{}^2$, over the range $0.5 \leq x \leq 0.93$ ($20 \leq M_X{}^2 \leq 140$ GeV^2). An average of the present $\pi^-p \to \pi^-X$ data for $x<0.8$ with a constant β produces a smaller t slope, $\beta=0.6\pm0.1$.

The parameters $\alpha(x)$ in the fit, which represent the average multiplicity at $t=0$, are plotted for $pp \to pX$, and $\pi^\pm p \to \pi^\pm X$ in Fig. 29. Also plotted are the total-cross-section multiplicities discussed in Sec. IV D at common $M_X{}^2=s$. Also indicated are fits to the world-average[44] total multiplicity data and the associated multiplicities[40] for $pp \to pX$ and $\pi^-p \to \pi^-X$. As has been previously noted,[45] the $pp \to pX$ associated multiplicities are systematically higher than the corresponding $pp \to X$ total multiplicities. Comparing the s dependence of the fits[40] to the associated multiplicities, it appears that the associated multiplicities at a fixed $M_X{}^2$ increase with increasing s. In comparison, the $\pi^\pm p \to \pi^\pm X$ multiplicity data are systematically lower than for the total-cross-section multiplicities at comparable s or $M_X{}^2$. Assuming a single exchange trajectory for $hp \to hX$ at high x or low $M_X{}^2$, one would expect identical behavior for associated multiplicities for all hadrons h, since all target fragments arise at the Pomeron-proton vertex.

The average multiplicities for the reactions

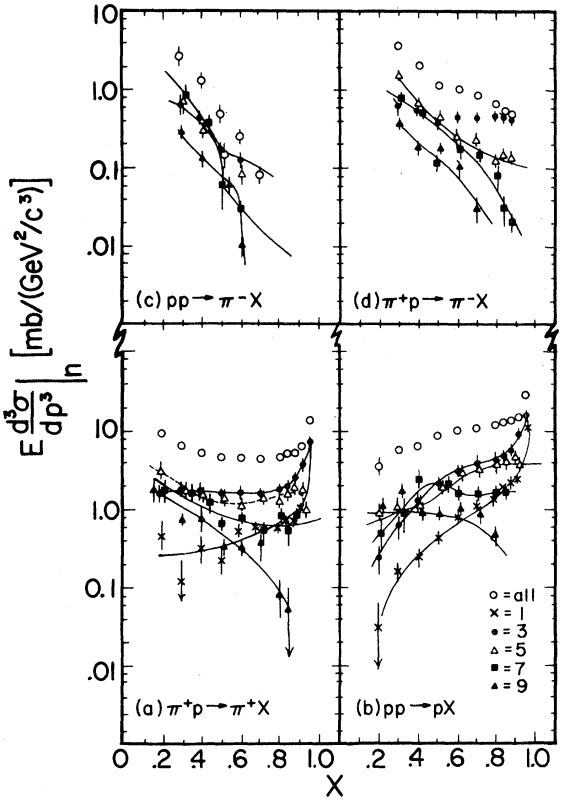

FIG. 25. Feynman-x dependence of contribution of n-prong cross sections $E\,d^3\sigma/dp^3\,|_n$ for $\pi^+p\to\pi^\pm X$, $pp\to pX$, and $pp\to\pi^- X$ at fixed p_T.

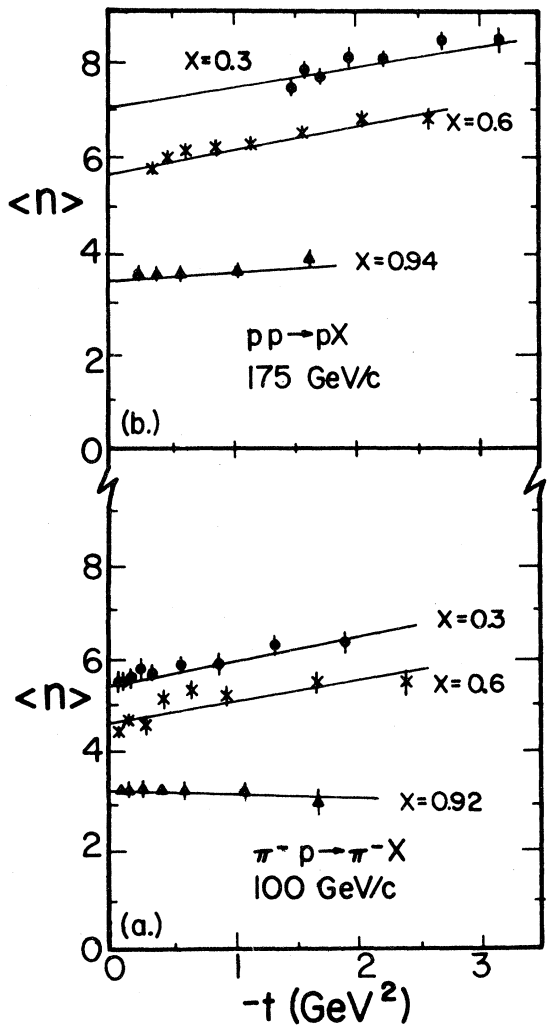

FIG. 26. Dependence of the associated-charged-particle multiplicity for $pp\to pX$ and $\pi^- p\to\pi^- X$ on the invariant momentum transfer t at fixed x. Linear-fit parameters are displayed in Figs. 28 and 29.

$\pi^\pm p\to\pi^\pm X$, $\pi^\pm p\to\pi^\mp X$, $K^\pm p\to K^\pm X$, and $p^\pm p\to p^\pm X$ at $t=0$ and a common $M_X{}^2=53$ GeV^2 are essentially the same with $\langle\bar{n}\rangle=4.62\pm0.18$. These agree well with the bubble-chamber[40] results for $pp\to pX$, $\Lambda^0 X$, and $\Delta^{++}X$ at the same $M_X{}^2$. This shows that at fairly low $M_X{}^2$ the multiplicity is independent of the exchange particle, whether there is a dominant *PPP* or *RRP* coupling, and primarily depends on $M_X{}^2$.

B. Angular distributions for the associated particles

Besides the associated multiplicities, correlations of the produced multiparticle state with the kinematics and identities of the trigger particles may provide further understanding of production and fragmentation processes. In the absence of momentum analysis, the associated particles are described by the pseudorapidity

$$\eta_{\rm lab}=-\ln\tan(\theta/2)\,, \tag{20}$$

where θ is the production angle relative to the beam direction.[46] Particles produced at 90° in the center of mass have $\eta_{\rm lab}=2.7$ and 2.9 for 100 and 175 GeV incident momenta, respectively. Due to limited statistics, all angular distributions for this experiment have been integrated over azimuthal angle and topology.

Figure 30 shows a similarity between the total and associated rapidity distributions at a common $s=M_X{}^2=190$ GeV^2. The associated η distribution for $pp\to pX$ measured in this experiment is compared to the total η distributions for $pp\to X$ (Ref. 47) and $\bar{p}p\to X$ (Ref. 48) at 100 GeV. The three data sets are in good agreement indicating that these processes can all be described by a common p_T-limited phase-space model.[41]

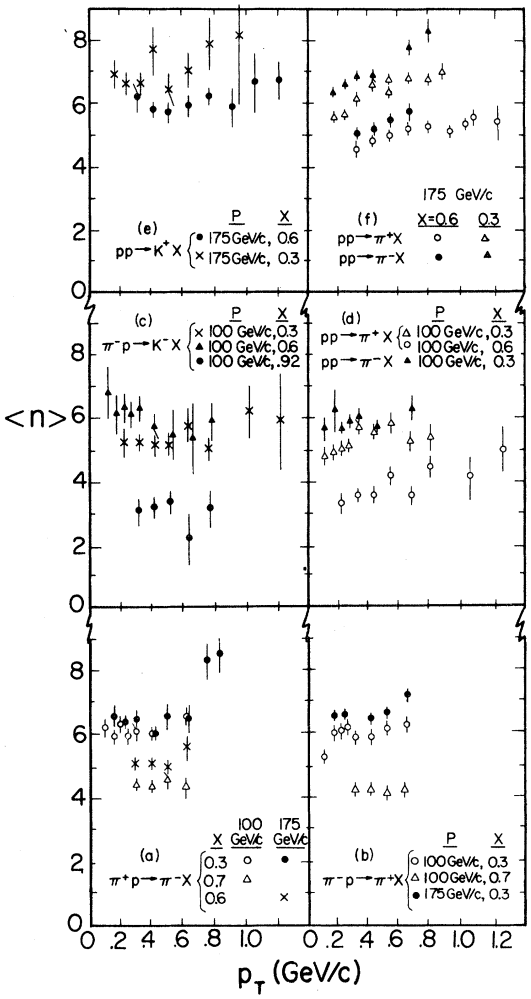

FIG. 27. Dependence of the associated-charged-particle multiplicity for particle-changing reactions $a+p\to c+X$ on the transverse momentum of particle c at fixed x.

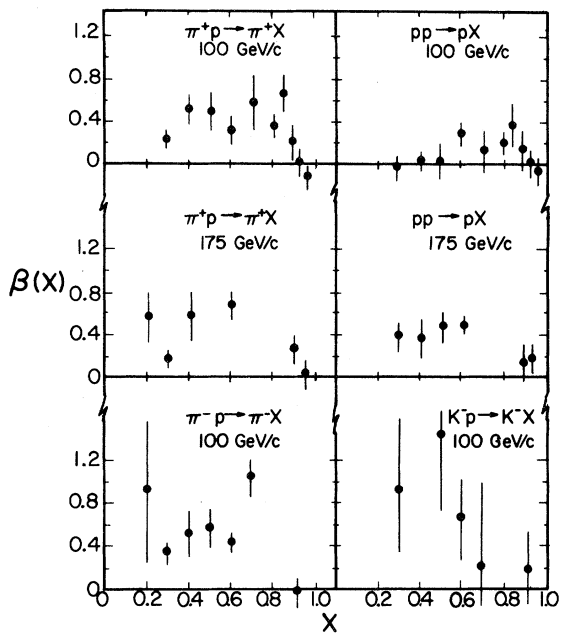

FIG. 28. Parameter $\beta(x)$ for fits of the form $\langle n(x,t)\rangle=\alpha(x)-\beta(x)t$ for leading-particle $a+p\to a+X$ channels.

The pseudorapidities of charged particles produced in $\pi^+p\to h^\pm X$ reactions are shown in Fig. 31. The angular distributions associated with leading $\pi^+p\to\pi^+X$ processes as a function of x at $p_T=0.3$ GeV/c show that the width of the pseudorapidity distribution increases as ln $M_X{}^2$ as expected. For $x\leq 0.4$, a central rapidity plateau appears. This is similar to the $pp\to hX$ data presented by the CHLM group[41] which were consistent with many of the detailed predictions of longitudinal or p_T-limited phase-space models.

There is very little dependence of the associated angular distributions on the identity of the particle detected in the single-arm spectrometer. The rise in the multiplicity with increasing p_T as seen for example in $\pi^+p\to\pi^+X$ at moderate x is due to an increase in the number of particles produced in the central rapidity region as shown in Fig. 13(c). The number of target or beam fragments is independent of p_T.

The process $\pi^+p\to\pi^-X$ at high Feynman x exhibits features not described by phase space. The associated charged-particle pseudorapidity distributions are shown in Fig. 32. As the spectrometer trigger π^- increases in momentum above $x=0.3$, the phase-space plateau narrows and a very large positive correlation emerges at $\eta\simeq 4$. At $x=0.88$, the integrated number of associated particles above $\eta\geq 3.5$ is one, representing the π^+ from the decay of the forward-produced vector meson.[2]

VII. DISCUSSION AND SUMMARY

This experiment provides new data on charged-particle production in low-p_T hadronic fragmentation for $\pi^\pm$, $K^\pm$, p and $\bar{p}$ beams. Compared to bubble-chamber[39,40] and spectrometer[15,34,49] experiments, it extends the kinematic range for complete identification of the charged secondary particles. The major contributions of this experiment to understanding production processes are discussed below.

Over most of the fragmentation range, the inclusive spectra are well represented by a power-law dependence such as $(1-x)^n$. This form qualita-

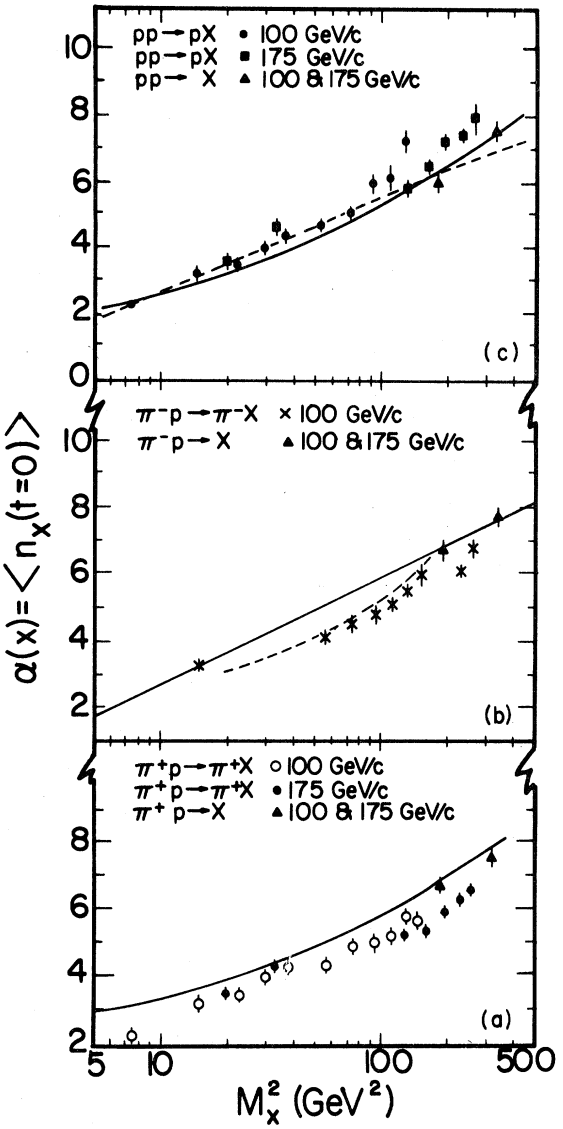

FIG. 29. Parameter $\alpha(x)$ for fits of the form $\langle n(x,t)\rangle = \alpha(x) - \beta(x)t$ for leading-particle $\pi^{\pm}p \to \pi^{\pm}X$ and $pp \to pX$ channels. Also plotted are the multiplicities for the $\pi^{\pm}p \to X$ and $pp \to X$ total-cross-section trigger of Table XI at a common $s = M_X{}^2$. The solid curve is a parametrization of Ref. 44, for $ap \to X$ total multiplicities. The dashed curve represents fits of Ref. 40 for $ap \to aX$ associated multiplicities as observed in bubble-chamber experiments.

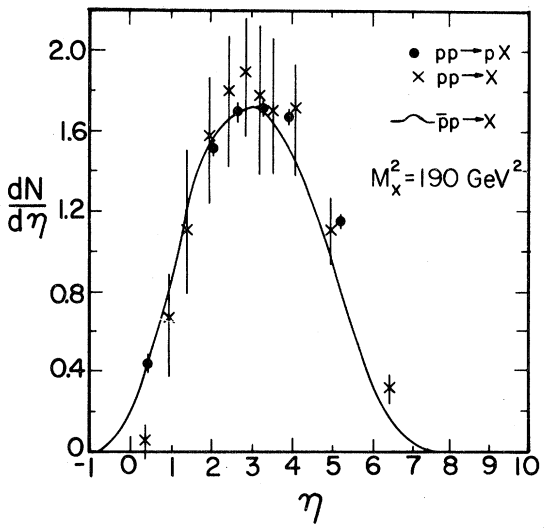

FIG. 30. Pseudorapidity distribution for associated particles in $pp \to pX$ compared with pseudorapidities for $pp \to X$ (Ref. 47), and $\bar{p}p \to X$ (Ref. 48) at a common $s = M_X{}^2 = 190$ GeV^2.

tively agrees with quark-counting-model predictions of Brodsky and Gunion.[31] Since the earlier publication of this data,[3] this production model has been modified to differentiate between hadronic and gluon bremmsstrahlung spectators in the counting rules to better represent the powers n for the large numbers of observed channels.[32] The modified model yields predictions in still better agreement with the data.

The pion and kaon data have been analyzed in the recombination[50] and valon[51] models. The meson structure functions may be derived from the data using this formulation.[4] The pion structure function determined in this manner agrees well with that derived from Drell-Yan dimuon production. However, the kaon valence structure function so derived using the recombination model is steeper[52] than those found from dimuon[53] or high-p_T π^0 production[54] by kaon beams. This disagreement is most likely due to uncertainties in the exact formulation of the recombination model and large resonance production backgrounds at high x for channels which determine the kaon structure function. Amiri and Williams[55] have studied the relative resonance and direct contributions to these channels and find reasonable agreement with the present data using the kaon structure functions of Ref. 53 and the valon phenomenology. The single-particle inclusive fragmentation data may also be well represented by the Lund model[56] as discussed in Ref. 17.

At high x, the leading-particle spectra may be well fitted using only scaling $PPP + RRP$ triple-Regge terms. The projectile-particle independence of the ratio of inelastic $a + p \to a + X$ to elastic $a + p \to a + p$ interactions at comparable t values is indicative of factorization of the aaP vertex from the ppP and PPP verticies. The agreement of the

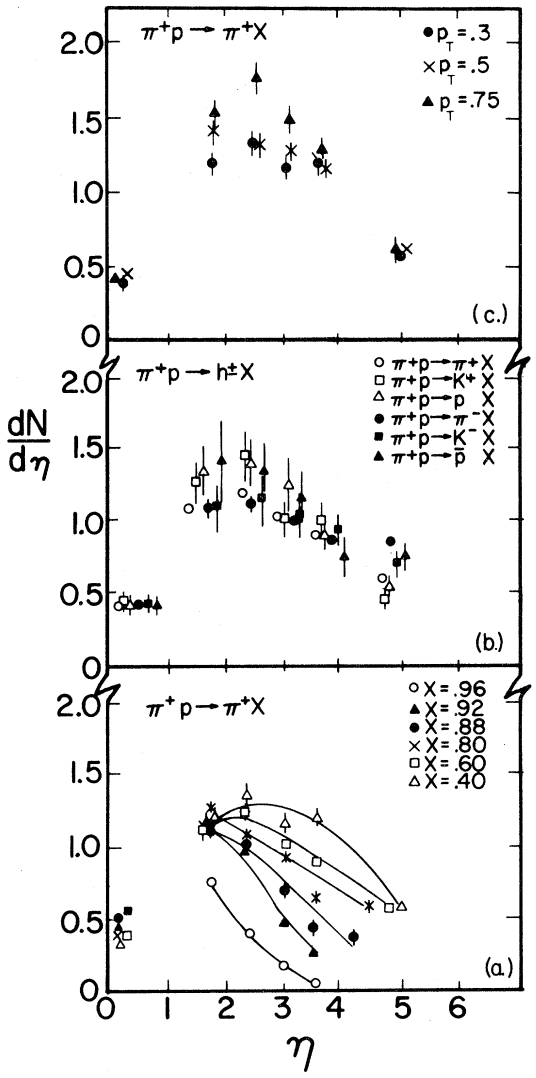

FIG. 31. Pseudorapidity distributions. (a) x dependence for $\pi^+p \to \pi^+x$ at $p_T=0.3$ GeV/c. Curves are drawn to guide the eye. (b) Trigger-particle dependence for $\pi^+p \to h^\pm X$ for 100-GeV/c incident π^+ at $x=0.6$ and $p_T=0.3$ GeV/c. (c) p_T dependence for $\pi^+p \to \pi^+X$ at $x=0.4$ for 100-GeV/c π^+.

production-cross-section ratio for $(\pi^-p \to K^-X)/(\pi^+p \to K^+X)$ with the the total-cross-section ratio of K^+p/K^-p gives strong evidence of factorization for K-exchange channels.

The average associated-charged-particle multiplicities increase with $\ln M_X{}^2$ as the total-cross-section multiplicities increase with $\ln s$. However, there are absolute differences in comparing the multiplicities for $ap \to aX$ and $ap \to X$ at comparable $M_X{}^2$ and s values. For leading-particle channels, the multiplicity increases as $|t|$ increases at constant x, except as $x \to 1$ where there is no t dependence. For

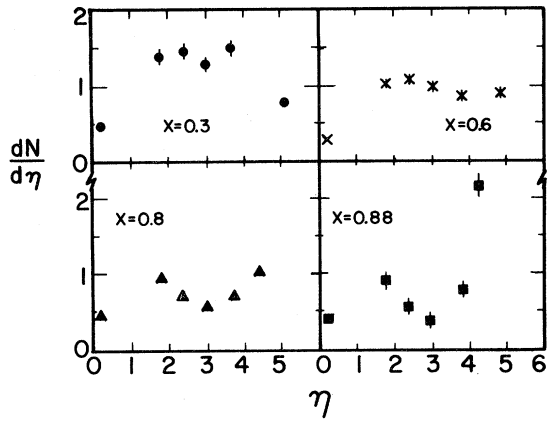

FIG. 32. x dependence of the associated pseudorapidity distribution for $\pi^+p \to \pi^-X$ at 100 GeV/c and $p_T=0.3$ GeV/c.

particle-changing reactions with sufficient statistics, there is also an increase of associated multiplicities with increasing p_T. The angular distributions of the associated particles indicate that this increase in the multiplicity is due to an increase of production in the central region.

ACKNOWLEDGMENTS

We would like to express our thanks to the many people at Fermilab who have contributed to the successful operation of the Single Arm Spectrometer and of the accelerator. Special thanks are due to the staffs of the Fermilab Meson Laboratory and Computing Center, MIT Physics Department and Laboratory for Nuclear Science, the Brown University Physics Department, and the Istituto Nazionale di Fisica Nucleare. Major credit is due for the technical efforts of Travis Minto from Fermilab and Roger Strong from MIT. This work was supported in part by the U. S. Department of Energy under Contracts Numbers EY76-C-02-3000 (Fermilab), EY76-C-02-3069 (MIT), and EY76-C-02-3130 (Brown), and by the Istituto Nazionale di Fisica Nucleare (Italy).

APPENDIX A: ČERENKOV PARTICLE IDENTIFICATION

The properties of the eight Čerenkov counters used in this experiment are given in Table IV. Any event within the spectrometer acceptance which has a valid beam Čerenkov pattern is assumed to be the result of one of the nine hadronic processes ($\pi Kp \to \pi Kp$). The beam identification

is the easier to deal with because any events with ambiguous beam Čerenkov patterns have been eliminated from both incoming flux and spectrometer rate, incurring no change in the measured cross section and only a small loss in statistics.

1. Beam identification

Valid beam particles used in the analysis required an unambiguous Čerenkov identification. The Čerenkov assignments used were

$$\pi = (\mathrm{BGAS}+\mathrm{BGAS0})\cdot\overline{\mathrm{BDISC}}\cdot\overline{\mathrm{BDIFR}}\ ,$$

$$K = \mathrm{BDISC}\cdot(\overline{\mathrm{BGAS}+\mathrm{BGAS0}})\cdot\overline{\mathrm{BIDFR}}\ ,$$

$$p = \mathrm{BDIFR}\cdot\overline{\mathrm{BDIFA}}\cdot(\overline{\mathrm{BGAS}+\mathrm{BGAS0}})\cdot\overline{\mathrm{BDISC}}\ .$$

Events not satisfying these criteria were discarded from further analysis due to ambiguous identification. Usually, the ambiguous signatures were caused by two particles in the same rf bucket or by Čerenkov-counter inefficiencies. Requiring strict beam-particle identification and readjusting the measured incident fluxes was more desirable than attempting to use all the flux and later applying corrections. The loss of events from application of this was 4% at 100 GeV and 8% at 175 GeV.

2. Spectrometer identification

Each event with valid beam and spectrometer particles reconstructed within the spectrometer aperture by fitting the multiwire proportional chamber data was assumed to correspond to a valid hadron scattering event regardless of the spectrometer Čerenkov pattern. A preliminary spectrometer identification was made for all possible spectrometer Čerenkov patterns. For each kinematic setting, a fitting program then solves for the efficiency and interference between spectrometer counters and corrects for those spectrometer particles mislabeled in the preliminary assignment.

A total of 32 Čerenkov patterns was available using the five spectrometer signals SDIFR, SDIFA, SGAS1, SGAS2, and SGAS3. The nominal settings of the Čerenkov pressures corresponded to the indentification in Table XXII. There are four important momentum-dependent efficiency changes. The first is a decrease in efficiency of SGAS1, SGAS2, and SGAS3 at high momentum. The second efficiency change is due to the proximity of the kaon and proton light in SDIF at high momentum, and the finite acceptance of the spectrometer. These circumstances lead to an overlap of the kaon and proton light at the edge of the SDIF ring. The third-effect is caused by the dispersion of Čerenkov light at low momentum. For momenta less than 50 GeV/c, the proton ring of light is wider than the SDIF ring, and protons count on both SDIFR and SDIFA. Finally, as the momentum becomes small, the light from pions and kaons, is emitted at very large angles in the SDIF counter. Therefore, the SDIFA efficiency for pions and kaons becomes quite small for low momenta.

TABLE XXII. Particle identifications associated with spectrometer Čerenkov signals.

	>100 GeV/c	≤ 100 GeV/c
SGAS1	π	π
SGAS2	π	$\pi+K$
SGAS3	π	π
SDIFR	p	p
SDIFA	$\pi+K$	$\pi+K$

For each spectrometer momentum, a fit was made for the efficiencies of each spectrometer Čerenkov counter for detecting π's, K's, and protons. The fitting program is applied to scattering data, using the identity of the beam particles, determining the reaction probability for a beam particle to produce a π, K, or proton in the spectrometer. Thus, 15 efficiencies E_{ic} and 9 reaction probabilities B_{ac} are fit where $i=$ the spectrometer Čerenkov counter (SDIFR, SDIFA, SGAS1, SGAS2, SGAS3), $a=$ the beam-particle type (π, K, or p), and $c=$ spectrometer particles (π, K, or p). The sum of the reaction probabilities for each beam particle is constrained to be 1. That is,

$$\sum_c B_{ac} = 1\ .$$

Thus, there are $15+9-3=21$ free parameters.

The input to the fitting program is an array of the number of events recorded for each spectrometer Čerenkov pattern. This is a 3×32 array where we have 3 beam-particle types and 32 spectrometer patterns. We then minimize χ^2 with respect to the 21 free parameters and calculated a complete set of efficiencies and reaction probabilities. From this we construct the "misidentification matrix" $M_{cc'}$ which gives the fraction of spectrometer particles c that are identified as c'. This matrix is applied during the run combination program of the analysis to correct the cross sections. For $\pi p\rightarrow \pi X$ and $pp\rightarrow pX$ reactions this correction is less than 1%. The correction for the $Kp\rightarrow KX$ cross section is typically 9%.

*Present address: Weizmann Institute, Rehovath, Israel.
†Present address: Brookhaven National Laboratory, Upton, N.Y., 11973.
‡Present address: U.S. Windpower, Burlington, Mass. 01803.
§Present address: Harvard University, Cambridge, Mass. 02138.
**Present address: Bell Laboratories, Holmdel, N.J. 07733.
††Present address: Bell Laboratories, Denver, Colo. 80234.
‡‡Present address: P.O. 796 APO, San Francisco, CA. 96555.

[1]For description and references see D. S. Ayres *et al.*, Phys. Rev. D 15, 3105 (1977).
[2]D. Cutts *et al.*, Phys. Rev. Lett. 40, 141 (1978).
[3]D. Cutts *et al.*, Phys. Rev. Lett. 43, 319 (1979).
[4]W. Aitkenhead *et al.*, Phys. Rev. Lett. 45, 157 (1980).
[5]W. Aitkenhead, Ph.D. thesis, MIT, 1979 (unpublished).
[6]W. Aitkenhead *et al.*, Report No. Fermilab-Conf-80/48-EXP (unpublished).
[7]L. G. Votta, Ph.D. thesis, MIT, 1979 (unpublished).
[8]J. Lach and S. Pruss, Report No. Fermilab-TM-298, 1971 (unpublished).
[9]R. L. Anderson and J. A. Grant, Nucl. Instrum. Methods 135, 267 (1976).
[10]M. Benot, J. Litt, and R. Meunier, Nucl. Instrum. Methods 105, 431 (1972).
[11]D. Ayres, ANL report, 1974 (unpublished).
[12]P. H. Garbincius, Nucl. Instrum. Methods 131, 273 (1978).
[13]E. F. Anelli, Rev. Sci. Instrum. 49, 1054 (1978).
[14]D. C. Carey, Nucl. Instrum. Methods 104, 173 (1972); K. L. Brown, F. Rothacker, D. C. Carey, and Ch. Iselin, Fermilab Report No. NAL-91, 1977 (unpublished).
[15]J. R. Johnson *et al.*, Phys. Rev. Lett. 39, 1173 (1977); Phys. Rev. D 17, 1292 (1978).
[16]F. Sannes *et al.*, Phys. Rev. Lett. 30, 766 (1973).
[17]W. W. Toy, Ph.D. thesis, MIT, 1978 (unpublished).
[18]B. G. Gibbard *et al.*, Phys. Rev. D 11, 2367 (1975), used a similar matrix unfolding procedure.
[19]T. Ferbel, private communication of reconstructed bubble-chamber events as described by J. W. Chapman *et al.*, Phys. Lett. 47B, 465 (1973).
[20]D. C. Carey and D. Drijard, J. Comput. Phys. 28, 327 (1978).
[21]S. Kahn, in *Particles and Fields—1975,* proceedings of the Meeting of the Division of Particles and Fields of the APS, Seattle, 1975, edited by H. J. Lubatti and P. M. Mockett (Univ. of Washington, Seattle, 1976), p. 292.
[22]R. L. Anderson *et al.*, Phys. Rev. Lett. 38, 880 (1977).
[23]A. Carroll *et al.*, Phys. Rev. Lett. 33, 928 (1974); 33, 932 (1974).
[24]W. M. Morse *et al.*, Phys. Rev. D 15, 66 (1977).
[25]E. L. Berger *et al.*, Nucl. Phys. B77, 365 (1974).
[26]V. E. Barnes *et al.*, Phys. Rev. Lett. 34, 415 (1975).
[27]D. Fong *et al.*, Nucl. Phys. B102, 386 (1976).
[28]R. E. Ansorge *et al.*, Phys. Lett. 59B, 299 (1975).
[29]G. Giacomelli, in *Proceedings of the 19th International Conference on High Energy Physics, Tokyo, 1978,* edited by S. Homma, M. Kawaguchi, and H. Miyazawa (Phys. Soc. of Japan, Tokyo, 1979), p. 53; Z. Koba *et al.*, Nucl. Phys. B40, 317 (1972).
[30]P. Slattery *et al.*, Phys. Rev. Lett. 29, 1624 (1972).
[31]S. J. Brodsky and J. F. Gunion, Phys. Rev. D 17, 848 (1978).
[32]J. F. Gunion, in *Proceedings of the XVth Recontre de Moriond, Les Arcs, Savoie, France, 1980* (Editions Frontieres, Dreux, France, 1980), p.151.
[33]G. J. Bobbink *et al.*, Phys. Rev. Lett. 44, 118 (1980).
[34]J. Singh *et al.*, Nucl. Phys. B140, 189 (1978).
[35]A. Mueller, Phys. Rev. D 2, 2963 (1970).
[36]R. D. Field and G. C. Fox, Nucl. Phys. B80, 367 (1974).
[37]W. Galbraith *et al.*, Phys. Rev. 138, 913 (1965).
[38]D. Brick *et al.*, Phys. Rev. D 25, 2248 (1982).
[39]J. Whitmore, Phys. Rep. 10C, 273 (1974); 27C, 187 (1976).
[40]D. Brick *et al.*, Phys. Rev. D 19, 743 (1979) and references listed therein.
[41]M. G. Albrow *et al.*, Nucl. Phys. B102, 275 (1976).
[42]A. Ramanauskas *et al.*, Phys. Rev. Lett. 31, 1371 (1973); T. S. Clifford *et al.*, *ibid.* 33, 1239 (1974); W. N. Schreiner, Ph.D. thesis, Virginia Polytechnic Institute (unpublished).
[43]C. deTar, Phys. Rev. D 17, 879 (1978).
[44]E. Albini *et al.*, Nuovo Cimento 32A, 101 (1976).
[45]S. J. Barish *et al.*, Phys. Rev. Lett. 31, 1080 (1973); J. Whitmore and M. Derrick, Phys. Lett. 50B, 280 (1978).
[46]Assuming all particles have $p_T=0.3$ GeV, a typical average transverse momentum, the maximum pseudorapidity available to an associated particle is

$$\eta_{\max}\simeq\ln\frac{2p_0(1-x)}{\langle p_T\rangle},$$

where p_0 is the beam momentum and x is the Feynman x of the trigger hadron. This estimate works reasonably well to define the η bin center and bin width corresponding to the MC detector region. Similarly, for backward particles $\eta_{\min}\simeq-1.1$, independent of x or p_0.
[47]J. E. Elias *et al.*, Phys. Rev. D 22, 13 (1980).
[48]R. Raja, 100 GeV $\bar{p}p\to X$ data set, private communication.
[49]R. T. Edwards *et al.*, Phys. Rev. D 18, 76 (1978).
[50]K. P. Das and R. C. Hwa, Phys. Lett. 68B, 459 (1977); R. C. Hwa and R. G. Roberts, Z. Phys. C 1, 81 (1979).
[51]R. C. Hwa, Phys. Rev. D 22, 1593 (1980).
[52]P. H. Garbincius *et al.*, in *High Energy Physics—1980,* proceedings of the XXth International Conference, Madison, Wisconsin, edited by L. Durand and L. G.

Pondrom (AIP, New York, 1981), p. 74.
[53]J. Badier *et al.*, Phys. Lett. 93B, 354 (1980).
[54]K. W. Lai and R. L. Thews, Phys. Rev. Lett. 44, 1729 (1980).
[55]F. Amiri and P. K. Williams, Phys. Rev. D 24, 2409 (1981).
[56]B. Andersson *et al.*, Phys. Lett. 71B, 337 (1977).